2014

Fabrication and Characterization of High Surface Area Gold Electrodes

Madhura S. Damle

FABRICATION AND CHARACTERIZATION OF HIGH SURFACE AREA GOLD ELECTRODES

A dissertation submitted in partial fulfillment of the requirements for the degree of Master of Science at Virginia Commonwealth University

by

Madhura Damle

Research Advisor: Dr. Maryanne M. Collinson

Department of Chemistry,

Richmond, Virginia

December 2014

ACKNOWLEDGEMENTS

I am grateful to Dr. Collinson for allowing me to be a part of her research group and for all her help and support over the last three years. I enjoyed doing research in her lab and this dissertation wouldn't have been possible without her. I am thankful to the research committee members: Dr. Arachhige, Dr. Alvarez and Dr. Ye for their valuable feedback. Heartfelt thanks to Dr. Dmitry Pestov for training me on the instruments and for all his help time and again. I would like to thank all the research group members for making our lab such a wonderful place to work in. I am thankful to Ahmed Farghaly for his help with HITACHI SEM and EDX. I would like to dedicate this dissertation to my parents for their unfailing moral support through very difficult times. I am also thankful to my friends back home and in Richmond for all the happy moments. My special thanks to Constance for her friendship, support and fun over endless cups of coffee.

OUTLINE

1 CHAPTER 1: INTRODUCTION

1.1 Introduction

1.1.1 Introduction to porous materials

1.1.2 Different fabrication strategies of porous materials

1.2 Fabrication of porous metal electrodes using templates

1.2.1 Synthetic Templates

1.2.2 Natural Templates

1.2.3 Applications of colloidal crystals and macroporous materials prepared using colloidal crystals

1.3 Summary of research

1.4 Characterization methods of high surface area films

1.4.1 Scanning Electron Microscopy (SEM)

1.4.2 Energy Dispersive Spectroscopy (EDS)

1.4.3 Electrochemistry: Cyclic Voltammetry (CV)

1.6 Applications of porous materials

2 CHAPTER 2: Use of Polystyrene Spheres as Templates for Fabrication

2.1 Different methods of synthesis of polystyrene spheres

2.2 Different methods of assembling a colloidal layer

2.3 Synthesis of Polystyrene Spheres

2.3.1 Materials and Methods

2.3.2 Results and Discussion

2.4 Preparation of Self Assembly of Colloidal Crystals

3 CHAPTER 3: Fabrication of High Surface Area Gold Electrodes

3.1 Fabrication of macroporous electrode using polystyrene spheres as template

3.1.1 Materials and methods

3.1.2 Results and discussion

3.2 Fabrication of macro-nanoporous gold electrode

3.2.1 Materials and Methods

3.2.2 Results and Discussion

3.3 Fabrication of nanoporous gold electrode

3.3.1 Materials and methods

3.3.2 Results and Discussion

4 CHAPTER 4: Electrochemistry

4.1 Surface area measurement

4.2 Cyclic Voltammetry in different redox molecules

4.2.1 Potassium Ferricyanide in KCl

4.2.2 Cyclic voltammetry in KCl

4.2.3 Ferrocene methanol in KCl

4.2.4 Dopamine

4.2.5 Ascorbic Acid

4.3 Surface adsorption of dopamine

4.4 Detection of dopamine in the presence of ascorbic acid

4.5 Conclusion and future work

LIST OF ABBREVIATIONS

PLD – Plused Laser Deposition

PET – Polyethylene Terephthalate

CTAC – Cetyl trimethylammonium chloride

SCE – Saturated Calomel Electrode

NPG – Nanoporous Gold

pNIPAm – poly(N-isopropylacrylamide)

TMV – Tobacco Mosaic Virus

PS – Polystyrene Sphere

PMMA – Poly-(methyl methacrylate)

SERS – Surface Enhanced Raman Scattering

SEM – Scanning Electron Microscope

EDS – Energy Dispersive Spectroscopy

CV – Cyclic Voltammetry

UA – Uric Acid

AA – Ascorbic Acid

DA – Doapmine

AP – Acetaminophen

CySH – Cysteine

DPV – Differential Pulse Voltammetry

hCG – Human Serum Chorionic Gonadotropin

GS – Graphene Sheet

NADH – Nicotinamide Adenine Dinucleotide

PEM – Proton Exchange Membrane

ADIB – azo-bis-isobutyronitrile

3D – Three Dimensional

2D – Two Dimensional

LB – Langmuir-Blodgett deposition

SDS – Sodium Dodecyl Sulfate

KCl – Potassium Chloride

Ti – Titanium

Au – gold

Ag – Silver

$NaNO_3$ – Sodium Nitrate

$HAuCl_4$ – Gold (III) Chloride

ABSTRACT

FABRICATION AND CHARACTERIZATION OF HIGH SURFACE AREA GOLD ELECTRODES

By Madhura Damle

M.S Chemistry

A dissertation submitted in partial fulfillment of the requirements for the degree of Master of Science at Virginia Commonwealth University

Virginia Commonwealth University, 2014

Research Advisor: Dr. Maryanne Collinson

Department of Chemistry

High surface area gold electrodes are very good substrates for biosensors, catalysis and drug delivery. Their performance is characterized by good sensitivity, low detection limit and high signal. As a result, extensive research is being carried out in this field using different approaches of fabrication to generate high surface area porous electrodes of different morphology, pore size and structure. The morphology of the electrodes can be changed based on whether the approach involves a template or not, types of metal deposition, method and time

of dealloying etc. The deposition of metal can be carried out using various approaches such as electroless deposition, electrochemical deposition, combination of electroless and electrochemical deposition, pulsed laser deposition, laser deposition etc. These electrodes can then be used in electrochemical measurements and their performance compared with an unmodified flat gold electrode.

We used a template based approach, combined with electrochemical deposition, to fabricate macroporous, macro-nanoporous and nanoporous gold electrodes. To generate nanopores, in case of macro-nanoporous and nanoporous gold electrodes, we used gold-silver alloy electrochemical deposition method, followed by chemical dealloying. The morphology of electrodes was later observed under HITACHI Scanning Electron Microscope (SEM) and their elemental composition studied using HITACHI Energy Dispersion Spectroscopy (EDS). The electrodes were used in electrochemical measurements and their voltammetric data was compared. These measurements involved the determination of surface area, faradaic current using redox molecules with fast and slow electron transfer and charging current in KCl. Surface adsorption of dopamine was studied and detection of dopamine in the presence of ascorbic acid was carried out.

CHAPTER 1: INTRODUCTION

1.1 Introduction

High Surface area porous materials have been extensively researched in the recent times because they exhibit higher current/signal, higher sensitivity, and lower detection limits as compared to the flat electrodes.[1],[2],[3],[4]. These features make high surface electrodes an attractive support for the construction of biosensors, catalysts, as tools of separation, for drug delivery. Various templating and non-templating procedures have been used to create macro, meso and nanopores in order to obtain high surface area porous materials.[5],[6],[7] This chapter aims at discussing the different procedures used to fabricate these electrodes followed by the applications of porous metal films.

1.1.1 Different fabrication strategies of porous materials

According to IUPAC definition porous films can be mainly classified in three categories: microporous (< 2 nm), mesoporous (2 nm – 50 nm) and macroporous (> 50 nm).[8] Some of the widely used methods to prepare these porous films are templating, electrochemical deposition, pulsed laser deposition (PLD) and electroless deposition techniques etc.[9],[10],[11] The following is an overview of the different methodologies implemented to fabricate high surface area porous electrodes.

a.) Electrochemical deposition:

Electrochemical deposition is a popular method for depositing metals/alloys on a conductive substrate. Electrodeposition followed by chemical or electrochemical dealloying is often used to obtain a uniform, porous film. Two electrode and sometimes three electrode cells are used to apply potential and deposit the metal on a thin substrate. A few examples of the value of electrodeposition to make high surface area metal electrodes are given in the paragraphs

below. Chen et al. have demonstrated the use of a two electrode cell to deposit gold on flexible metal substrate to obtain porous metal films.[9] Layers of Ti and Au were evaporated on polyethylene terephthalate (PET)[9]. Depositing Ti and Au on the flexible PET surface made it conductive.[9] The electrodeposition solution consisted of $HAuCL_4$, $NaNO_3$ and Cetyl-trimethylammonium chloride (CTAC).[9] A two-electrode cell consisting of gold as the anode and carbon as the cathode was used to apply a voltage to reduce $HAuCl_4$ and electrodeposit gold on the flexible, conductive substrate.[9]

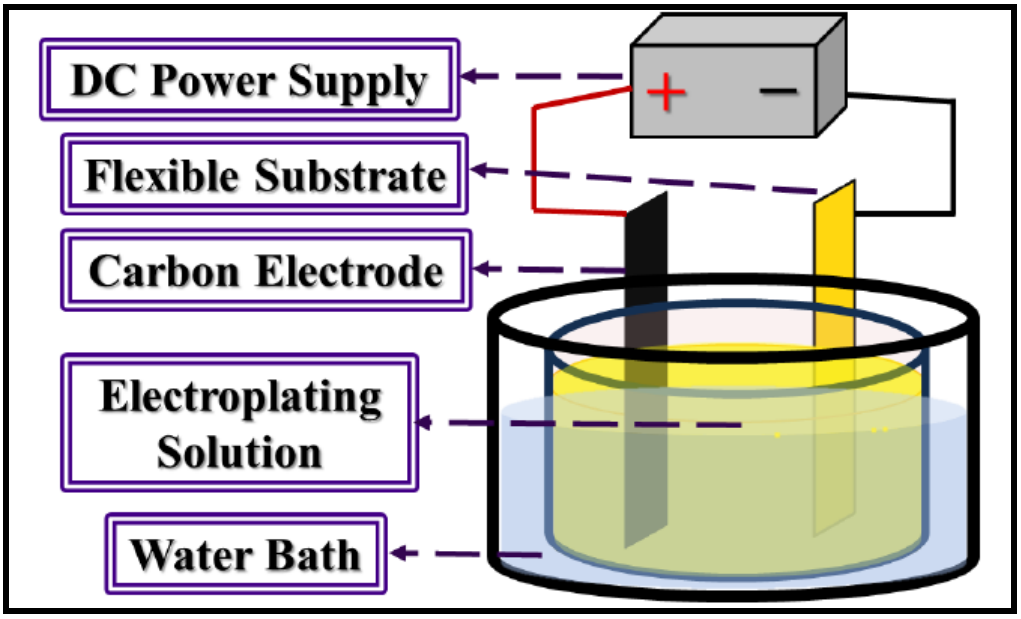

Figure 1: Design of the two-electrode cell used for gold electrochemical deposition. Reproduced from Ref. 9 with permission from the Royal Society of Chemistry

Further modifications to the basic procedure of electrodeposition such as the addition of surfactant, changing the electrodeposition voltage, changing the quantity of $NaNO_3$ helped achieve a variety of gold nanostructures with different morphologies like gold nanothorns, nanocorals, nanowires and nanoslices which can be seen in the figure below.[9]

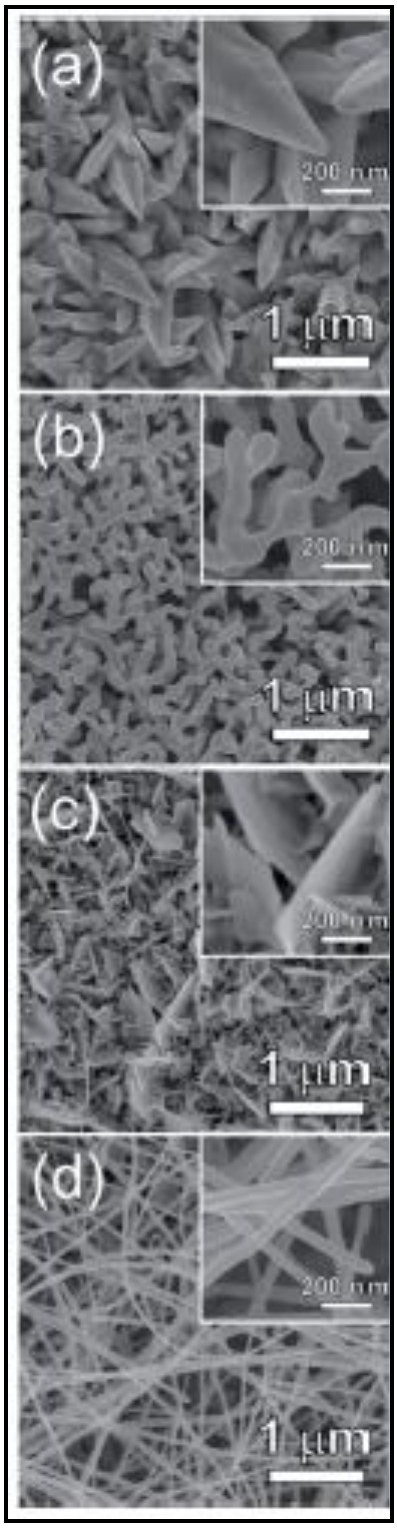

Figure 2: a.) Nanothorns **b.)** Nanocorals **c.)** Nanoslices **d.)** Nanowires

Reproduced from Ref. 9 with permission from The Royal Society of Chemistry

Hsu et al prepared gold nanostructures on flexible PET substrates. A thin gold film along with a Ti film was grown onto the PET substrate by e-gun evaporation.[12] The flat gold electrode acts as the seeding layer and using the technique of electrodeposition, the gold nanostructures were grown on the substrate.[12]

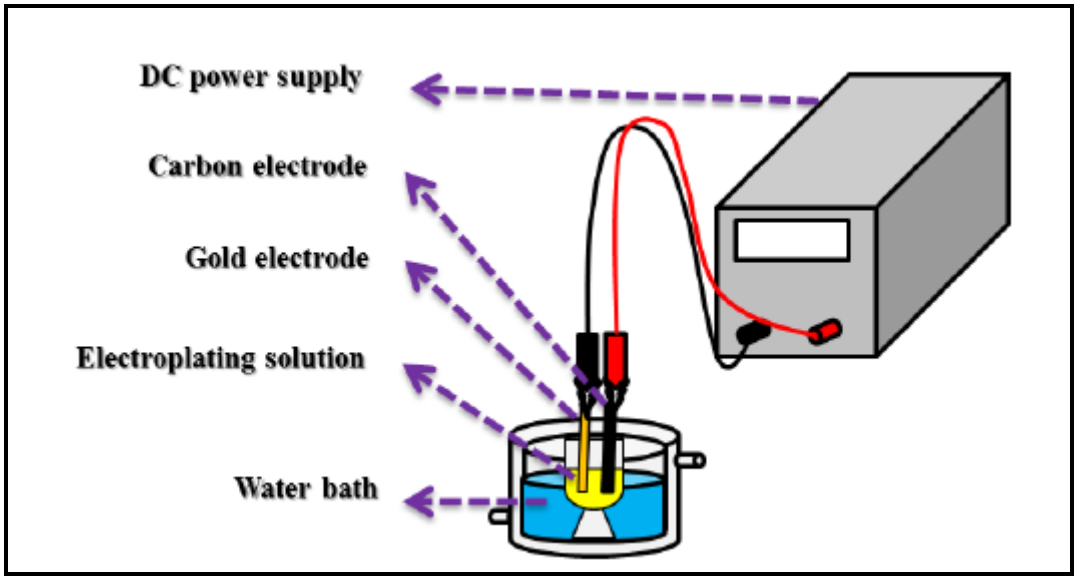

Figure 3: Two-electrode cell used by Hsu et al. for electrodeposition

Reprinted from Ref. 12 with permission from American Chemical Society. Copyright 2012 American Chemical Society

They modified the electrodeposition parameters to get different gold nanostructures.[12] Jia and co-workers investigated an electrodeposition method where Zinc was electrodeposited on the gold substrate using an electrolyte composed of anhydrous $ZnCl_2$ and benzyl alcohol at 60^0C.[13] They scanned the potential cathodically and Zn was electrodeposited on the substrate which then formed an alloy with gold at a high temperature.[13] When they reversed the potential i.e. performed the anodic scan, the electrodeposited Zn was electrochemically dealloyed forming a nanoporous gold film.[13] In the second cathodic potential scan Zn was electrochemically deposited again and reversing the potential scan initiates dealloying for the second time.[13] After

performing these four steps, the authors were able to obtain a perfect nanoporous gold electrode.[13] For the process of electrodeposition, a three-electrode cell was used with Zn plate as the counter electrode and gold wire as the working electrode.[13]

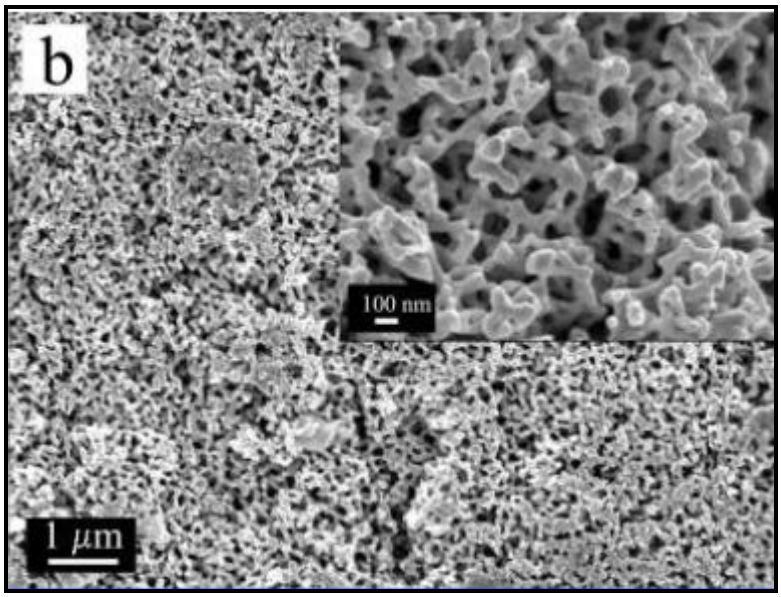

Figure 4: Field-emission SEM images of Nanoporous Gold at 120^0C

Reprinted with permission from Ref. 13. Copyright 2007 American Chemical Society

In order to obtain completely hollow gold microtubules, Brumlik et al. used flow assisted electroplating technique.[14] The flow assisted electrolysis apparatus is shown in Figure 5 below.

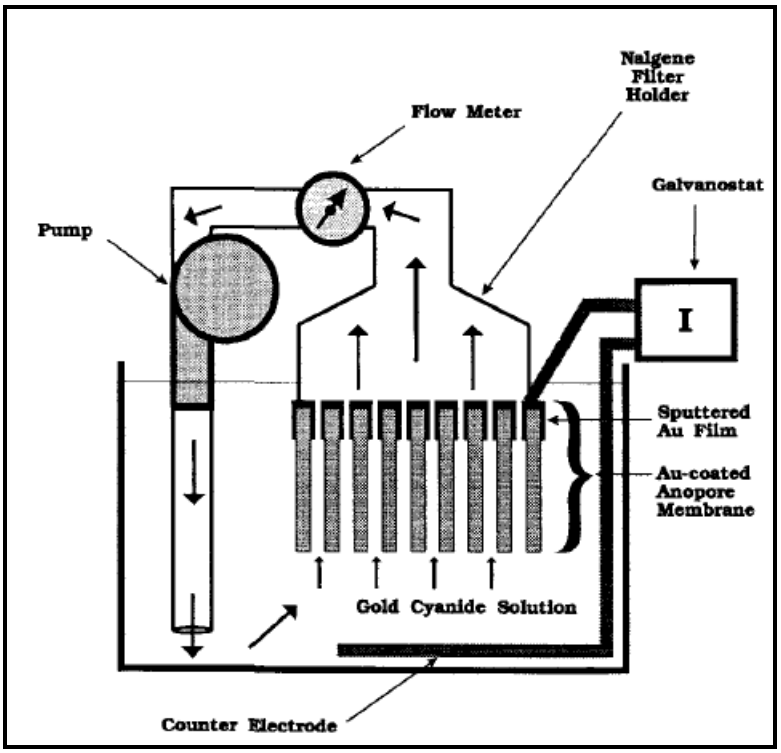

Figure 5: Flow assisted electroplating.

Reproduced from Ref. 14 with Permission from Cambridge University Press

The microtubules were sputtered with a thin film of gold as so that the microtubule ensemble can be used as a cathode in the electroplating cell.[14] The microtubule ensemble was immersed in the gold cyanide solution and a high area platinum mesh electrode was used as the counter electrode.[14] The gold electroplating solution was pumped through the membrane with the help of the peristaltic pump at the flow rate of 5-100 mL/ min.[14] Pressure was carefully monitored during the entire process. Mounting pressure indicated increasing thickness of the microtubules[14]. The template was later dissolved in hydrofluoric acid to obtain the microtubules.[14]

The beauty of the electrodeposition process is that it can be easily controlled. Controlling the parameters like the alloy composition, applied voltage and deposition time helps fabricate desirable porous films. Jia et al. successfully prepared nanoporous films of copper, silver and

gold using electrodeposition. They used zinc as a template to deposit the other metals and chemically dealloyed zinc at a later stage to obtain porous films.[15] The zinc deposition was carried out in a three electrode electrochemical cell consisting of Zn plate as the counter electrode, saturated calomel electrode (SCE) as the reference and the foil of the chosen metal substrate as the working electrode.[15] Holding the current density at 20 mA/cm^2, zinc was deposited on the foil.[15] The thickness of the deposition was controlled by monitoring the deposition time.[15] The deposited foil was exposed to thermal treatment to help form the zinc-metal alloy.[15] After the thermal treatment, the foil was immersed in a suitable electrolyte to etch out zinc and obtain a porous metal film.[15]

b.) Electroless metal deposition:

Electroless deposition has an advantage over the traditional electrochemical deposition in that the non conductive surfaces can be easily plated with the metal of choice.[11] The surface to be coated is selected and a catalyst is used to speed up the metal ion reduction process[11]. Electroless deposition is considered a cheap and a relatively easy technique that helps to uniformly coat a substrate of any geometry.[16] Electroless methods are described as being universally applicable and not confined to a particular kind of substrate surface.[17] Moreover, surface roughness can be varied by modifying the deposition time and the type of precursor used.[17] It works with most, if not all, metals.[17] Menon et al. implemented electroless deposition by using a chemical reducing agent to deposit metal. They used a “sensitizer” (in their case, Sn^{2+}) to modify the surface and later immersed it into a solution of $AgNO_3$.[11] A redox reaction is initiated which results in reduction of silver on the surface[11]. The silver-coated surface is then immersed in a gold plating bath so that gold particles may replace the silver ones as gold is a more noble metal.[11] Similar procedure of electroless deposition was used by Delvaux and Demoustier-Champagne to fabricate nanotubes arrays.[18] Zhang et al. added the gold nanoparticle hydrosol to the template solution and extracted the Au coated template. They later

added hydroxylamine hydrochloride as the reducing agent and $HAuCl_4$ to the gold-coated template.[19] The reducing agent reduces the gold onto the surface of the template[19]. Ding and Erlebacher introduced a novel method to confine the coating of the metal within the porous structure called the "gas-phase electroless plating technique".[20] Using the fact that the nanoporous gold (NPG) leaf floats on the water surface, they floated it on the plating solution free of any reducing agent.[20] Reducing agent in the vapor form (hydrazine, in this case) was floated onto the NPG leaf.[20] The reaction that followed helped coat the metal (silver) only on the inside of the porous structure and the reaction stops as soon as the pores are clogged with the metal.[20] Lang et al. used hydrazine in gaseous form to reduce MnO_2 within the pores of nanoporous gold by floating the NPG leaf on $KMnO_4$ and KOH.[21] Electroless ways like hydrothermal and solvothermal techniques to deposit platinum have been explored.[22] Hydrothermal methods use aqueous solvents for the reaction that is carried out in high temperature and pressure conditions.[22] Solvothermal methods use non aqueous solvents and the main difference between the two methods lies in the use of a different platinum precursor[22]. Both methods are similar in few aspects in that they: are carried out in closed containers such as autoclaves in steel vessels, are economical and do not require templates and surfactants.[22]

c.) Pulsed Laser deposition:

Quite a few research papers have been dedicated to the preparation of porous thin films using electroless deposition. Pulsed laser deposition (PLD) is one of these methods. PLD is carried out in vacuum. Figure 6 below shows the schematic diagram of the apparatus.[23]

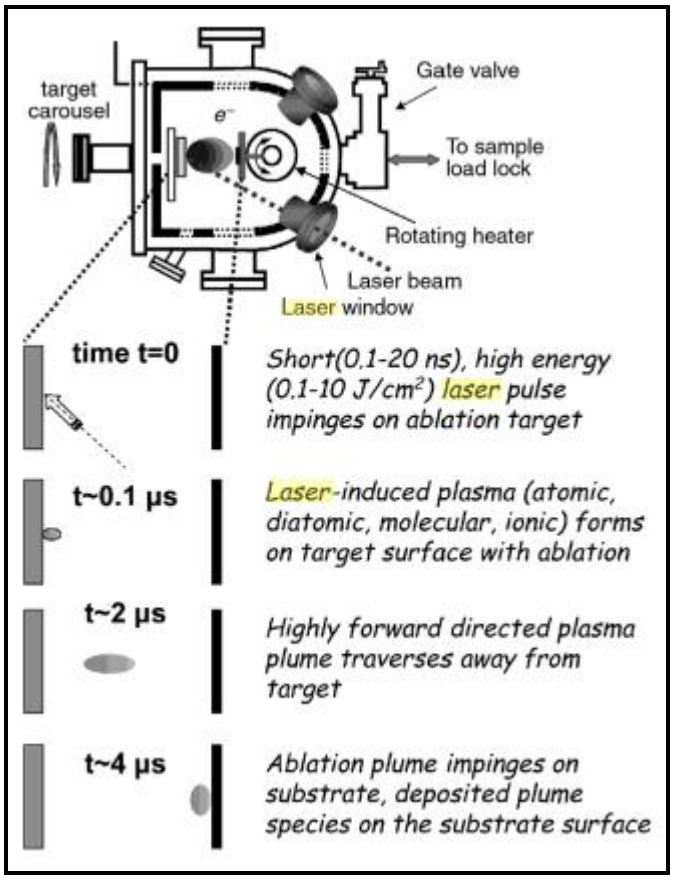

Figure 6: Schematic diagram of Pulsed Laser Deposition (PLD) apparatus.

Reproduced from Ref. 23 with permission from John Wiley and Sons

The material of choice is used as a target and a high energy laser beam is directed onto it in order to “ablate” or vaporize the material. The vaporized material turns into a “plasma plume” and is ejected onto another substrate and forms a thin film.[23] The vaporization conditions can be altered depending upon the material to be ablated.[23] Inorganic, organic and polymeric films have been prepared using this technique.[23] Navasery and co-workers used the PLD technique to produce porous $La_{0.7}Na_{0.3}MnO_3$ thin porous films on different kinds of substrates such as MgO, Si and glass substrates.[24] They used Ng-YAG laser to deposit the films at a wavelength of 500 nm.[24] The deposition was carried out in an oxygen atmosphere under the pressure of 12 mTorr.[24] The substrates were cleaned and heated to 750^0C prior to deposition.[24] Vinodkumar et

al. used Nd:YAG laser at a frequency of 532 nm with a pulse width of 7 ns to deposit porous ZnO films.[25] They used a repetition frequency of 10 Hz. Pure ZnO pellets were used a target for pulsed laser ablation.[25] The procedure of deposition was carried out under oxygen at 0.02 mbar pressure and deposition was performed on a quartz substrate.[25] The distance between the target and the substrate was 6 cm and the deposition time was 30 minutes.[25] Sun et al. demonstrated the use of a krypton fluoride (KrF) laser to prepare a porous, thin ZnO film[26], while Chen et al. used the PLD technique to obtain a conductive La-Sr-Co-O film[27]. Pulsed laser deposition has many advantages over other commonly used deposition methods: control over the crystalline state of the material being deposited, successful use of the procedure under a variety of environments, avoids interference of contaminants, variety of materials that can be used as a target such as superconductors, insulators etc. and easily modifiable parameters such as types of targets, distance between the target and the substrate, laser energy and oxygen pressure.[25]

d.) Alloying/Dealloying

It is also possible to fabricate porous metal films without using templates. A most widely used method is to prepare alloys and then etch out the less noble metal which results in the formation of pores. A wide variety of metals such as gold, silver, platinum, copper, zinc etc. have been used as binary and ternary alloys to form porous metals films. Xu et al. used platinum as one of the metals to prepare nanoporous electrodes as it is characterized by its noble nature, high electrocatalytic activity and the ability to be easily functionalized.[28] They prepared a bimetallic nanoporous structure by a “galvanic replacement reaction”.[28] The procedure included using commercial silver-aluminium and copper-aluminium alloy foils and dealloying them in NaOH to remove aluminium[28]. As a result, nanoporous silver and copper structures were obtained. These structures were then added to H_2PtCl_6.[28] They explain that “etch pits” form on the nanoporous silver and copper surface and when added to H_2PtCl_6, the silver and copper from inside the

ligaments is etched out and platinum is plated on top forming silver-platinum and copper-platinum alloy structures.[28] The morphology depends on temperature, concentration of the H_2PtCl_6.[28] Aburada and co workers used a ternary alloy for the preparation of nanoporous copper.[29] They also demonstrated the changes brought about by the addition of nickel to the nanoporous structure.[29] They used amorphous spun ribbons, $Al_{70}Cu_{18}Mg_{12}$ and $(Al_{75}Cu_{17}Mg_8)_{97}Ni_3$ atomic percent.[29] The ribbons were chemically dealloyed in 1M HCl to etch Al and Mg, keeping Ni and Cu intact.[29] They proved that the presence of Ni produced a nanoporous Cu with a finer structure than the one obtained without Ni[29]. This observation is based on the fact that addition of Ni lowers the surface diffusion of Cu atoms thus inhibiting the growth of nanoporous structure.[29] Liu et al. used a binary alloy Al-Cu to produce nanoporous copper.[30] The Al-Cu ribbons of different compositions were prepared and etched in an alkaline media (10 wt % aqueous solution) and Al atoms were removed.[30] They studied the two different phases of the alloy Al_2Cu and AlCu and proved that the composition of the alloy influences the phases, the dealloying mechanism of the alloy and the nature of the nanoporous structure.[30] Using the similar principle of etching the less noble element, Zhao et al. prepared nanoporous copper from Mg-Cu ribbons of different compositions by dealloying in 5 wt. % HCl.[31] Zhang and co workers used Al-Au ribbons of varying atomic percent compositions and dealloyed them in an alkaline medium such as 20 wt % NaOH as well as acidic medium such as 5 wt % HCl.[32] In another paper, these researchers used Al-Au ribbons of similar compositions and etched them electrochemically at 1.5 V to obtain nanoporous gold ribbons with alloy ribbon as anode, graphite as cathode and NaOH as the electrolyte.[33] Similar examples are those of the Al-Pd alloy ribbon etched in NaOH to leach the aluminium[34] and the Co-Pd alloy electrochemically etched in 0.1 M sulfuric acid at 0.5 V.[35]

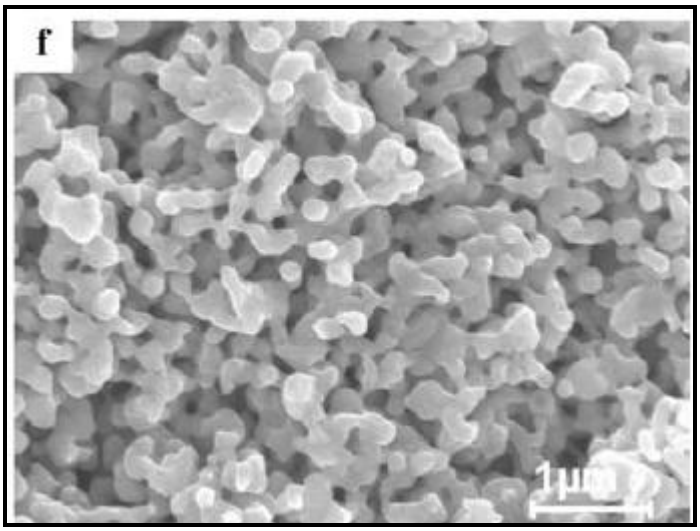

Figure 7: Nanoporous copper formed after dealloying of $Mg_{50}Cu_{50}$ ribbon

Reproduced from Ref. 31 with permission from Elsevier

1.2 Fabrication of porous metal electrodes using templates

Another popular method to fabricate porous metal films involves templating. The method includes deposition of the template on a substrate, deposition of the metal in/around the template and removal of template. The templates can be broken down into two broad categories: synthetic templates and natural templates. This part of the chapter aims at giving an idea of the wide variety of templates being used to obtain porous electrodes.

1.2.1 Synthetic Templates

Singh and coworkers used gold nanoparticles as a template to synthesize nanogels.[36] A shell of poly(N-isopropylacrylamide) (pNIPAm) was grown around the Au nanoparticles followed by the dissolution of the gold nanoparticles.[36] They used the phase transition quality of the pNIPAm to their advantage in that they increased the temperature above its lower critical solution temperature, thus making them hydrophobic.[36] They collapse and encapsulate the Au nanoparticles.[36] After dissolution of the Au nanoparticles, soft pNIPAm shells are obtained.[36] A

templating method that uses liquid crystals was introduced by Kresge et al.[37] They used aminosilicate gels as the template to form mesoporous solids.[37] Few groups used anodically oxidized aluminium as a template.[38],[39],[40] Zhao et al. sputtered silver onto the AAO film surface and removed the metal film by immersing it in NaOH.[39]

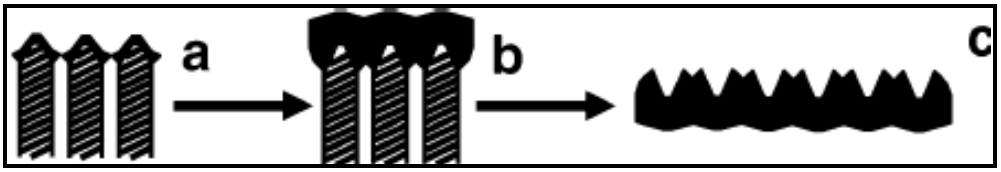

Figure 8: Schematic diagram of preparation of silver porous film using anodized aluminum as a template.

Reprinted from Ref. 39 with permission from American Chemical Society. Copyright 2006 American Chemical Society

Molares and co-workers prepared etched polycarbonate foils as templates to prepare copper nanowires[41] while Schonenberger et al. used commercial porous polycarbonate membranes to obtain nanowires of Ni, Cu, Au and Co.[42] They irradiated the polycarbonate foil with heavy ions such as gold and lead and they were then chemically etched in NaOH.[41] The diameter of the pores formed on the membrane increased with the etching time.[41] They then electrodeposited copper in the template and the copper wires were freed from the template by dissolving the foil in dichloromethane.[41] Many groups have succeeded in using other templates to prepare nano materials. Wu and Bein used mesoporous material as a template; they prepared carbon nanowires using channels of the mesoporous material MCM-41.[43] Carbon nanotubes, their use as a template and the principles behind filling the tubes with metals or their compounds to form nanostructured materials has been studied.[44] Hydrogen bubbles were used as a template to deposit copper and then galvanostatically replace it with gold.[45]

1.2.2 Natural Templates

Many groups have investigated the performance of biological entities as templates. Among many, Tobacco Mosaic Virus (TMV) is quite widely studied.[46],[47],[48] Many groups have explored a wide range of biotemplating methods such as use of *Bacillus subtilis* to prepare nanostructured silica materials[49], two kinds of wood were used to fabricate a porous ZnO film[50], sea urchins or echinoids used to prepare porous gold[51], outer egg shell membrane used to prepare TiO_2 tubes[52], use of pollen grains to form porous particles of inorganic materials.[53] The disadvantage of biotemplating is that there is no control on the dimension of the pores since the biological organisms/entities determine it.[6]

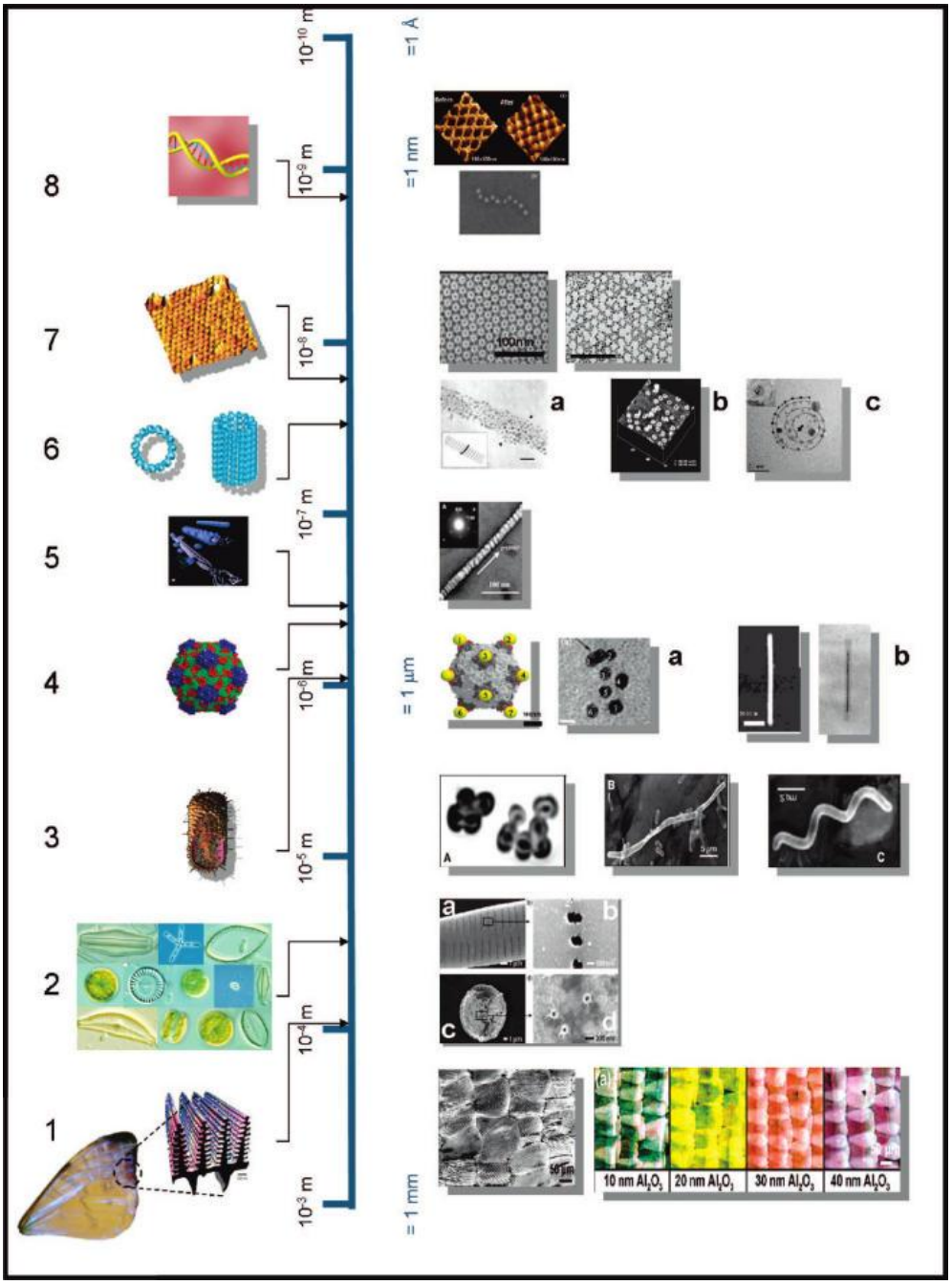

Figure 9: Examples of biological templates and their corresponding structures.[54]

1.2.3 Use of polystyrene spheres (PS) as templates

Polystyrene spheres (PS) or colloidal crystals have been widely used to manufacture porous metal films. They are a type of synthetic templates but because of their extensive use, this sub chapter has been dedicated only for PS spheres and their use as templates. The following sub chapters will explain in depth the different methods of fabrication and the deposition of these crystals.

Colloidal crystals, as the name suggests, are the colloidal particles that can be deposited in an ordered arrangement to obtain an ordered porous structure. The pore size of the structure can be controlled by tuning the diameter of the polystyrene spheres to the desired size. One of the simplest and the most time saving method of deposition was introduced by Bartlett et al. in 2000.[55] They used commercially available polystyrene spheres and deposited them on the substrate by the evaporation method.[55] They deposited the metal around the crystals by applying the appropriate voltage and filled the interstices of the spheres with metal.[55] Upon removal of the spheres in toluene, a metal mesh was obtained.[55]

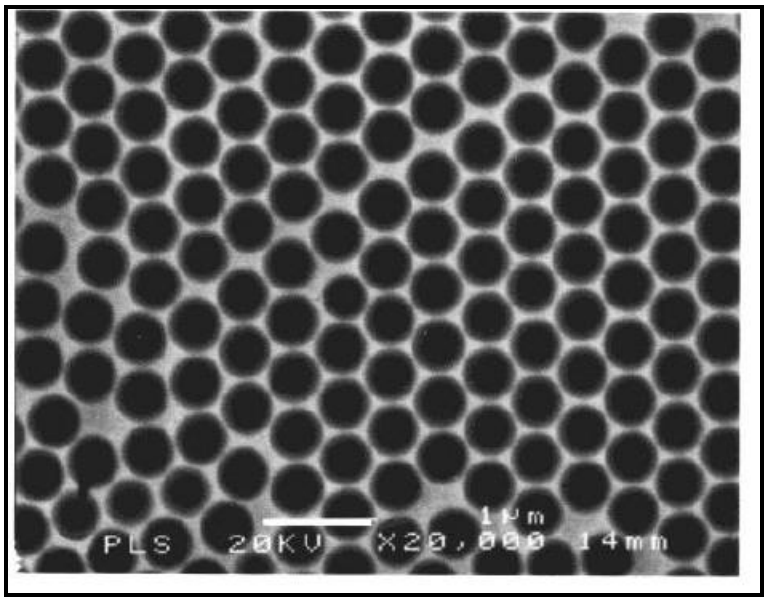

Figure 10: Macroporous gold electrode prepared using polystyrene spheres

In yet another paper, Bartlett and co workers list the advantages of the polystyrene spheres as templates that make them an attractive choice as a template.[56] During electrodeposition the metal being deposited is high in density in the interstices of the spheres than the surface around the spheres.[56] This avoids any volume shrinkage after removal of the template and no steps like annealing are needed to remedy the shrinkage.[56] Both aqueous and non-aqueous solutions can be used for electrodeposition without affecting the template.[56] The surface topography can be changed with the deposition and the deposition bath conditions.[56] The metal film obtained under these conditions is very uniform and hence has applications as photonic mirror.[56] Chen et al. combined polystyrene spheres and electroless deposition to obtain hollow silver spheres.[57] The colloidal crystals were deposited in a microchannel and the channel was immersed in the silver plating solution.[57] The silver ions were reduced to Ag and deposited on the surface of the beads.[57] The reducing agent in the plating solution continued to reduce the silver ions and

deposit it on the surface of the spheres.[57] The thickness of the silver shell can be controlled by modifying the immersion time of the crystals in the plating bath.[57] Removal of these spheres would give hollow silver spheres.[57] Functionalization of the colloidal crystals or the latex beads was studied in order to uniformly deposit different metal particles on the surface of the bead.[58] The paper describes functionalizing the PS spheres with amine or carboxylic groups, treating these charged spheres with a polyelectrolyte of opposite charge facilitating adhesion of the metal colloids on the surface of these spheres.[58] The researchers carried out the successful adsorption of the metal colloids on the neutral PS bead surface.[58] They established yet another way to deposit metal colloids on the PS surface which was to deposit a precursor hydroxide or metal oxide on the PS surface which will reduce to deposit metal particles on the surface of the PS bead.[58] Yan and co workers used poly-(methyl methacrylate) (PMMA) beads instead of regular polystyrene beads on account of PMMA having better wettability than PS.[59] Better wettability ensures better penetration of the metal solutions and hence less structural defects.[59] Salt of the desired metal was dissolved in ethanol or methanol and colloidal PMMA crystals were soaked in it and later dried.[59] The dried assembly was then soaked in oxalic acid in order to form metal oxalate and 3D macroporous materials were obtained after calcinations.[59] One research group synthesized carbonaceous polysaccharide microspheres and used them as templates to prepare Ga_2O_3 and GaN hollow spheres.[60] Porous carbons were prepared using silica opal crystals[61], semiconductors were electrodeposited in the spaces between colloidal crystals[62], and zeolitic microporous frameworks were prepared using PS spheres as the templates.[63] The short review of the research on the use of colloidal crystals as templates makes it clear that the colloidal crystals are compatible with a wide range of materials, different metal deposition techniques and the fabrication procedure is relatively hassle free.

1.2.3 Applications of colloidal crystals

Other than the obvious use as templates, colloidal crystals have other potential applications such as photonic crystals that increase the efficiency of light emitting diodes, for surface processing of metals, and catalysis.[64]

The macroporous or mesoporous materials prepared using colloidal crystal templating technique have applications in catalysis, separation, sensing and optics.[65] The dielectric 3 dimensional macroporous materials can be used in photonic crystals, measuring stop band position and intensity, tuning the photonic bandgaps using birefringent liquid crystals, as substrates in surface enhanced Raman scattering (SERS).[65]

1.3 Summary of Research

This sub chapter is designed to give a gist of the research carried out in our lab. We aimed at preparing high surface area gold electrodes because of their higher sensitivity, lower detection limit, and higher current and, of course, higher surface area as compared to the flat gold electrodes. We proceeded to do so by using a templated and non-templated approach. Macroporous and Macro-nanoporous electrodes were prepared via electrodeposition using 1200 nm polystyrene sphere (PS) templates. The templates were deposited on the gold-coated glass substrate using the evaporation method described by Vogel et al. and gold or gold-silver alloy was deposited in the interstices by applying appropriate electric potential. While macroporous gold was fabricated from a deposition solution containing gold ions, macro-nanoporous were obtained by electrodepositing a gold-silver alloy solution and later, by etching out the silver by chemical dealloying. Nanoporous gold electrode was fabricated by electrodepositing the gold-silver alloy solution on a flat gold surface without the assistance of a template and then silver was etched out chemically to give nanopores. To obtain a clear idea of their morphology and chemical composition, they were characterized by Scanning Electron

Microscope (SEM), Energy Dispersive Spectroscopy (EDS) and in case of macroporous gold electrode, a Nikon Digital Microscope. The performance of these electrodes was compared to that of flat gold electrodes which included the measurement of their surface area, non faradaic current and faradaic current from the reduction-oxidation of specific redox probes. These electrodes were used to detect biomarkers like dopamine and ascorbic acid and the superior performance of the high surface area gold electrodes (compared to the flat gold electrode) observed underlines their potential as biosensors. Subsequent chapters will explain the fabrication and characterization procedures in detail.

1.4 Characterization Methods of High Surface Area Porous Metal Films

The morphology and the porosity of the high surface area gold electrodes were investigated using a Scanning Electron Microscope (SEM) and their chemical composition was determined using Energy Dispersive Spectroscopy (EDS). Their behavior and performance was compared to the flat gold electrode using electrochemical techniques like Cyclic Voltammetry (CV) and amperometry.

1.4.1 Scanning Electron Microscopy

Images obtained using a scanning electron microscope involve a high energy electron beam scanning the surface of the sample. The interactions between the electron beam and the sample surface helps obtain information about the morphology and the topography of the sample. The gun generates an electron beam at an energy level of 0.1 to 3 keV and the accelerated electrons hit the sample surface.[66] Various parameters of the electron gun can be adjusted according to the sample in question: current, spot size and energy dispersion. Tungsten electron guns are most widely used in SEMs today as they are able to produce high current and low energy dispersion.[66] An electron gun consists of a tungsten hairpin filament that acts as the cathode and an anode.[66] The tungsten filament is heated up to a temperature of

about 2,800 K by applying a current and electrons are generated which accelerate toward the anode.[66] Electromagnetic condenser lenses help focus the electron beam to a spot on the sample surface.[67] The electron beam bombards the sample and the electrons penetrate the surface up to about 100 nm to 5 micron deep.

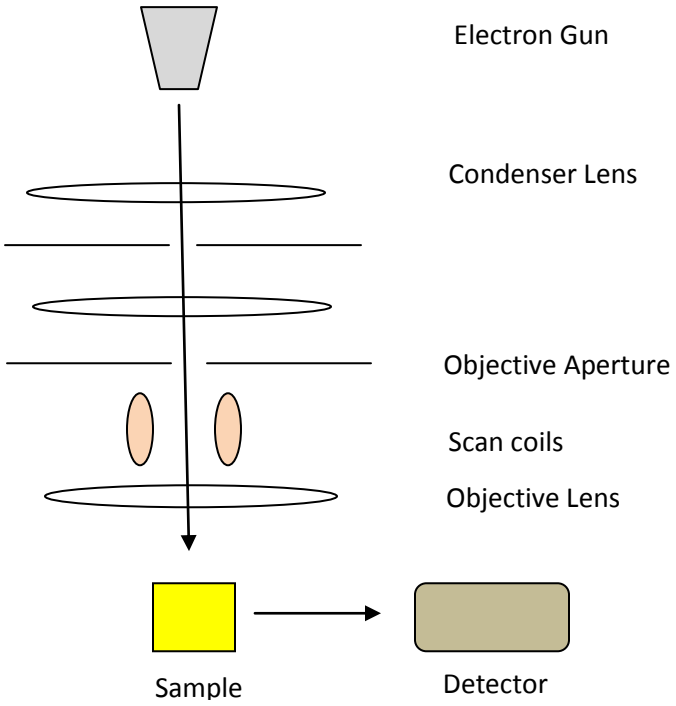

Figure 11: Schematic diagram of a SEM[67]

Two kinds of interactions occur once the electrons hit the sample: elastic and inelastic scattering.[66] These interactions produce three different kinds of electrons: secondary electrons, backscattered electrons and X-ray photons.[67] In case of an inelastic scattering, the energy of the primary electron collides with the atomic electron and transfers its energy to it, thus resulting in its emission.[67] Such an electron, with energy less than 50 eV, is called a secondary electron.[67] The secondary electrons provide information about the morphology of the sample.[67] In case of inelastic interactions, the primary electron collides with the atomic electron and backscatters without transferring its energy to the atomic electron.[67] These scattered electrons

are called backscattered electrons which are responsible for the contrasts in composition.[67] The backscattered signal provides information about the elemental composition of the sample and the X-rays produced during inelastic collision are characteristic of the elements present in the sample.[67]

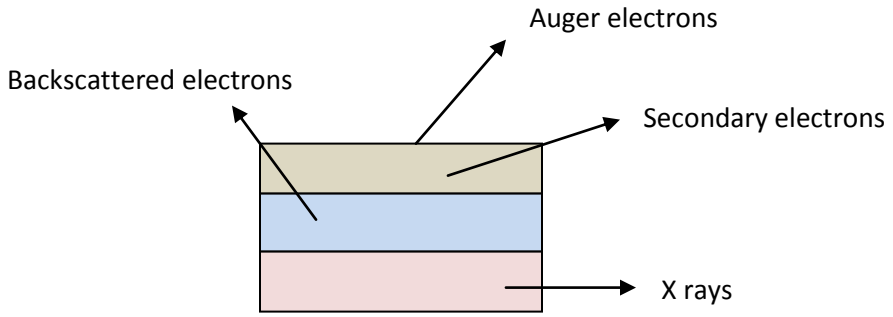

Figure 12: Different species obtained after incidence of the primary beam on the sample surface[66]

The characteristic X-rays produced by the sample can be analyzed by coupling EDS with SEM for elemental analysis. The advantage of SEM is that it's a non destructive technique and hence the samples stay intact. In order to be used for imaging the samples have to electronically conducting. Hence, metal samples – in our case, gold electrodes – were used as is, whereas the polystyrene spheres coated surfaces were sputtered prior to imaging.

1.4.2 Energy Dispersive Spectroscopy

X-rays are photons with an energy range of 10 eV to 100 keV.[68] A primary electron beam emitted by the cathode excites the atomic electrons which make them leap to higher energy states. The excited atoms lose energy in the form of X-rays and fall back to the ground state. The amount of energy released is equal to the energy difference between the two shells.[69] These emitted X-rays are characteristic of the atom that generated them. These X-rays are analyzed by the energy dispersive spectrometer and elemental composition of the sample is

determined. Different energy shells are represented as K, L, M etc. and the emitted X-ray represents the energy shell from which it was emitted.[69] This hole formed in the energy shell after excitation of the electron is filled by an electron from a higher shell.[69] K shell is the closest to the nucleus, L shell (n = 2) is higher in energy as compared to K, M is higher in energy than L and so on[67]. The spectral lines are named as $K\alpha_1$, $K\alpha_2$, $K\beta_1$, $K\beta_2$, $L\alpha_1$ etc. α and β indicate the sub shells and the number indicates the intensity of the sub shell. The EDS is made of a silicon crystal diode with lithium atoms diffused (p-i-n diode).[69] EDS involves an X-ray tube which is an evacuated glass tube which encloses the cathode and anode.[67] The generated X-rays pass through the beryllium window and are of two types: white radiation and discontinuous spectrum.[67] The lithium diffused detector measures the kinetic energy of the X-ray photon.[67] The spectrum is recorded as the intensity versus energy of the X-rays.

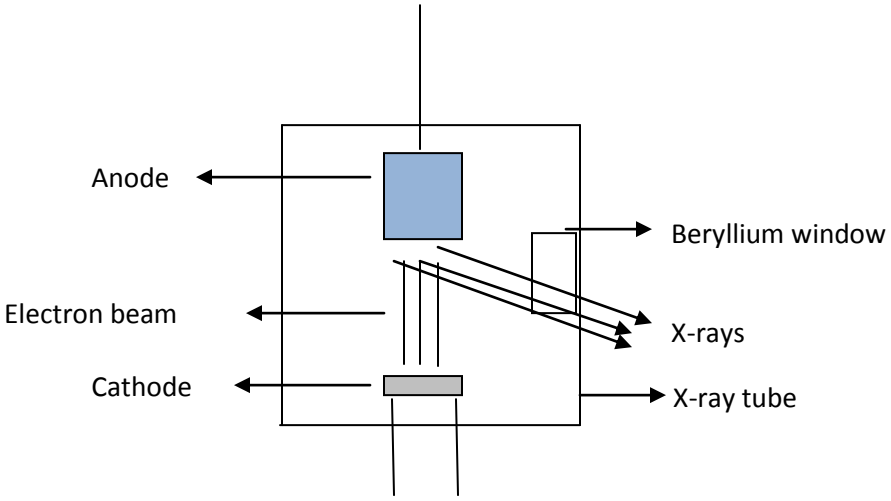

Figure 13: X-ray Tube[67]

1.4.3 Cyclic Voltammetry

Cyclic Voltammmetry is a widely used electrochemical technique that involves measuring the current as the potential is changed linearly with time. It is widely used to study a compound or an electrode surface.[70] To run a cyclic voltammetric experiment, usually a three electrode cell is used that consists of a reference electrode such as silver chloride (Ag/AgCl), a counter electrode such as a platinum wire and a working electrode which in our case is a gold electrode. Depending on the redox molecule being used the potential limits are set such that the reduction and oxidation of the redox molecule occurs between the two switching potentials. When the potential is applied between the reference electrode and the working electrode and is scanned from the more negative end to the more positive end, oxidation occurs and the current recorded is the anodic current. When the scan is reversed and the potential is scanned from the more positive end to the more negative end cathodic current is recorded. It must be noted that oxidation and reduction are not dependent on the negative or positive potential. Oxidations can occur at a negative potential and reduction can occur at a positive potential.

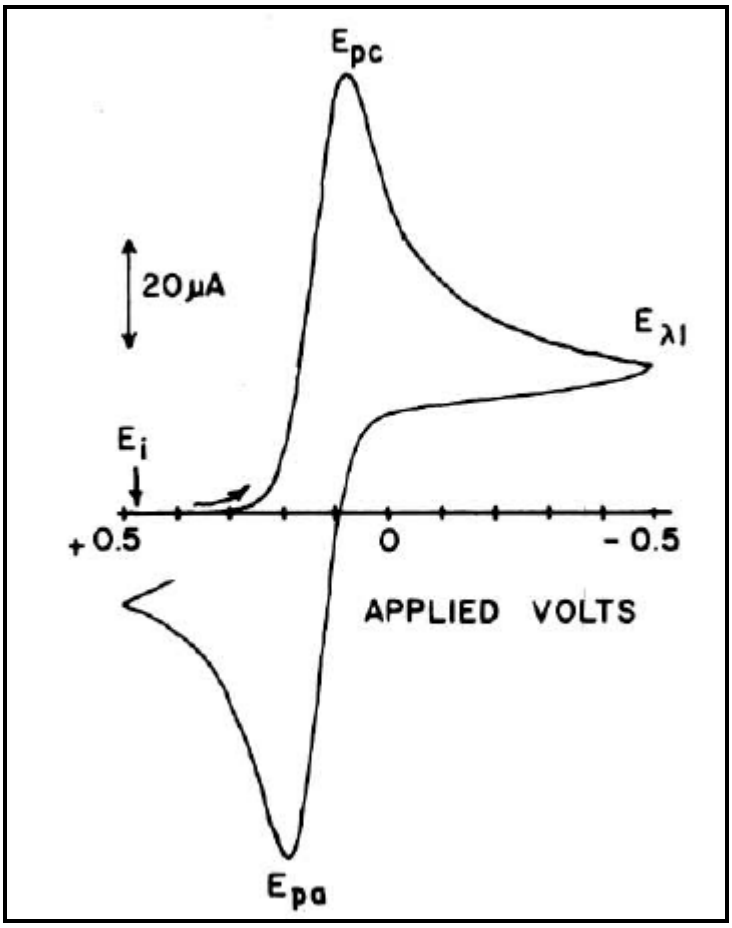

Figure 14: Cyclic Voltammogram (CV)[71]

Figure 14 above shows a typical cyclic voltammogram of a reversible redox couple in solution. When the potential is scanned from -0.5 V to +0.5 V, oxidation of the electroactive species occurs. If we just consider the forward scan where the potential scans from negative to positive the electroactive species (R) closest to the surface of the electrode oxidizes to form O species thus forming a depletion layer. The electroactive species must diffuse across this depletion layer to reach the electrode surface.[72] The rate of oxidation slowly increases giving an anodic peak which is indicated as Epa in the above figure. When the potential is reversed the oxidized species O at the electrode surface is slowly reduced to species R. The diffusion controlled current slowly increases until we get a cathodic peak indicated as Epc. The rate of diffusion of O

to the electrode surface and the current is limited hence giving a low current. The rate of scanning can be controlled as desired.

1.6 Applications of porous materials

As mentioned before, porous films exhibit higher surface areas, higher signals and higher sensitivities making them potential candidates for biosensors. This part of the chapter gives a brief overview of the applications of the metal porous films, but with a focus on the biosensing applications. Lee and Park prepared the macroporous binary alloy electrode in order to detect cholesterol.[73] Au nanoparticles were aggregated to form coral like structures and the surface was roughened by further deposition of platinum nanoparticles using the electroplating technique.[73] The large gold macropores not only enhance the surface area but also allow the redox molecules access. The platinum nanoparticles increase the catalytic activity of the electrode.[73] Cyclic voltammograms (CVs) were run in varying concentrations of cholesterol and an increase in the response current was observed at 0.3 and 0.2 V.[73] The current response increased with the concentration of cholesterol.[73] Figure 15 below shows the CV response to increasing concentrations to cholesterol.[73]

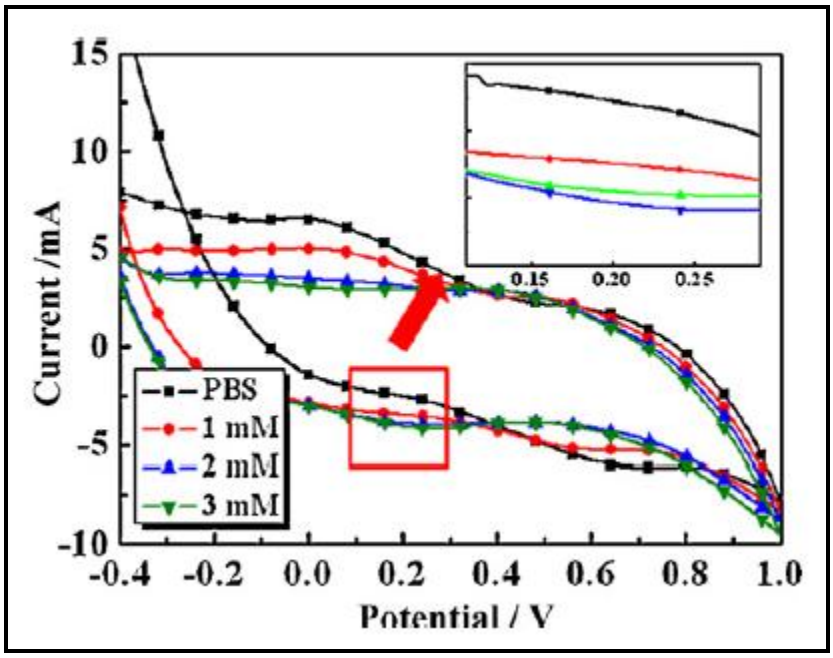

Figure 15: Cyclic voltammograms (CVs) of macroporous Au/n-Pt in varying concentrations of cholesterol

Reproduced from Ref. 73 with permission from Elsevier

Based on the CV data, an amperometric response of the macroporous Au/np-Pt to the cholesterol was recorded that is shown below in Figure 8.[73] With each addition of increasing concentration of cholesterol at regular intervals, the current showed an increase.[73] Moreover, additions of uric acid (UA), ascorbic acid (AA) and acetaminophen (AP) did not interfere with the amperometric response.[73]

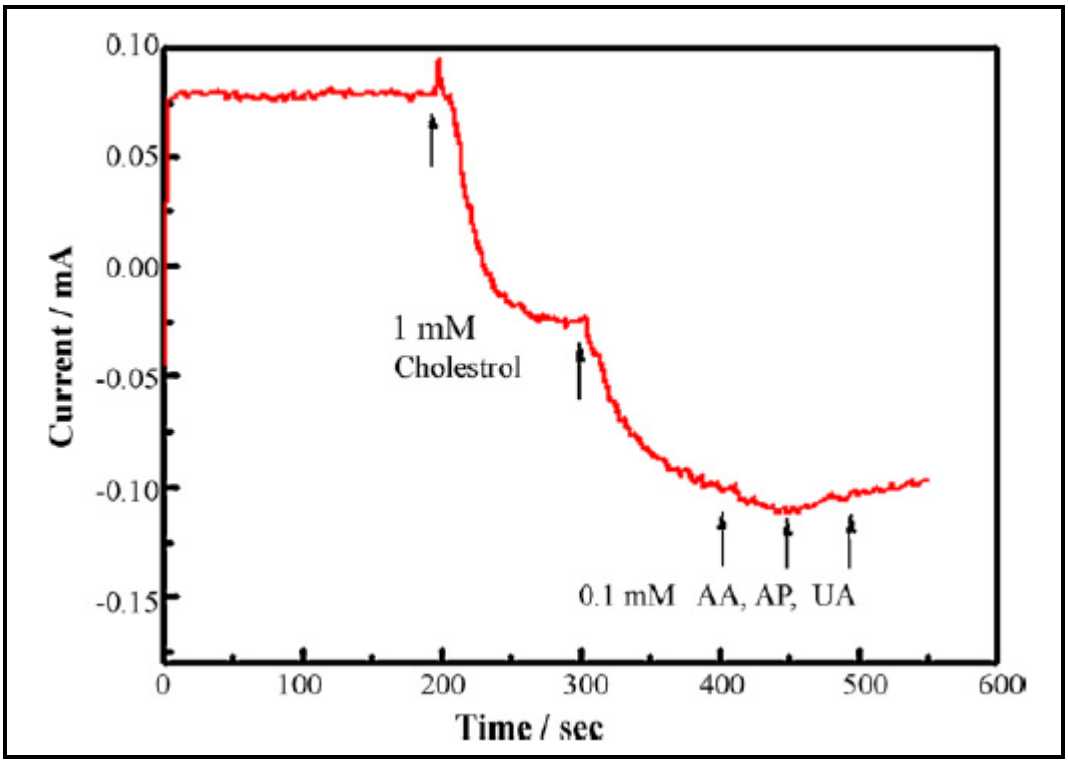

Figure 16: Amperometric response of macroporous Au/np-Pt to cholesterol, AA, AP and UA Reproduced from Ref. 73 with permission from Elsevier

El-Said et al. electrochemically deposited a nanoporous gold film (NPGF) on a gold substrate and used the fabricated electrode to detect dopamine and ascorbic acid using differential pulse voltammetry (DPV).[74] Figure 17 below shows the DPV response to the mixture of dopamine and ascorbic acid.[74] The NPGF electrode showed pronounced oxidation peaks and a peak shift as compared to the flat gold electrode in response to these individual biomarkers and also their mixture.[74]

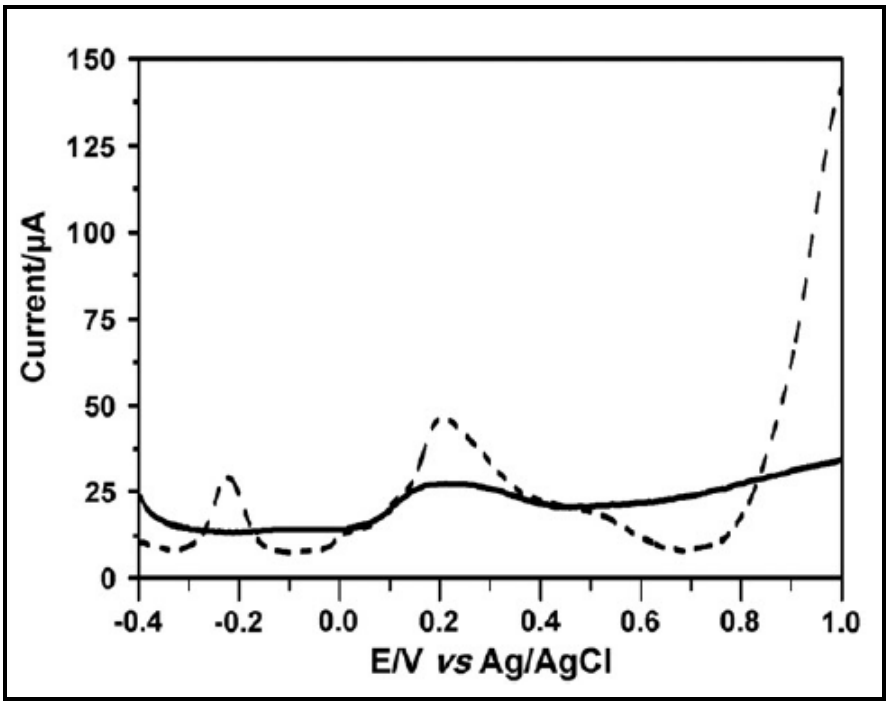

Figure 17: DPV Response of NPGF to the mixture of ascorbic acid and dopamine

Reproduced from Ref. 74 with permission from Elsevier

The dashed line in the figure 17 above is the NPGF electrode with its higher, sharper peaks as compared to the flat gold electrode (solid line).[74] The peak shift was explained on account of the electroactive species being trapped inside the pores and hence undergoing a fast electron transfer with the metal electrode and hence being oxidized at a reduced potential.[74] Ding et al. designed an electrochemical immunoassay of Hepatitis B antigen that involved nanoporous gold electrode and gold nanoparticles.[75] The electroactive product was formed and subsequently reduced and the peak current was measured to determine the concentration of antigen in the analyte.[75] Hsu et al. prepared gold nanowires, nanocorals and nanoslices and tested their response to dopamine.[12] A gold film electrode showed poorer results as compared to the nano electrodes; the dopamine reaction on the surface of the flat gold electrode was not reversible either unlike on the surface of the other nano electrodes.[12] They checked the nano electrodes

for fouling and proved that about 95% of the original current is measured with no degradation in their morphology.[12] The nano electrodes also showed that the additions of uric acid and ascorbic acid did not interfere with the dopamine measurements.[12] The nano electrodes showed higher current, better peak separation as compared to the gold film electrode owing to their higher surface area and more number of active sites on the surface.[12]

Human serum Chorionic Gonadotropin (hCG) is a biosensor for ovarian and testicular cancer.[76] Li et al. developed an amperometric sensor to detect the level of hCG using nanoporous gold (NPG) foils and graphene sheets (GS) that have high surface areas.[76] They modified the glassy carbon electrode with NPG foils and GSs and incubated it in hCG solutions of varying concentrations[76]. The current response increases with the concentration of hCG.[76] They attributed the success of this label free sensor to the high surface area of graphene and the NPG foil acting as the immobilization matrix which increased the anti-hCG immobilization.[76] Liu and coworkers used nanoporous gold electrode for the detection of cysteine – another biomarker.[77] They used cyclic voltammetry and amerometric responses to prove the superiority of nanoporous gold electrode as biosensor compared to the flat gold electrode.[77] Qiu and co workers ran CVs to detect nicotinamide adenine dinucleotide (NADH); the excellent performance of the nanoporous gold electrodes was characterized by decrease in overpotential, higher current and lesser peak separation than the flat gold electrode.[78] They also recorded the amperometric responses toward hydrogen peroxide (H_2O_2) and glucose.[78] Use of nanoporous gold as catalyst for CO oxidation was studied by two groups[79],[80] while its use as a catalyst in the electrooxidation of methanol was also studied.[81] Gold is not only known to catalyze oxidation reactions at low temperatures but it is also a selective catalyst.[81] These properties make nanoporous gold an attractive choice as a catalyst in “green chemistry”.[81] Nanoporous gold was used as a glucose sensor[82] and as a catalyst in the aerobic oxidation of D-glucose to D-gluconic acid[83] opening the many possibilities of its use as a sensor in the medical field. Zeis and co-

workers prepared platinum plated nanoporous gold leaf electrode and used it as a catalyst in the proton exchange membrane (PEM) fuel cells.[84]

CHAPTER 2: USE OF POLYSTYRENE SPHERES AS TEMPLATES

Polystyrene spheres (PS) can be purchased commercially or synthesized in lab. We used commercial as well as synthesized spheres to fabricate macroporous and macro-nanoporous gold electrodes; however most of our work featured the ones we synthesized in lab. We used the synthesis method described by Telford et al. and synthesized 1200 nm carboxylic polystyrene spheres in lab. We used two methods to deposit the spheres on the gold slide: vertical evaporation method[5] and Langmuir-Blodgett deposition method.[85] Following sections describe the most commonly used methods of synthesis of different types of colloidal crystals, different methods of self assembly of the spheres and the methods we used in our lab.

2.1 Different Methods of Synthesis of Polystyrene Spheres

This part of the chapter deals with various synthesis strategies of colloidal spheres but with a focus on polystyrene spheres. Monomer, emulsifier and initiator are needed to synthesize the colloidal spheres.[86] The most commonly used method to synthesize polystyrene spheres (PS) is the "emulsion polymerization" method.[86] Zhang et al. described a one pot synthesis that included adding sodium lauryl sulfate (emulsifier) and potassium persulfate (initiator) to a flask followed by the addition of the monomer which is styrene (anti-polymerizer free).[86] Nitrogen was passed through the flask to remove oxygen and the emulsion was heated to 70^0 C to polymerize.[86] Another group used the same method except for different chemicals – 4,4' azobis 4-cyanovaleric acid as the polymerization initiator and polyvinyl pyrrolidone as the surfactant.[87] It was concluded from their research that varying the concentrations of surfactants and initiators changes the diameter of spheres.[87] Increasing surfactant concentration decreases the size and the same effect is observed when the initiator concentration is increased.[87] The spheres obtained from this process have a narrow size distribution.[87]

Reese and co workers suggested a slightly different method where they added water and sodium bicarbonate to the reaction container followed by addition of nitrogen treated Aerosol MA-80-1 (surfactant).[88] Deoxygenated and inhibitor-free monomers such as styrene and divinyl benzene was injected to the mixture in the container followed by injection of the ionic comonomer sodium 1-allyloxy-2-hydroxypropane sulfonate (COPS-1).[88] Changing the concentration of the aerosol influences the diameter of the PS particles.[88]

Silica colloids are just as widely used as the polystyrene spheres. Stöber et al. devised a strategy early on to prepare silica colloidal spheres.[89] The same strategy was and is adapted even today with small modifications in the procedure as necessary. Alcohol, alcoholic ammonia solution, ammonium hydroxide and water are added to a container followed by addition of tetraalkyl silicate.[89] Increasing opalescence indicated the initiation of the condensation reaction which later changed to a turbid white solution.[89] Usually the above described procedures give spherical sphere shaped colloidal crystals – be it polystyrene, silica or polymethyl acrylate (PMMA). In order to obtain hollow core and shell structure, various particles can be added to the container during the synthesis of these colloidal crystals.[90],[91] As a result, the silica or polystyrene is deposited on the particle forming just a shell. Processes like calcination or solvent extraction assist in the removal of cores giving mere shells of the colloidal crystals.[90] However, the success of preparing perfect hollow core-shell colloidal crystals largely depended on the proper ratio of reactants to the core particles.[91] Carbonaceous spheres are another type of colloidal spheres that are used. Sun and Li introduced the method and explained the mechanism of formation of the carbon spheres using glucose as the staring material.[92] Glucose was dissolved in deionised water and the resulting solution was sealed in autoclave for 4-20 hours at 160 to 180^0 C. Rinsing and oven drying at 80^0 C helped obtain the final products.[60] Sun and Li explain that the temperature of 160-180^0 C initiates “carbonization and aromatization”.[92] Nucleation takes place at the supersaturation and carbonization may occur due to cross linking

between the materials formed in the previous steps.[92] The newly formed nuclei grow and form the spheres. The diameter can be controlled by controlling the growth factors.[92] Antl et al. described the synthesis of poly(methyl methacrylate) spheres in non-aqueous media in 1986.[93] They added azo-bis-isobutyronitrile (ADIB), stabilizer and the monomer to a closed flask followed by the addition of hexane/high boiling hydrocarbon fraction and octyl mercaptan.[93] The flask was heated without stirring for two hours at 80^0 C.[93] Few groups slightly modified the procedure described by Antl and co workers and prepared non-aqueous fluorescent PMMA colloids.[94], [95], [96] Yamada and co workers modified the conventional method of preparing PS spheres by introducing a "soap-free emulsion polymerization method".[97] They added the monomer at multiple stages which helped the particles attain a bigger average diameter, added a pH buffer during synthesis to control the electric potential on the particle surface and stabilize them.[97] Gu et al. introduced a new synthetic method of preparing magnetic polymer particles by tailoring the conventional PS particles synthesis method.[98]

2.2 Different Methods to Prepare an Ordered Colloidal Crystal Packed Layer

Colloidal spheres can be easily assembled into an ordered array on any kind of substrate quite easily. This part of the chapter deals with the different methods employed by the researchers to form an ordered colloidal crystal layer.

Brinker and co workers explain precisely what an assembly of colloidal crystals is. They say – "…a spontaneous organization of materials through non covalent interactions (hydrogen bonding, Van der Waals forces, electrostatic forces, π-π interactions etc.) with no external intervention".[99] The colloidal crystals may be neutral, or may possess a positive or a negative surface charge. Denkov et al. explained the mechanism of formation of a 2D colloidal crystal assembly. They spread the latex solution on a hydrophilic glass substrate and covered it with a Teflon ring and let the aqueous solution evaporate giving an ordered layer.[100] Deckman and Dunsmuir prepared an ordered colloidal array of negatively charged polystyrene spheres on a

positively charged substrate.[101] They immersed an aluminum substrate into the negatively charged colloidal solution of pH 5.[101] There is electrostatic attraction between the polystyrene spheres and the substrate.[101] Excess or unbound spheres were rinsed off and the substrate was allowed to dry.[101] They also described another procedure – (spin coating) – to produce an ordered array.[101] A slow spin coating speed results in deposition of multilayers while a high one gives rise to gaps in the layering of colloids.[101] Few other groups also used spin coating to form an ordered colloidal layer on a flat substrate.[102], [103]

Sedimentation is another popular method used to prepare ordered arrays of colloidal spheres.[104],[105],[106] Park and co workers introduced a method that eliminated the drawbacks of sedimentation and electrostatic interaction methods.[107] Both these methods were time consuming and the method of electrostatic interaction, in particular, required monitoring of many parameters and precise experimental conditions.[107] Park et al. prepared an aqueous solution containing PS spheres and injected it into a cell.[107] Pressure was applied through the glass cell using nitrogen to force the PS solution to come out through the other end onto the top substrate.[107] Under sonication, the PS spheres assembled into an ordered array. The cell was placed into the oven to evaporate the solvent.[107] The top substrate was removed and an ordered array was obtained on the bottom substrate.[107] Adjusting the cell thickness can help attain the desired number of PS layers.[107] Controlling the nitrogen pressure can help control the rate of packing of the spheres.[107]

A similar procedure of templating involving microchannels was used to prepare macroporous membranes.[108],[109] Capillary forces were used to their advantage by Denkov et al.[110] They explained the formation of the self assembly in two main stages: 1.) Capillary forces helping the nucleus formation 2.) Crystal growth through convection after evaporation of water.[110] Other groups also used the capillary forces to form self assembled colloids.[111],[112],[113] This technique allows rapid formation of self assembled colloids on any substrate. Pieranski et

al. introduced a novel method which could be described as the “confinement” method between two repulsive boundaries.[114] They confined the colloidal spheres between two flat glass surface and a glass sphere.[114] They were able to obtain a very thin, 3D layer by this method.[114] Velev and co workers used the method of filtration to form ordered self assembly of colloids.[115] The PS solution was filtered through a 25 mm diameter polycarbonate membrane.[115] The membrane was mounted on a filter stand that had back pressure control.[115] The filtration was maintained by a back pressure of about 5 kPa.[115] After about 2-3 hours, the colloidal crystals accumulated on the membrane surface were ordered into a 3D array.[115] Holland et al. implemented a slightly modified procedure of filtration.[116] They deposited latex solution on the filter paper in Buchner funnel under vacuum and soaked the latex in ethanol.[116] Huang and co workers used the method of electrophoresis to deposit the spheres on an electrode surface.[117] The sphere suspension was prepared and its pH was adjusted.[117] The suspension was subjected to zeta potential measurement in order to deposit them electrophoretically on the surface.[117] The actual deposition involved two electrodes – one of which was Si.[117] The two electrodes had widely differing areas with the counter electrode having a higher surface area.[117] Voltage was applied for 0-2 hours and afterwards, the sample was left to dry.[117] Other research groups also successfully tried out electrophoretic deposition of colloidal crystals as this method improves the order of the colloidal crystal array.[118],[119],[120] Wijnhoven et al. managed to deposit colloidal crystals in flat, thin, long glass capillaries. They filled the capillaries with sphere solution and the spheres were sedimented and centrifuged for 2-48 hours.[121] Kim and co workers used a “confined convective assembly” where they held together two glass substrates with a gap in between of about 100 microns.[122] They immersed the glass substrates into the sphere solution and then gently removed the back glass substrate while blowing hot air at the same time in order to evaporate the solvent.[122] The lifting of the back glass substrate thinned the meniscus and affected the number of layers deposited and whether the assembly formed is 2D or 3D.[122] Ye et al. used the method of “vertical deposition” to form an ordered self assembly of colloidal

crystals.[123] They prepared the sphere solution in a vial and dipped a clean substrate into it.[123] They kept the vial in an oven in order to facilitate the evaporation of the solvent.[123] The drying process begins from the top and ordered layers of colloids on the substrate are obtained.[123] A method of dip coating was introduced by Lu and co workers which was easy and lithography-free and involved arranging the substrate in such a way so that the spheres are deposited in selective places.[124] Figure 18 below shows a summary of the different methods implemented to obtain a colloidal crystal.[125]

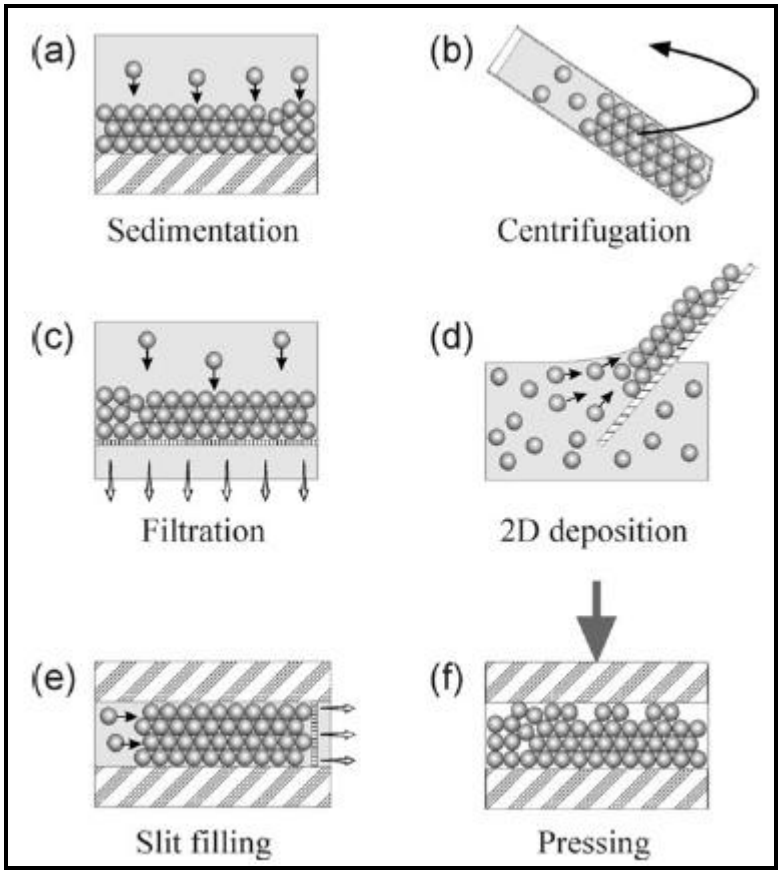

Figure 18: Different methods implemented to obtain an ordered self assembly of colloidal spheres

Reproduced from Ref. 125 with permission from Elsevier

2.3 Synthesis of Polystyrene Spheres

To synthesize the polystyrene spheres, we decided to use the surfactant-free emulsion polymerization procedure[126] described by Telford and co-workers rather than the conventional emulsion polymerization procedure widely used in the literature before. Emulsion polymerization method relies largely on the nucleation step of the process – the longer the nucleation process, the broader the size distribution.[126] In the presence of surfactant, the nucleation occurs inside the monomer swollen micelles whereas in the surfactant-free emulsion polymerization water insoluble polymer chains form that collapse to form precursor particles that aggregate to form clusters and then mature particles.[126] The main reasons that make this kind of synthesis an attractive method are: 1.) It's a one-pot synthesis method and hence very easy to execute 2.) Need for deoxygenation of reaction mixture eliminated by using enough initiator 3.) Narrow size distribution can be obtained in spite of skipping the deoxygenation step 4.) Time saving 5.) Economical.[126]

2.3.1 Materials and Methods

The commercial styrene (monomer) contained stabilizer that needed to be removed before using the monomer for synthesis. A small glass column was filled with basic alumina resting on glass wool plugged at the end, Figure 19. Commercial styrene was added to the column and the stabilizer-free styrene was collected at the other end.

Figure 19: Column of basic alumina to remove the stabilizer from the styrene

The initiator azobis-(cyanovaleric acid) was weighed (90 mg) and added to a glass flask with 50 mg of NaOH and 5 g of deionised water (Millipore). This initiator solution was heated in the oil bath for 1 minute. In another 50 ml round bottom flask, the stabilizer-free styrene was mixed with 17 g of deionised water and the mouth of the flask was sealed with a rubber septum. The flask was heated in an oil bath at 70^0 C for 5 minutes with continuous stirring. The initiator solution prepared earlier was injected into the styrene flask with the help of a syringe. The entire reaction mixture was retained overnight in the oil bath at 70^0 C. The milky white colour of the reaction mixture signals the end of the reaction, Figure 20. A small amount of sphere solution had coagulated at the bottom of the flask and was almost sticking to the glass. On observing it under SEM, we found it to be a mere residue of the reaction (unformed spheres) which we later

discarded. The sphere solution was repeatedly centrifuged in ethanol (each centrifugation cycle lasted 30 minutes) to make sure all traces of NaOH were removed. The sphere solution was diluted to 8 weight % in ethanol (same weight percent as the commercial sphere solution we used initially). The 8 weight % sphere solution was stored at room temperature. The spheres were later characterized by Scanning Electron Microscope (SEM).

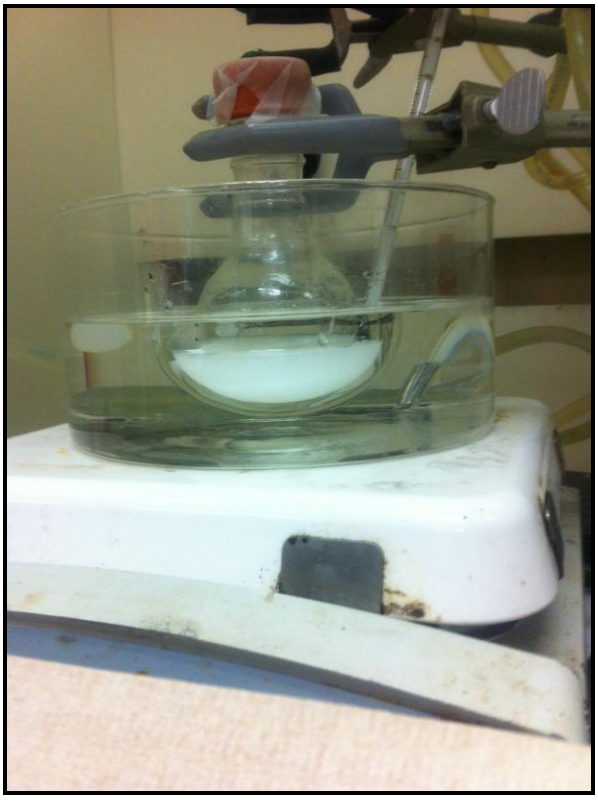

Figure 20: Milky white reaction mixture signalling the end of the polymerization reaction

2.3.2 Results and Discussion

The process of emulsion polymerization includes four components: a monomer, an emulsifier, a medium and an initiator. The process consists of two steps: nucleation and growth. In this case, the monomer is the styrene, the medium is deionised water and initiator is azobis-(cyanovaleric

acid). The conventional technique of the synthesis of PS spheres includes a surfactant that exists in the form of micelles swollen by the monomer.[90] The initiator decomposes to generate free radicals. This period is referred to as the nucleation period. The nucleation period decides the size distribution of the spheres formed. The longer the nucleation period, broader is the size distribution. However, in this case, the concentration of the initiator is pretty high which led to a short nucleation period and narrow size distribution.[126] The large amount of initiator decomposes to give large number of free radicals and is polymerized by the monomer to give styrene oligomers.[126],[90] The oligomers are stable particles as opposed to the unstable monomers.[126] The stable aggregate of precursor particles forms mature particles that are swollen with the monomer.[126] The monomer particles grow in size as the polymerization process proceeds. The oligomers keep forming in the medium till the monomer in the reaction mixture runs out.[126] The oligomers are captured onto the surface of the swollen mature particles; they retain their original appearance that gives the mature particle a rough surface.[126] The oligomers have a tendency to coagulate on the surface of mature particles – in other words – heteroagulate, than homoagulate.[126] This is because the high ionic strength compresses the double layer which affects the smaller particles more than the larger ones.[126] This procedure is diagrammed in Figure 21.

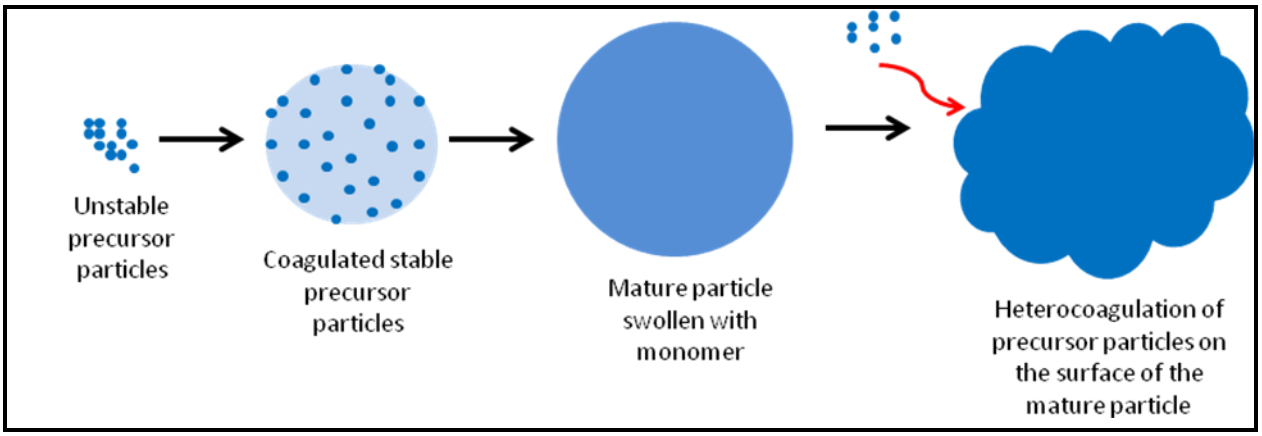

Figure 21: Mechanism of polystyrene sphere formation.

Adapted from Ref. 126. With Permission from John Wiley and Sons

Owing to the initiator used, the spheres formed in this process have carboxylic acid groups on the surface and the rough surface makes it possible to accommodate a very high number of them on the surface.[126] The negative charge on all the spheres helps stabilize them and avoids coagulation in spite of the high solid content in the medium.[126] The spheres obtained were relatively monodisperse. Although we did observe small particles that hadn't reached full maturity, they were low in number. Figure 22 shows JEOL SEM image of the lab synthesized polystyrene spheres. The spheres in this image were used as is i.e. without undergoing sputtering. The purpose of this image was to observe the size of the freshly synthesized spheres and hence they have not been assembled into an ordered layer. We merely dipped a clean gold coated glass slide into the 8 weight percent sphere solution and allowed it to air dry before imaging it.

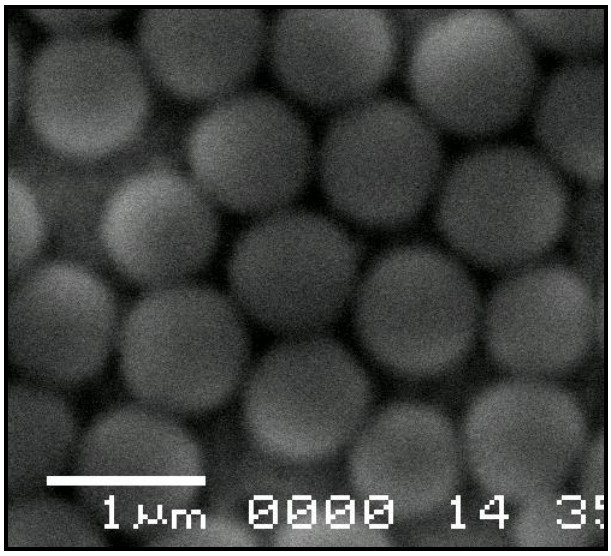

Figure 22: 1.2 micron polystyrene spheres synthesized in lab

2.4 Preparation of Self Assembly of Colloidal Crystals

To prepare the colloidal crystal the polystyrene spheres had to be uniformly self assembled on a gold coated glass slide first in order for them to be used as templates for further electrodeposition. We used two methods to prepare the colloidal crystal: vertical evaporation method or "convective assembly"[127] and Langmuir-Blodgett deposition as described by Vogel and co-workers.[85]

a.) Vertical Deposition method:

A glass vial was mounted onto a small glass flask which was filled with water. Commercial sulfate stabilized polystyrene latex spheres of a diameter of 500 nm were used to prepare the colloidal crystal. A dilute latex solution was prepared by mixing 308 microlitre of the sphere solution with 7 ml of ethanol. The gold coated glass slide is cleaned in the piranha solution (dangerous) and rinsed with deionised water. Cysteamine (2-aminoethanethiol, figure 23) of 10 mM concentration was prepared in ethanol and piranha cleaned gold slide was soaked in this

solution for 24 hours. During this time the gold slide was chemically modified with the thiol and the modified slide was inserted in the glass vial at an inclined angle and the latex solution in ethanol slowly added to the vial from the side. The entire assembly (shown in Figure 24) was kept in a hot water bath at 50^0 C for a little more than 24 hours or until the latex solution in the vial has completely evaporated and the gold slide appeared dry. Care must be taken not to let the moisture drops splash on the sphere coated gold slide.

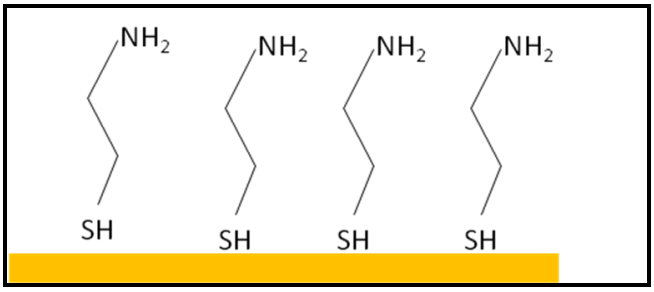

Figure 23: Cysteamine modified gold slide

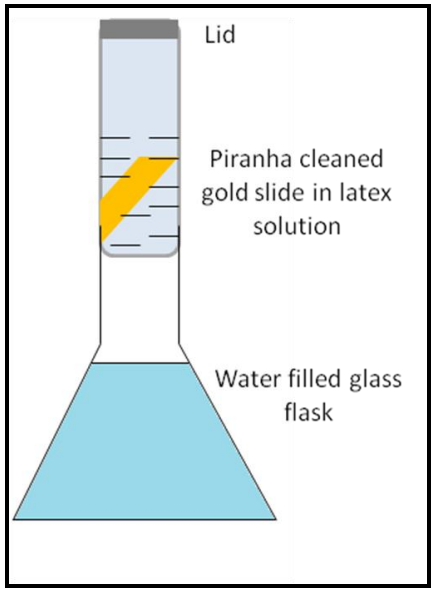

Figure 24: Vertical deposition assembly for deposition of PS spheres

Multilayer deposition in this kind of method is common and the entire deposition process takes about 2 days to reach completion. Two forces are at play in this process of forming 2D colloidal layer: attractive capillary forces between two neighbouring spheres and convection forces, Figure 25. The elevated temperature of the water bath starts the slow solvent evaporation process that initiates a convective flow of spheres from the bulk toward the drying point.[127] The capillary forces and the convective forces balance to form 2D arrays of spheres on the substrate.[127] When the convective forces triumph over the capillary forces, a multilayer 3D colloidal layer is formed.[127] The spheres, that are caught in the solvent flux and driven toward the drying end of the layer, end up pressing against the crystal front.[127] Capillary bridges are formed between particles because of the strong capillary forces that may cause cracks in the colloidal layer.[127] Although it's difficult to exercise precise control on the evaporation, the water bath temperature, type of substrate used, inclined angle of the substrate, type of solvent, humidity conditions and concentration of colloidal solution can affect the quality of colloidal layer formed.[127]

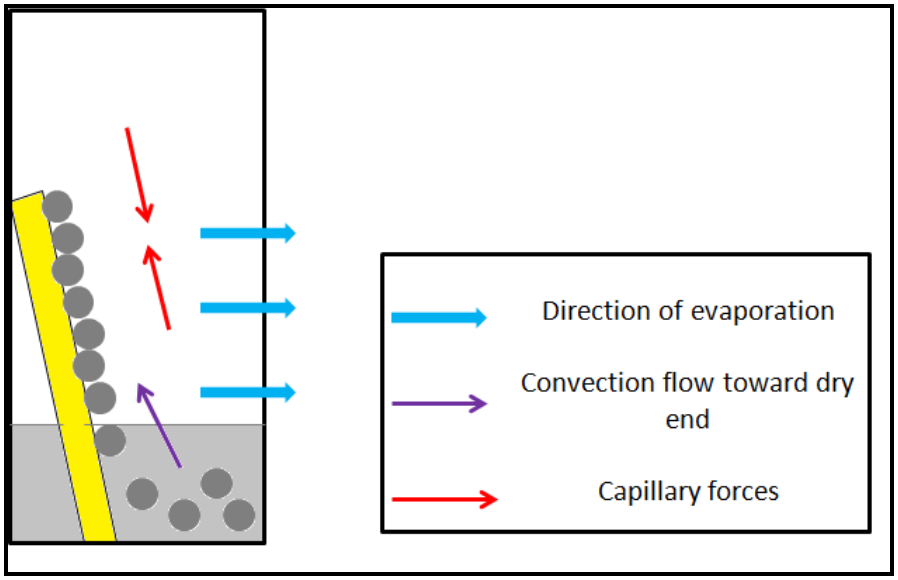

Figure 25: Different forces participating in the formation of 2D colloidal crystal assembly.

Adapted from Ref. 127 with Permission from Royal Society of Chemistry

This method was time consuming with no control over the evaporation process. It also consumed a high amount of sphere solution and the deposition was often multilayered and "furrowed". Maintaining humidity conditions proved tricky which meant we had to keep the lid of the water bath and the glass vial closed. Often condensation droplets would splash on the gold slide ruining the deposition despite our best efforts to avoid it. Hence, we switched to an alternate method called Langmuir-Blodgett (LB) deposition to suit our purposes.

b.) Langmuir-Blodgett (LB) deposition:

This method involves forming a colloidal layer at the air-water interface and transferring this layer onto the surface of plasma etched gold slide as shown in Figure 26. This method had been used previously in the literature[85] and is based on the Langmuir-Blodgett (LB) deposition principle.[127]

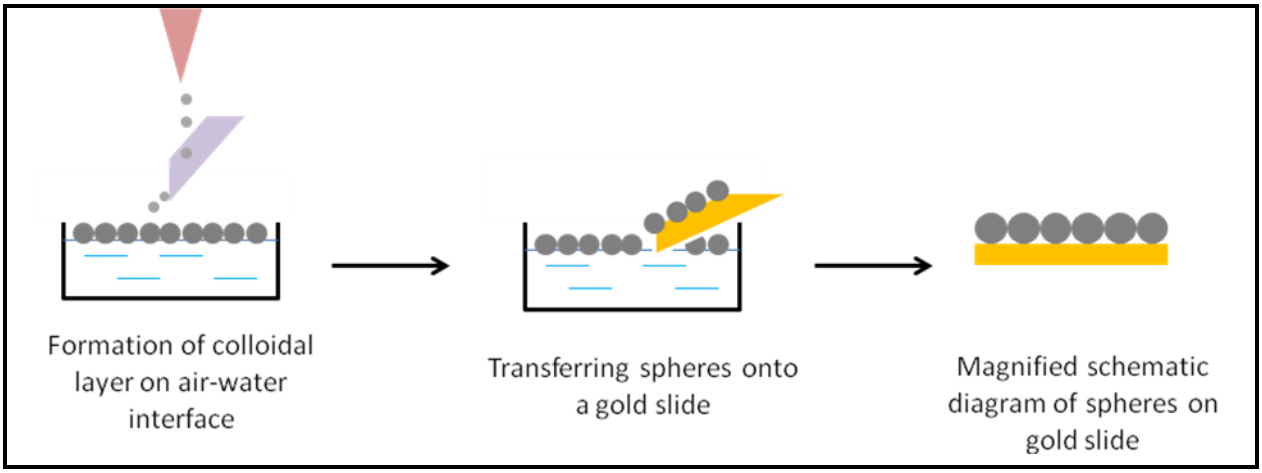

Figure 26: Schematic diagram of transfer of preassembly of colloidal crystal assembly

Adapted from Ref. 85 with Permission from John Wiley and Sons

A glass vessel was filled with tap water (pH 11) and 140 microliter of 0.1 mM Sodium Dodecyl Sulfate (SDS) was added to the water surface. Water must not be stirred after the addition of SDS. A dilute sphere solution was prepared by adding 172 microliter sphere solution to 1 ml ethanol. A clean glass slide was held in an inclined position on the air-water interface and the sphere solution is slowly dropped onto the glass slide such that the latex solution slides onto the air-water interface from the tip of the glass slide and forms patches of colloids on the surface of water. The process must be stopped before the entire air-water interface is covered with colloidal patches and buckles under it. Gold slides were cleaned by exposing them to an oxygen at 15 W for 5 minutes (Bias value -86) and were held at an inclined angle of ~45^0 at the interface to scoop the spheres. The gold slide, after scooping, was removed from the water at an inclined angle and then left on a flat surface to dry. The SDS amphiphilic molecules float on the surface of the water and form a “cushion” for the colloids that are added to the water. As a result the spheres (when added to the interface) end up pushing against the SDS layer effectively getting closer to each other and forming an ordered 2D colloidal crystal layer.[85] The spheres used in this process have carboxylic groups on their surface (owing to the initiator used) giving them a negative charge. The carboxylic groups on the sphere surface are deprotonated upon increase in the pH of the tap water, thus increasing the charge density on the surface. As a result the spheres are electrostatically repulsed from each other, thus increasing the energy barrier between them.[85] In order to minimize this barrier the spheres move around and form a hexagonally ordered lattice.[85] Plasma cleaning the gold slides under oxygen increases their wettability making them an ideal substrate for the transfer of the colloidal layer.[85] Deposition must be done immediately after plasma etching the gold slides. Figure 27 shows a colloidal crystal formed using Langmuir-Blodgett deposition.

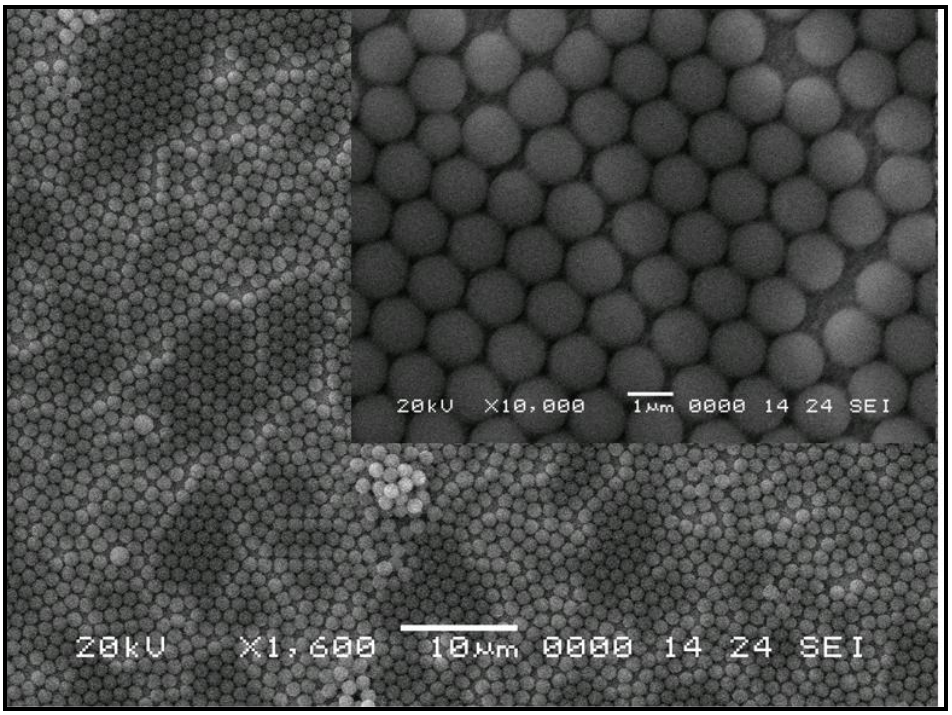

Figure 27: SEM image of 2D colloidal crystal layer prepared by Langmuir-Blodgett (LB) deposition

This method saved on time and resources with little or no hassle. The number of times the gold slide is used to scoop the spheres decides the number of layers deposited and it takes only 20-25 minutes to air dry the gold slide. This method can be used for any kind of substrate.

CHAPTER 3: FABRICATION OF HIGH SURFACE AREA GOLD ELECTRODES

Macroporous electrodes were fabricated using 1200 nm sized polystyrene spheres as templates and electrodepositing gold around the spheres. Macro-nanoporous and nanoporous gold electrode were prepared by electrodepositing a binary alloy (gold-silver) followed by chemical dealloying, to generate the nanoporosity. The following sections explain in depth the fabrication procedure of each electrode.

3.1 Fabrication of Macroporous Electrode Using Polystyrene Spheres as Template

Ordered macroporous gold electrodes have been reported in the literature and extensively studied.[128]. This fabrication method helps fabricate robust, mechanically stable macroporus gold electrodes.

3.1.1 Materials and Methods

Electrodeposition was performed using commercial cyanide-free gold solution (Gold Tech 25). Polystyrene spheres with a diameter of 1.2 micron were synthesized using surfactant-free emulsion polymerization method as described in the previous chapter. Gold slides were prepared by cleaning in hot piranha solution (caution: dangerous) for 1 minute and thoroughly rinsed with deionised water. Polystyrene spheres (1200 nm in size) were deposited on the gold slide using the Langmuir-Blodgett method as described earlier. The sphere coated slides were allowed to dry for 24 hours before exposing them to cyanide-free gold solution. Electrochemical deposition was done using CH instrument potentiostat at a potential of -0.9 V for about 200 seconds using a three electrode assembly: silver/silver chloride electrode as the reference electrode, platinum gauze as the counter electrode and the sphere deposited gold slide as the working electrode. The electrochemically deposited gold slide was immersed in chloroform for 4-5 hours to dissolve the polystyrene spheres and then rinsed with deionised water and dried

under nitrogen. Figure 28 shows the schematic diagram of the steps involved in the fabrication of the macroporous gold electrode.

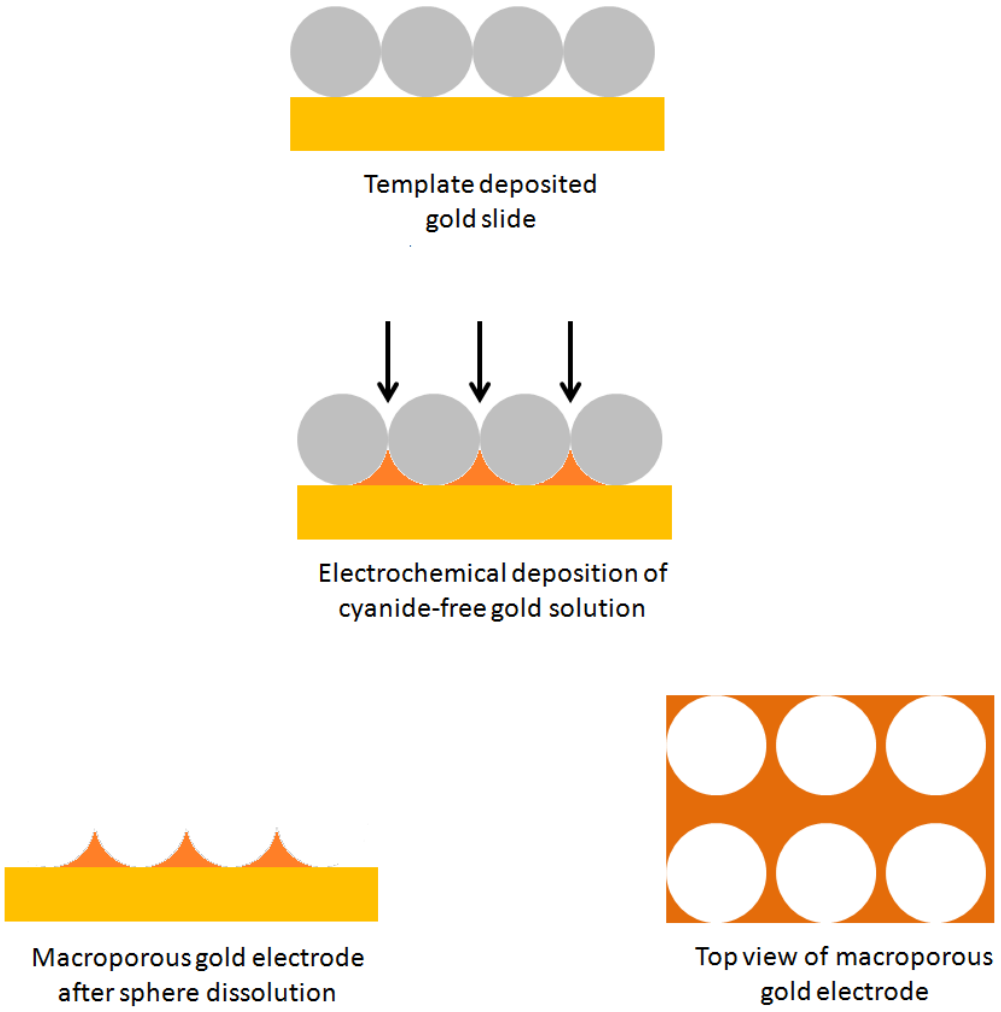

Figure 28: Schematic of the fabrication of the macroporous gold electrode

3.1.2 Results and Discussion

The deposition of polystyrene spheres on the gold slide has to be as uniform as possible in order to get an ordered macroporous gold electrode. A potential of -0.9 V was applied and the deposition was closely monitored using the current-time curve.

The deposition usually starts from the lowest layer of spheres and proceeds in the upward direction. On account of this, the area under deposition constantly changes as the deposition proceeds and, as a result of changes in the substrate area, the current changes too. These current fluctuations observed in the current-time curve are used as a “scale” to monitor the layers of gold being deposited.

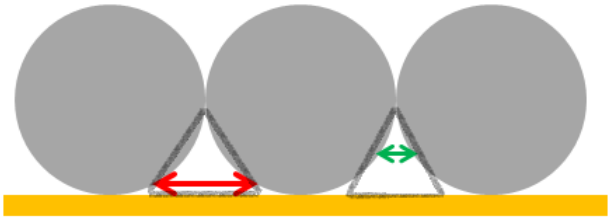

Figure 29: Changing area between two neighboring spheres

As can be seen in figure 29 above, the deposition starts from the bottom layer where the interstitial area is high as indicated by the red arrow. As a result, the current slowly increases. As the gap between the two spheres slowly starts filling up, the interstitial area decreases (indicated by the green arrow) and so does the current. Thus, the “troughs” observed in the current-potential curve, Figure 30, are used to count the number of layers being deposited.

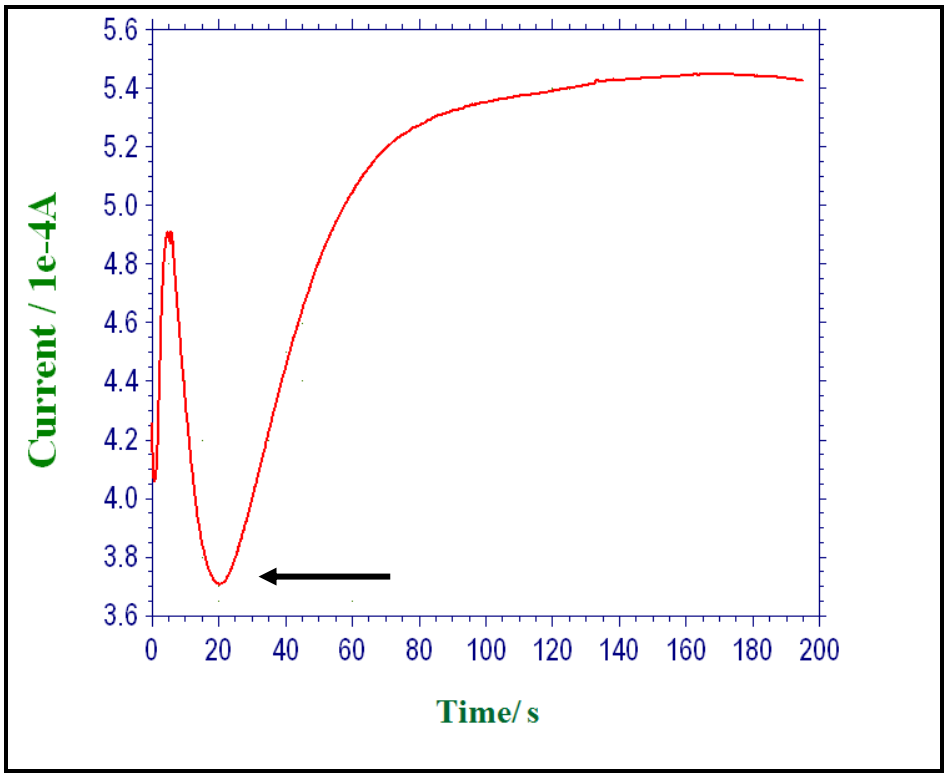

Figure 30: Current-time electrodeposition curve of macroporous gold electrode

The trough (indicated by a black arrow) observed in the curve in Figure 30 indicates that 0.5 layers have been deposited. Had the deposition continued, a second trough would have been observed which would have indicated 1.5 layers being deposited and so on and so forth. The reason we stopped at 0.5th layer was that the spheres deposited on the gold slide were a monolayer thick and hence continued deposition would have made the gold deposit on top of the spheres. Figures 31 and 32 exhibit the formation of macropores observed after using monolayered and multilayered spheres as templates.

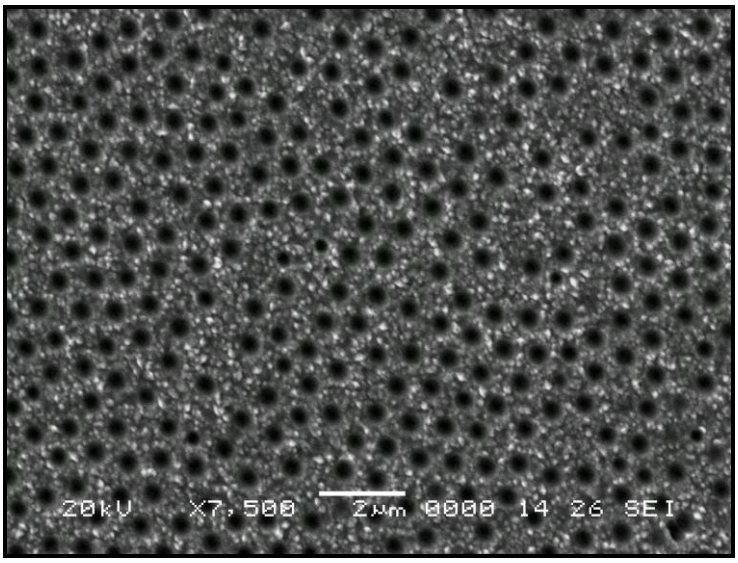

Figure 31: SEM Image of macroporous gold electrode (monolayer deposition)

SEM image in Figure 31 shows the macroporous gold electrode obtained after depositing gold in the interstices of a monolayer of polystyrene spheres followed by the removal of spheres. The deposition appears to be uniform with no cracks, incomplete deposition or “windows” which are frequently observed in the multilayered gold deposition as shown in Figure 32. The voids or hollow macropores observed are due to the presence of the template which was dissolved prior to imaging. The gold has deposited in the interstices of the spheres and appears to have a rough texture. The hollow macropores also indicate that the gold deposition was stopped in time and that gold did not deposit over the top of the spheres.

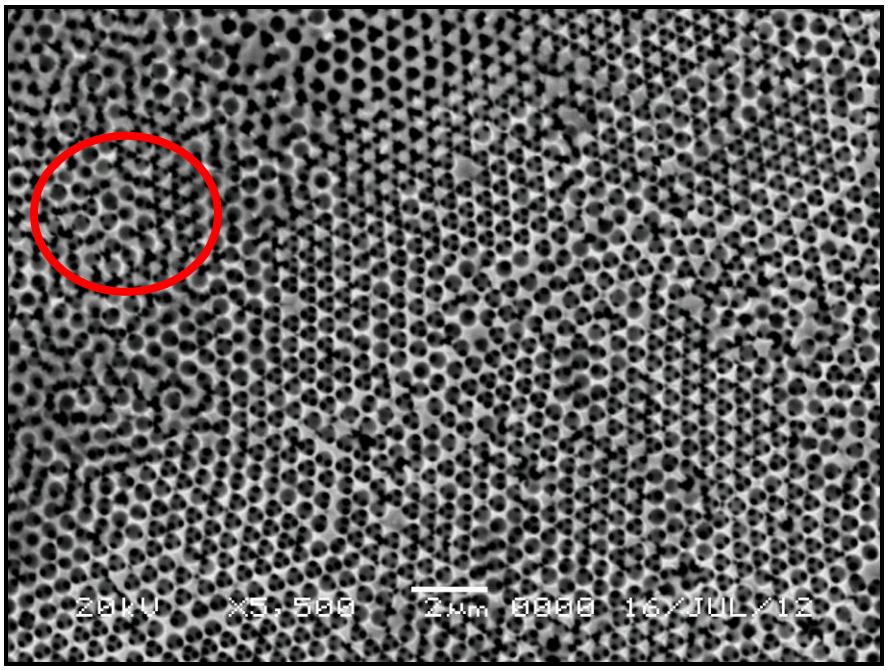

Figure 32: SEM image of macroporous gold electrode (multi-layered deposition)

The vertical evaporation method of sphere deposition described previously exhibited multilayered deposition of spheres. The electrochemical deposition in this case generated macropores with “windows” or the three spherical voids seen inside the macropore. These voids are observed due to the interconnections between the spheres which the gold solution is unable to fill in.[128] The red circle in figure 32 indicates the portion of the electrode where the electrochemical deposition is unable to occur due to the lower layer of spheres and hence the gold deposition is incomplete.[128] On account of these defects in the multilayered structure, we preferred macroporous gold electrodes that were fabricated using a monolayer of polystyrene spheres.

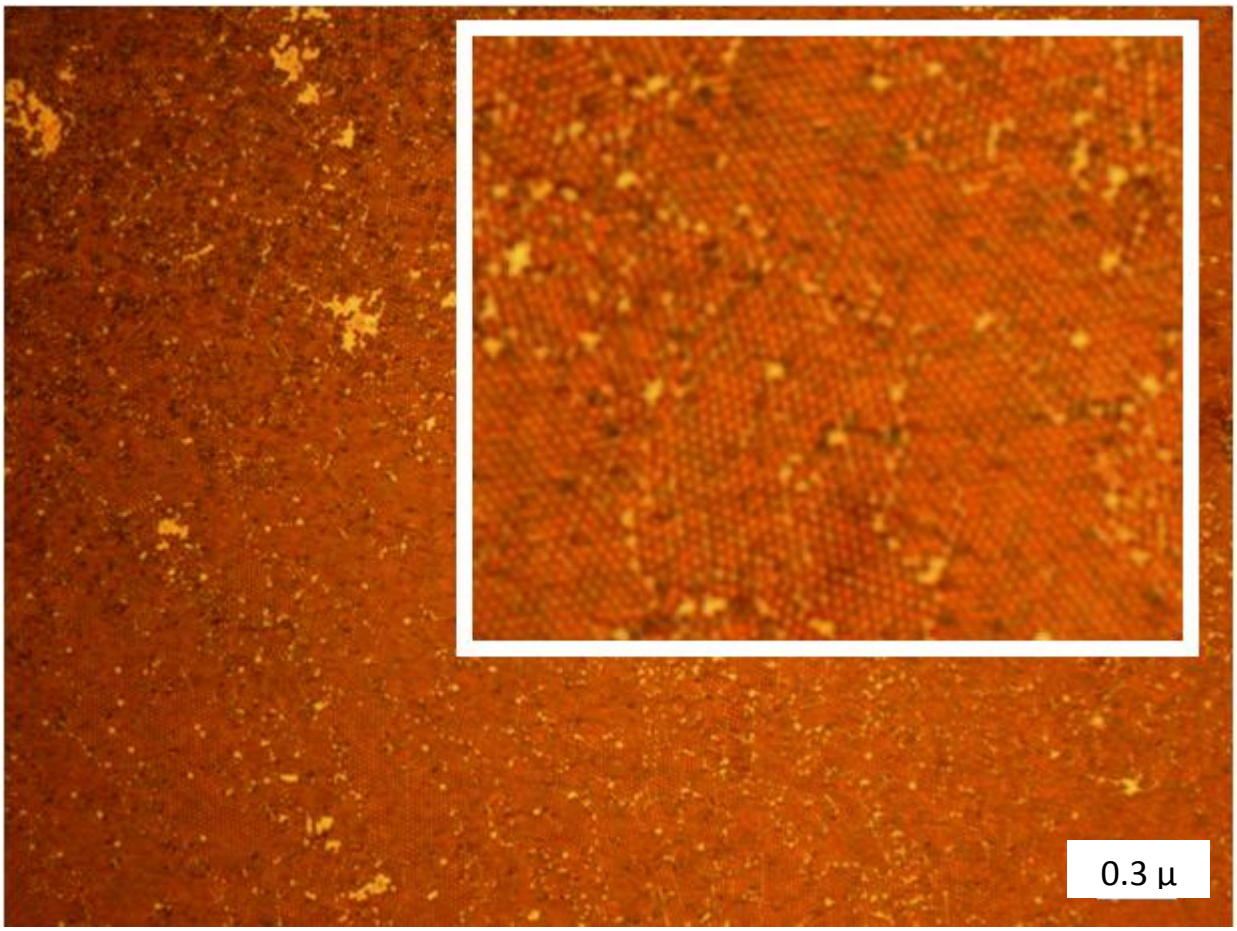

Figure 33: Nikon digital optical microscope image of macroporous gold electrode

Figure 33 shows the image of macroporous gold electrode taken using a Nikon Digital Optical Microscope. The macroporous electrode was imaged after the removal of the spheres and was used as is. The inset, which shows ordered macropores, is a small portion of the original image that was magnified on the computer to better see the macropores.

The electrochemical deposition method of fabrication is easy to execute and can be easily controlled by changing the parameters like deposition potential, deposition time. By modifying these parameters one can modify the porous film as desired as demonstrated above: the number of layers being deposited can be controlled, the density of the material being deposited can be controlled by controlling the deposition potential. The primary advantage of

electrodeposition is that the metal deposited in the gaps between spheres is highly dense.[128] As a result, the procedure is ruled by volume templating rather than surface templating.[128] This gives rise to a strong, stable metal structure that shows no shrinkage upon template removal and hence no cracking.[128] As a result, the electrode does not require annealing and can be used as is for electrochemical measurements. Another attractive feature of this procedure is the easy removal of spheres that does not involve calcification, etching or any other complicated/time consuming methods. Simple removal of template ensures no damage to the macroporous film on the gold substrate.

3.2 Fabrication of Macro-nanoporous Gold Electrode

Macro-nanoporous gold electrode was fabricated using polystyrene spheres as templates and electrodepositing a gold-silver alloy solution around the spheres followed by sphere removal and etching. The principle behind the fabrication of macropores is the same as that of the macroporous gold electrode, while the nanopores are generated in the macropores by etching the less noble metal – silver.

3.2.1 Materials and Methods

Commercial gold cyanide and silver cyanide solutions (caution: dangerous!) were used for electrochemical deposition. Extreme care must be taken while handling the solutions and the actual deposition must be performed in a closed chamber. No acids must be allowed near or inside the chamber and it must be made sure that the hood of the closed chamber is working properly. Lab-synthesized polystyrene spheres of size 1200 nm were used as templates. A three electrode assembly was used to carry out the electrochemical deposition: silver/silver chloride as the reference electrode, platinum wire as the counter electrode and the sphere deposited gold slide as the working electrode. Concentrated nitric acid was used to chemically

etch out the silver from the electrodeposited electrode. An oxygen plasma etcher was used to make the sphere coated gold slides more hydrophilic.

The gold slide was piranha cleaned (caution: piranha solutions are dangerous) and the spheres deposited on the surface via the Langmuir-Blodgett deposition method as described earlier. The spheres were dried for at least 24 hours before using them as templates. The gold-silver alloy solution was prepared by adding 10 drops of silver-cyanide solution to 40 drops of gold-cyanide solution. The intention was to keep the gold percentage around 80% and silver around 20% to provide stability to the structure. The alloy solution was mixed and used for electrochemical deposition. Prior to deposition the sphere coated gold slide was exposed to an oxygen plasma at 15 W for 30 seconds to make the spheres more hydrophilic. The sphere coated gold slide was transferred straight from the plasma etcher to the cell and the electrochemical deposition was performed at a potential of -1100 mV for approximately 100 seconds in a closed chamber. The deposition was monitored using the current-time curve, as described above. After the deposition the electrodeposited gold slide was rinsed with deionised water and soaked in chloroform for 4-5 hours to dissolve the spheres. The gold slide was rinsed again, dried under nitrogen and immersed in concentrated nitric acid for two hours to etch the silver. After the etching process, the gold electrode was rinsed and soaked in deionised water for an hour to make sure all the traces of nitric acid were removed from the pores. The electrode was then dried under nitrogen and used for electrochemical measurements. Imaging was done using HITACHI SU 70 scanning electron microscope (SEM) and HITACHI Energy Dispersive Spectroscopy (EDS) was used to study the alloy composition after etching.

3.2.2 Results and Discussion

The formation of the macropores is based on the same principle as described in the previous sub-chapter and outlined in Figure 34. The alloy solution was electrodeposited in the interstices

between the spheres and macropores were obtained after dissolution of the template. The alloy solution that was deposited reached only about a quarter of the height of the spheres before the electrodeposition was stopped. As a result, the macropores are really shallow and give the electrode surface a wavy/ crest-trough pattern.

Template deposited
gold slide

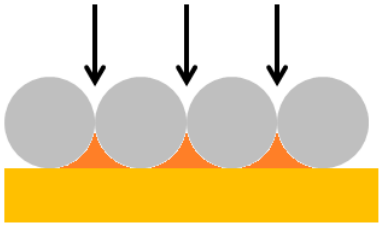

Electrochemical deposition of gold
cyanide-silver cyanide alloy solution

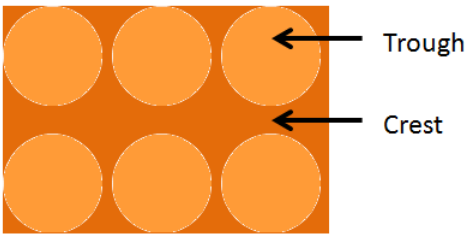

Top View: Macropores
after template dissolution

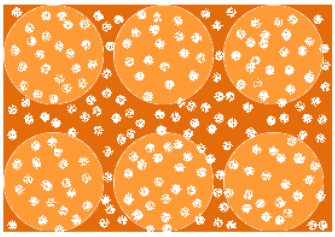

Top View: Nanopores observed on
the crests and troughs after etching

Figure 34: Schematic diagram of the fabrication of macro-nanoporous electrode

Figure 34 above shows the steps involved in the fabrication of the macro-nanoporous electrode. As the name suggests, the electrode has “wells” or macropores resulting from the presence of the polystyrene spheres and nanopores on account of the etching of silver. The current-time curve showed in Figure 35 below was used to monitor the thickness of the film being deposited.

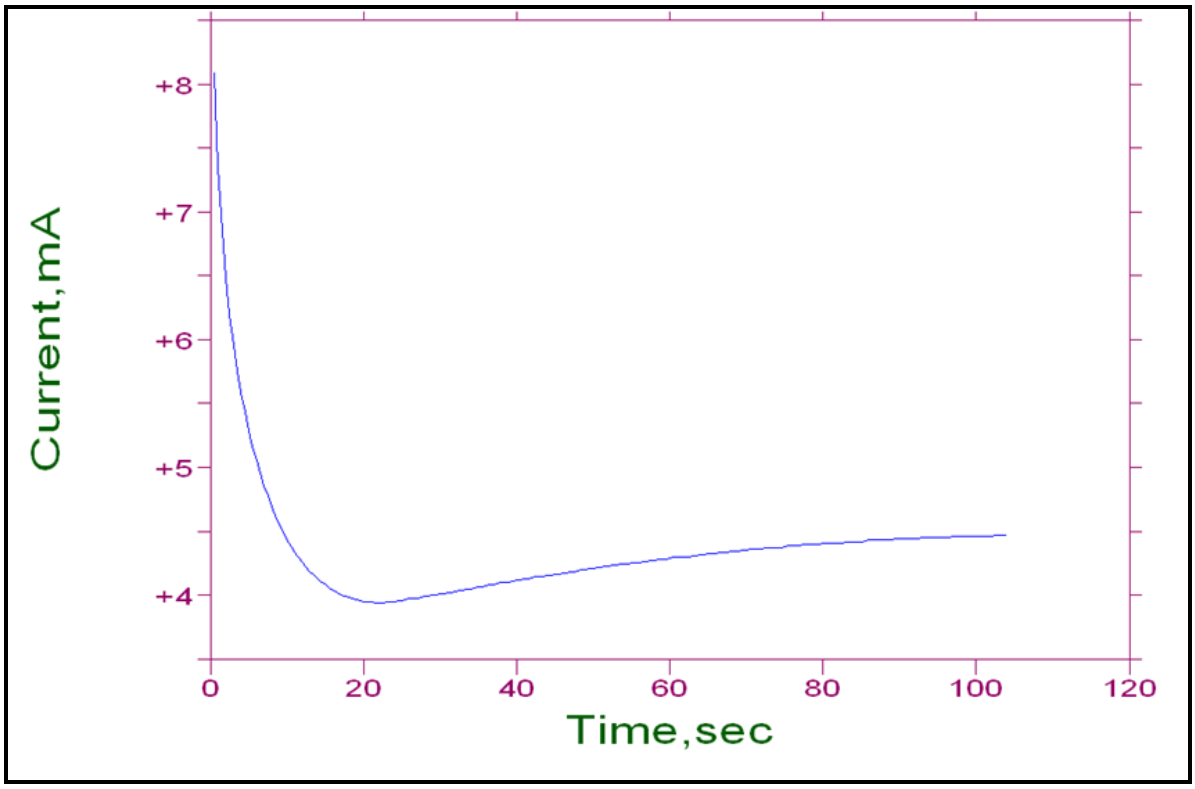

Figure 35: Electrochemical deposition current-time curve of macro-nanoporous electrode

The current gradually increases as the interstitial area increases. We stopped the deposition around 100 seconds when the current reached a fairly stable value in order to avoid the alloy forming over the spheres. After the template dissolution, the electrodes were etched in concentrated nitric acid. The more noble metal, gold is unaffected by nitric acid whereas the less noble element, silver, is etched from the electrode leaving behind nanosized pores. The

mechanism of etching is discussed in detail in the following section of nanoporous gold electrode.

Table 1: Effect of varying concentrations of gold and silver in the alloy solution

Composition	Effect	Annealing
1:4 Ag:Au	No cracking	None
1:1 Ag:Au	cracking	24 hours
2:1 Ag:Au	cracking	24 hours

Table 1 above summarizes the different concentrations of gold and silver used in the fabrication process. A large amount of silver in the deposition solution gives rise to films that are not mechanically stable and the porous films were observed to crack after etching in concentrated nitric acid. Effects of annealing have been studied in the literature and annealing at 300^0 C seemed to work best in controlling the cracking.[129] The films can't be annealed at higher temperatures than that since annealing coarsens the gold ligaments that are not easily distinguishable.[130] The ligaments also grow in size thus decreasing the surface area.[130] We tried to remedy the cracking by annealing the electrodes at 300^0C for 24 hours. However, no significant amount of reduction in cracking was observed. Fabrication was done at -1000 mV, -1100 mV and -1200 mV but -1100 mV seemed to give the best results. The silver:gold 1:4 ratio produced mechanically robust macro-nanoporous electrodes which effectively eliminated the need for annealing, thus making the fabrication procedure time saving. Different etching times were experimented with and ultimately optimized to two hours of etching in concentrated nitric acid which seemed to etch out most of the silver present in the film giving fine nanopores, Figures 36, 37 and 38.

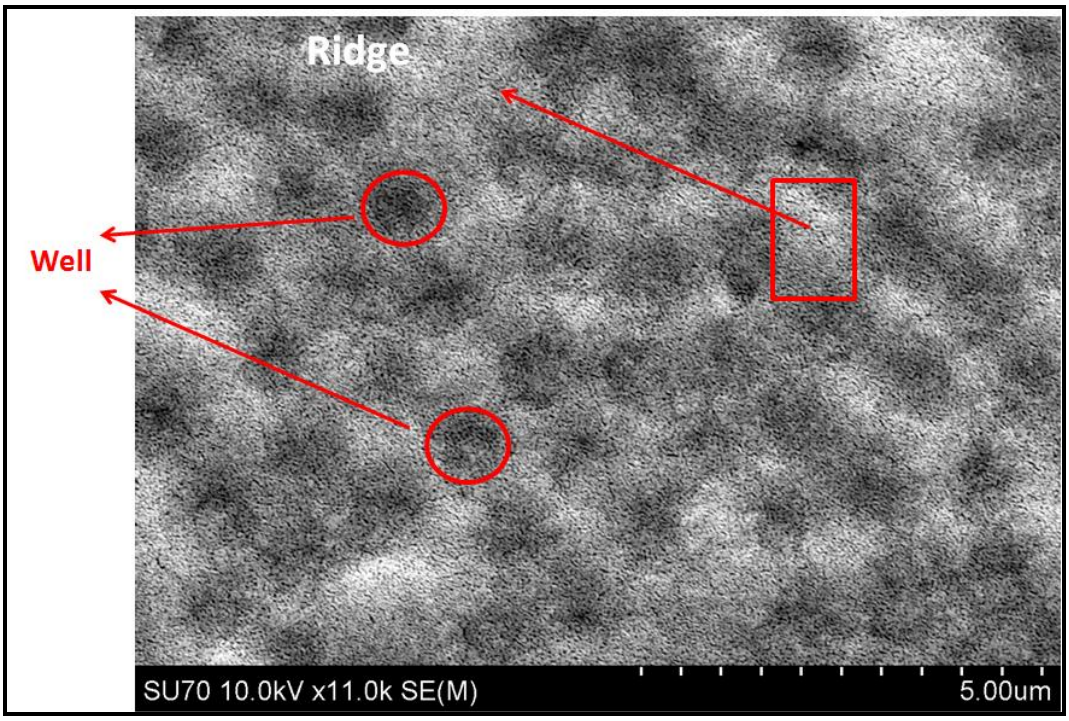

Figure 36: SEM image of a macro-nanoporous electrode

Figure 36 shows the SEM image of the surface of macro-nanoporous electrode after the removal of spheres and etching. The red circles mark the position of wells or depressions caused by the presence of polystyrene spheres and the red rectangle marks the border of the well or a crest. Nanopores are observed on the macropores as a result of the silver etching. The etching time determines the diameter of the pores. The longer is the etching time, the larger the pores.

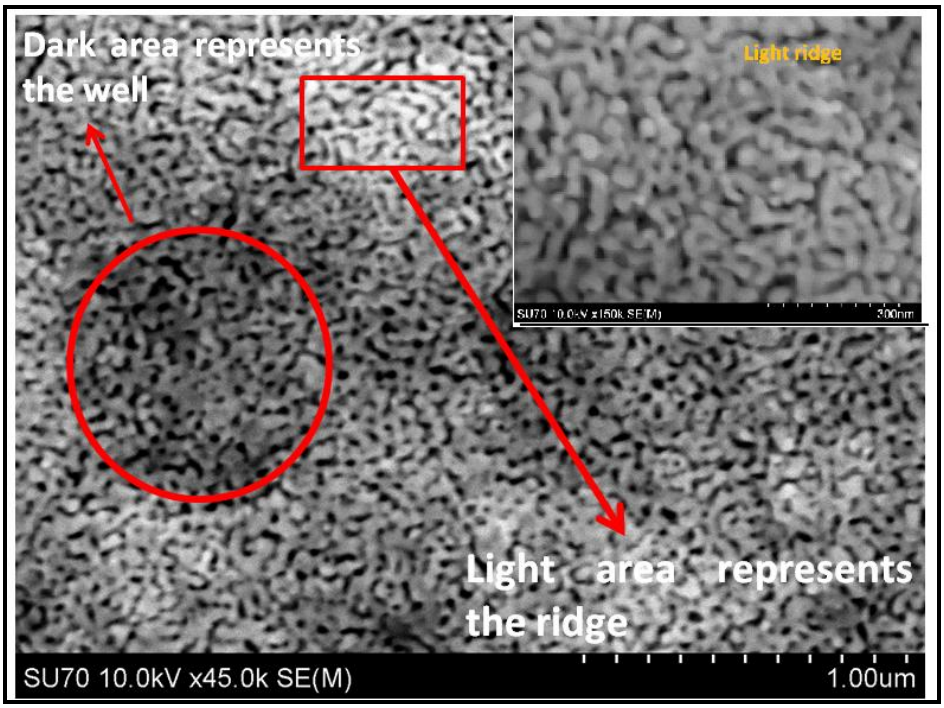

Figure 37: Magnified SEM image of the crest-trough pattern of the electrode surface

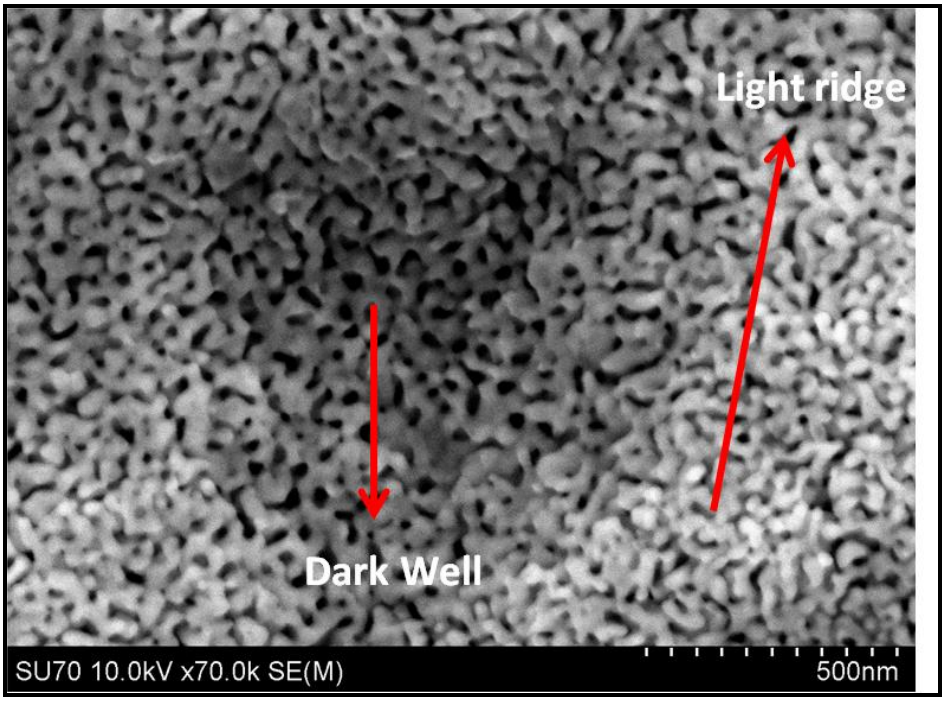

Figure 38: Magnified SEM image of the crest-trough pattern of the electrode surface

Figure 37 and 38 above show a magnified image of the electrode surface where the dark hollow region represents the macropore or the well and the light area represents the ridge or the border of the well. The inset in Figure 37 shows a magnified image of the ridge which shows a nanoporous bicontinuous gold ligament structure.

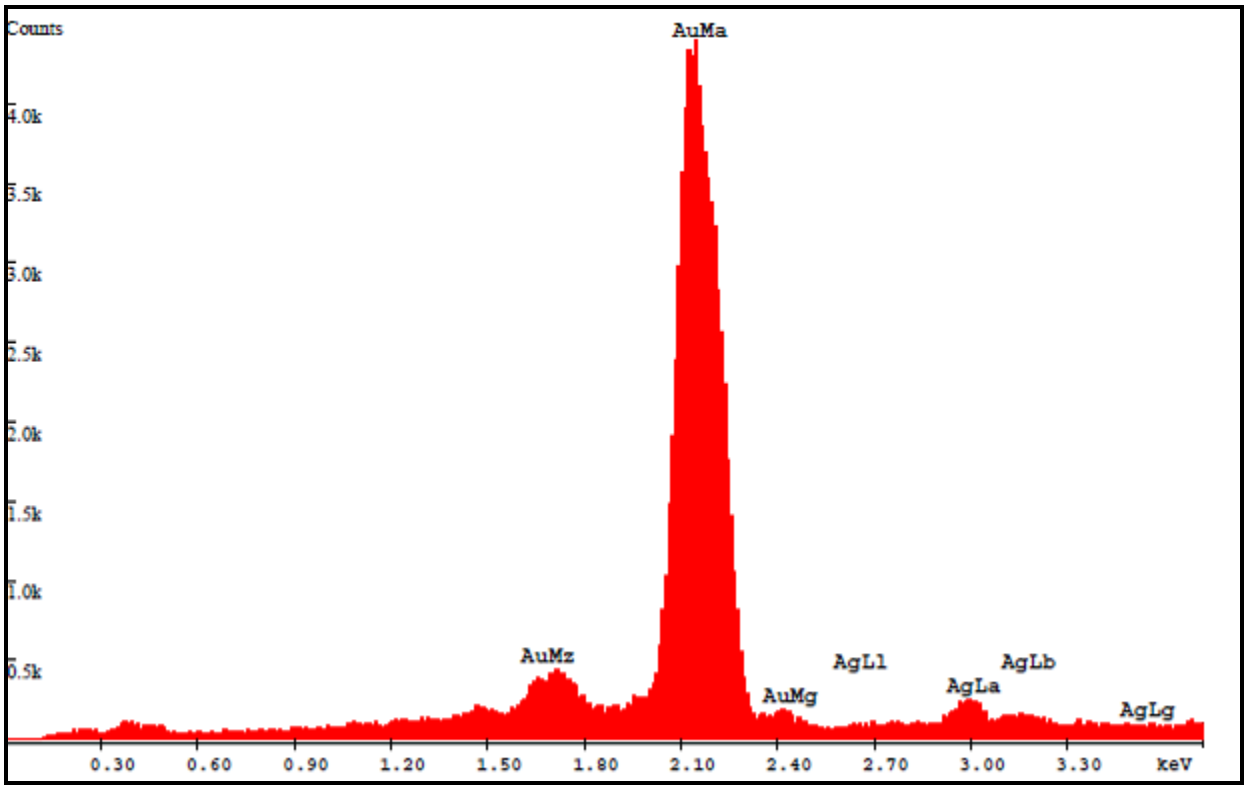

Figure 39: EDX spectrum of the inside of a well of the macro-nanoporous electrode

Table 2: Elemental composition of the well obtained using EDX

EDAX ZAF Quantification (Standardless)
Element Normalized
SEC Table : Default

Element	Wt %	At %	K-Ratio	Z	A	F
AgL	5.52	9.64	0.0300	1.0953	0.4970	1.0000
AuL	94.48	90.36	0.9359	0.9903	1.0002	1.0000
Total	100.00	100.00				

Figure 39 shows the EDX spectrum of the inside of the macropore. The elemental composition obtained from the EDX spectrum (Table 2) suggests that the silver composition is 5.52 weight % while gold is 94.49 weight %. This percentage seemed ideal in that such a low silver amount doesn't interfere with the electrochemical measurements carried out at a later stage and the high gold weight percentage provided mechanical stability to the electrode. EDX spectra of other macropores indicated the presence of 4.46 weight % of silver and 95.54 weight % gold which suggested that the etching in nitric acid was uniform.

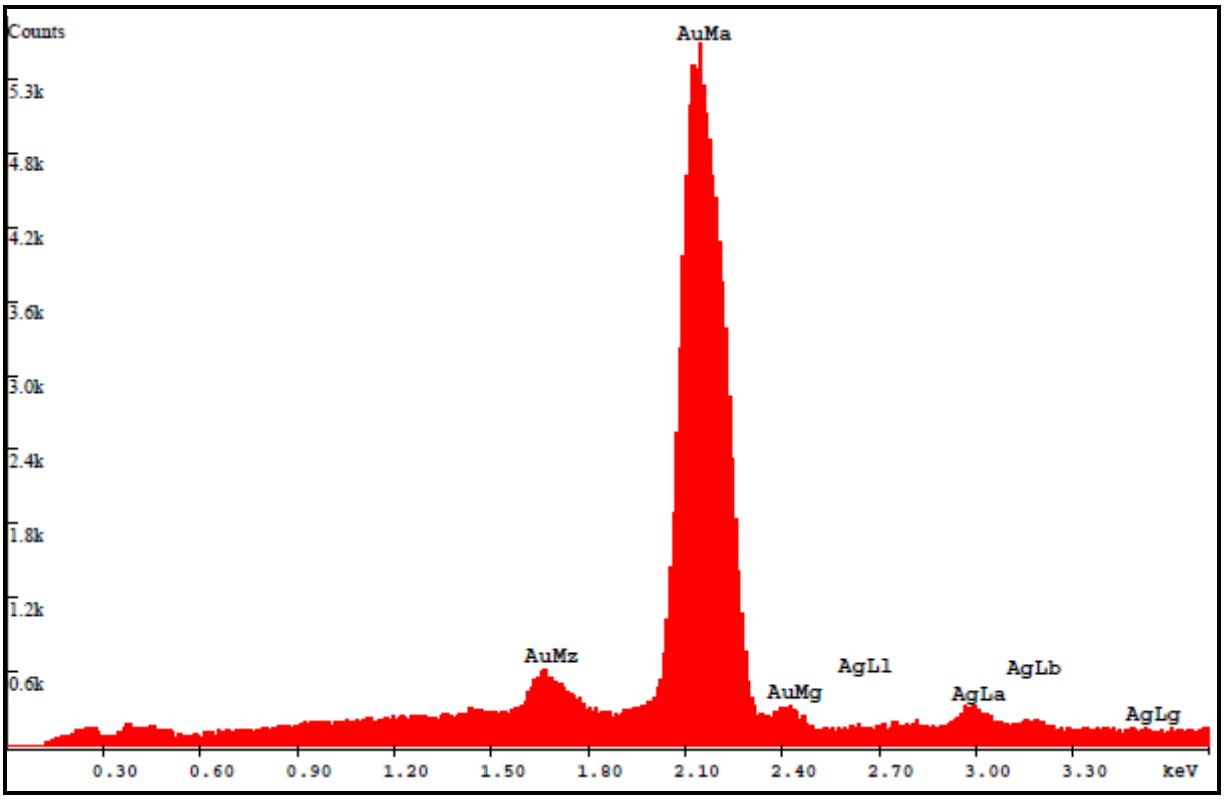

Figure 40: EDX spectrum of the ridge on the surface of the macro-nonporous electrode

Table 3: EDX elemental composition of the ridge of macro-nanoporous electrode

EDAX ZAF Quantification (Standardless)
Element Normalized
SEC Table : Default

Element	Wt %	At %	K-Ratio	Z	A	F
AgL	5.94	10.34	0.0324	1.0948	0.4984	1.0000
AuL	94.06	89.66	0.9310	0.9896	1.0002	1.0000
Total	100.00	100.00				

Figure 40 shows the EDX spectrum of the ridge of the macro-nanoporous electrode seen in Figure 37. Table 3 shows the elemental composition of the ridge which is quite similar to that of the well: 5.94 weight % silver and 94.06 weight % gold. Other electrodes were tested for the elemental composition of both the well and the ridge and the results were consistent.

Using the widely used binary alloy method, we fabricated a robust, mechanically stable electrode that is a cross between the macroporous and the nanoporous electrode.

3.3 Fabrication of the Nanoporous Electrode

Various fabricating procedures have been documented in the literature to prepare nanoporous gold electrode. Nanoporous gold electrode has been fabricated in our lab using 12 K white gold leaf and biofouling studies have been successfully performed using the gold leaf electrode.[131] We decided to go ahead and fabricate electrodeposited nanoporous electrode for this study for purposes of fair comparison. Binary alloy was electrodeposited on the conductive substrate without the assistance of a template and was later chemically dealloyed to generate nanopores. Care must be taken while (a.) Handling highly toxic cyanide salts (b.) fabricating a very thick film since it's more prone to cracking.

3.3.1 Materials and Methods

Gold and silver cyanide commercial solutions were mixed together and used for deposition. A three electrode assembly was used for deposition – silver/silver chloride reference electrode, platinum wire as the counter electrode and a clean, gold coated glass substrate as the working electrode. Etching was performed in concentrated nitric acid and the electrodes were later characterized using HITACHI Scanning Electron Microscope (SEM) SU 70 and HITACHI Energy Dispersive Spectroscopy (EDS).

The gold slides were cleaned in piranha solution (dangerous) and thoroughly rinsed in deionised water. The electrochemical deposition was carried out in a closed chamber by mixing the two metal cyanide solutions – 35 drops of gold cyanide solution and 15 drops of silver cyanide solution. A potential of -1100 mV was applied and deposition was performed for 100 seconds. The deposition was monitored using the current-time curve. After the electrodeposition, the

electrodes were rinsed with deionised water, dried under nitrogen and annealed at 300^0 C for two hours. The electrodes were later soaked for two hours in concentrated nitric acid. They were then soaked in deionised water to remove all the traces of the acid and dried under nitrogen.

3.3.2 Results and Discussion

Figure 41 shows the steps involved in the fabrication of the nanoporous electrode. The deposition film was kept very thin in order to avoid cracking. Figure 42 shows the current-time curve used to control the electrochemical deposition process. The curve shows no fluctuations, unlike the other two curves, since no template was used in this case.

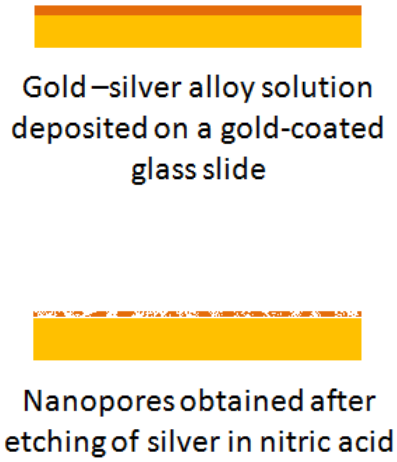

Figure 41: Schematic diagram of fabrication of nanoporous gold electrode

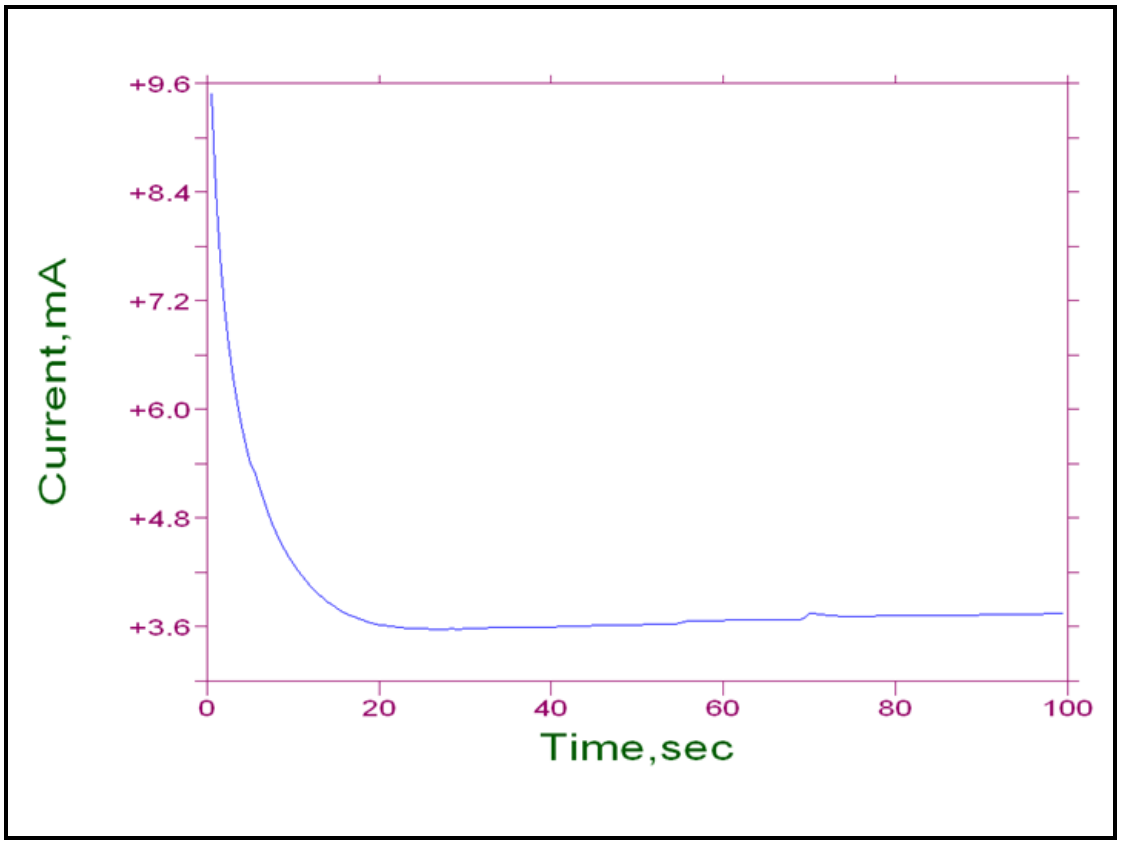

Figure 42: Current-time electrodeposition curve for nanoporous gold electrode

Table 4 gives the results of a series of experiments undertaken via the modification of certain parameters. We wanted to obtain good porosity and hence we kept the silver amount high (2:1) and the deposition time short to produce very thin films. Inspite of the thin thickness, cracking was observed which could not be remedied after annealing for 24 hours. Increasing the gold:silver ratio to 1:1 and shorter deposition time (20 seconds) gave certain stability to the film and showed no cracking. However, increasing the deposition time to 100 seconds showed cracking again. This is because after immersion in concentrated nitric acid, most of the silver is leached out causing significant volume shrinkage. Annealing these films doesn't help either as volume shrinkage is dominant over the effect of thermal treatment.[129] 7:3 gold-silver ratios produced a good, robust, mechanically stable electrode

Table 4: Effect of different parameters on the fabrication of nanoporous electrode

Composition	Effect	Deposition Time	Annealing
3:7 Ag:Au	No cracking	100 seconds	24 hours, 300^0 C
1:1 Ag:Au	No cracking	20 seconds	24 hours, 300^0 C
1:1 Ag:Au	cracking	100 seconds	24 hours, 300^0 C
2:1 Ag:Au	cracking	100 seconds	24 hours, 300^0 C
2:1 Ag:Au	cracking	50 seconds	24 hours, 300^0 C
2:1 Ag:Au	cracking	30 seconds	24 hours, 300^0 C
2:1 Ag:Au	cracking	20 seconds	24 hours, 300^0 C

Figure 43 shows the SEM image of nanoporous gold electrode. The nanoporous, bicontinuous ligament/pore structure can be seen after two hours etching in concentrated nitric acid. The pore size can be tailored by monitoring the etching time in the acid. Longer etching time generates bigger pores with smaller surface area.

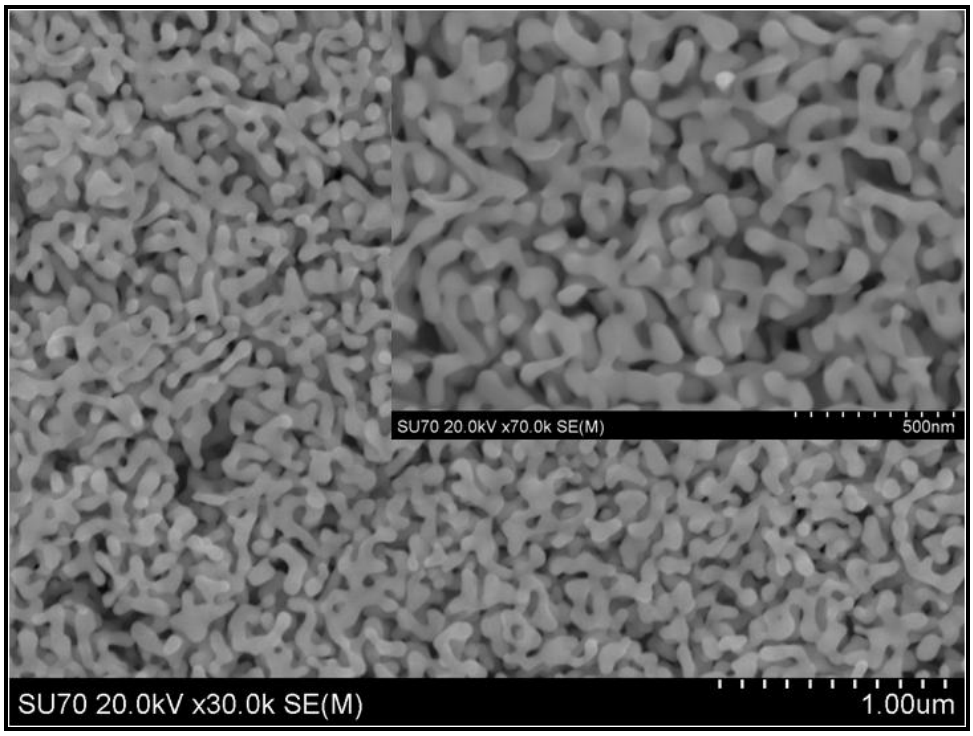

Figure 43: SEM Image of nanoporous gold electrode

The mechanism of etching has been explained by Erlebacher and co-workers using a Monte Carlo model.[132],[133]. When the electrode is immersed in nitric acid, selective dealloying takes place. The more noble metal (gold) stays intact whereas, less noble metal (silver) is dealloyed. The process of etching starts at the interface of the electrode surface and acid.[132] The less noble atoms start dissolving, leaving behind the gold atoms that diffuse to the surface.[132] During etching, the gold atoms move around and form clusters.[132] This allows the acid to penetrate into the lower layers and etch more silver atoms.[132] With the passage of time, the gold clusters coarsen and form 3D hills. With continued etching, the hills are undercut and the bulk of the film is etched by the acid.[132] Longer the electrode stays in the acid, more silver atoms are depleted. These processes are shown in Figure 44.

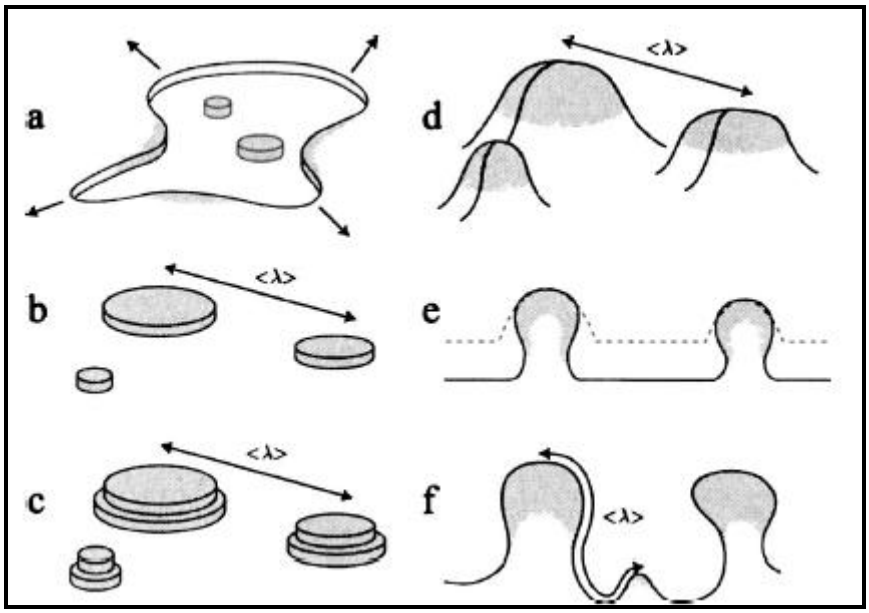

Figure 44: Mechanism of etching.

Reprinted with Permission from Ref. 132, Copyright 2004. The Electrochemical Society

In order to deduce the elemental composition post etching, the electrode was analysed by Energy Dispersive X-ray Spectroscopy (EDX) and the results shown in Figure 45 and Table 5. The silver was found to be 2.07 weight % which indicated that most of the silver had been dealloyed and would not interfere with the electrochemical measurements.

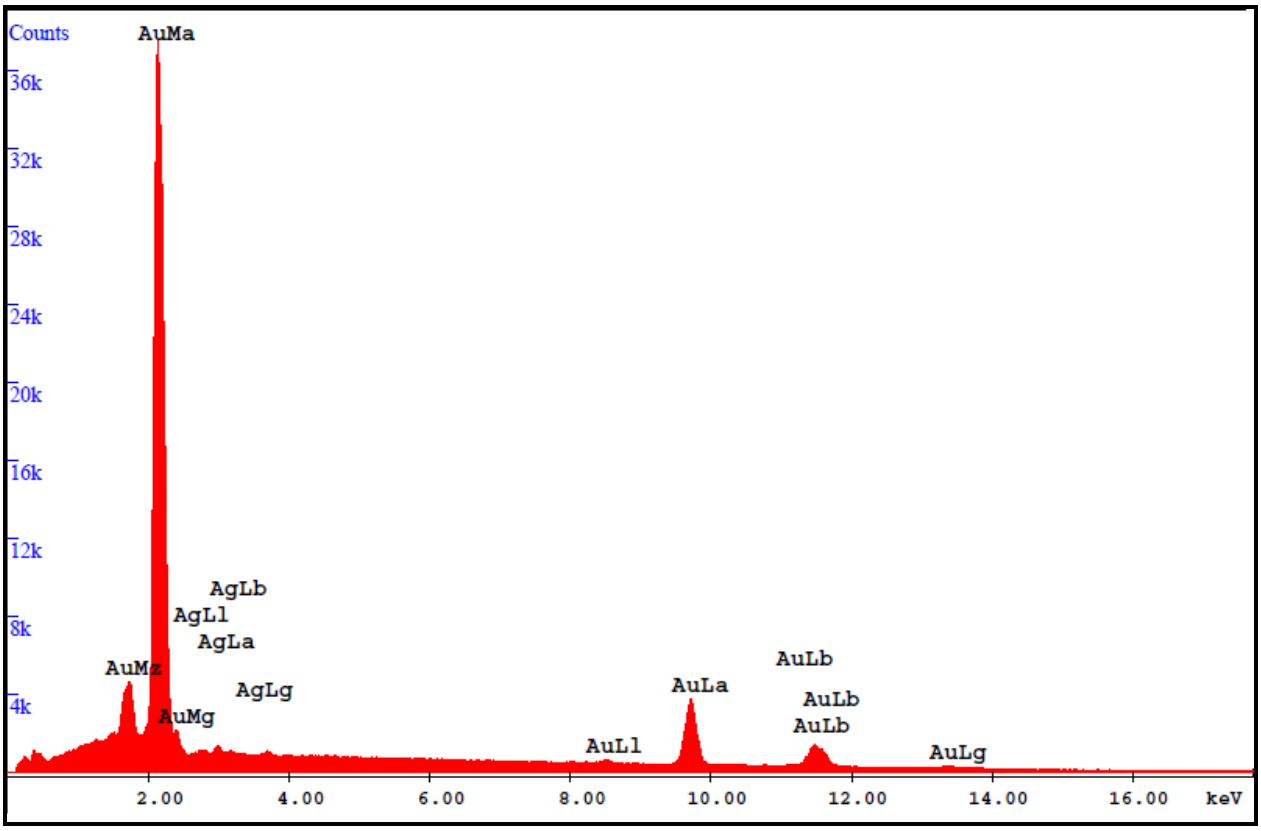

Figure 45: EDX spectrum of the nanoporous gold electrode

Table 5: EDX elemental composition of the ridge of nanoporous gold electrode

EDAX ZAF Quantification (Standardless)
Element Normalized
SEC Table : Default

Element	Wt %	At %	K-Ratio	Z	A	F
AgL	2.07	3.71	0.0110	1.0997	0.4857	1.0000
AuL	97.93	96.29	0.9758	0.9963	1.0001	1.0000
Total	100.00	100.00				

Modifying parameters like deposition potential, deposition time, thickness of the film, alloy composition and etching time can help fabricate an electrode of desired morphology. The

following chapter will explain the electrochemical and surface fouling studies carried out using these electrodes.

CHAPTER 4: ELECTROCHEMISTRY

Electrochemical experiments were performed using the high surface area electrodes described in the proceeding chapters and comparisons made to unmodified flat gold electrodes. Electrochemical experiments involved running cyclic voltammograms (CVs) in electrolytes containing redox molecules exhibiting fast electron transfer, redox molecules with slow electron transfer, measurement of surface area, testing surface fouling with redox molecules that adsorb on the surface and testing the electrodes' ability to detect dopamine in the presence of ascorbic acid. Using the data obtained from the CVs, the faradaic and non-faradaic currents were measured.

4.1 Surface Area Measurement

In order to determine the surface area of the electrodes, CV curves were run in 0.5 M sulphuric acid at a scan rate of 50 mV/s from 0.2 V to 1.8 V. An adhesive tape with a $1/8^{th}$ of an inch diameter hole was attached to the surface of the electrode to define the electroactive area of the electrode. The ratio of the real surface area to geometric area gives the roughness factor.[73] The geometric area in this case is the spherical area defined by the hole in the tape while the area obtained by integrating the area under the gold oxide reduction peak is the "real" surface area. Figure 46 shows a typical CV scan recorded in 0.5 M sulphuric acid.

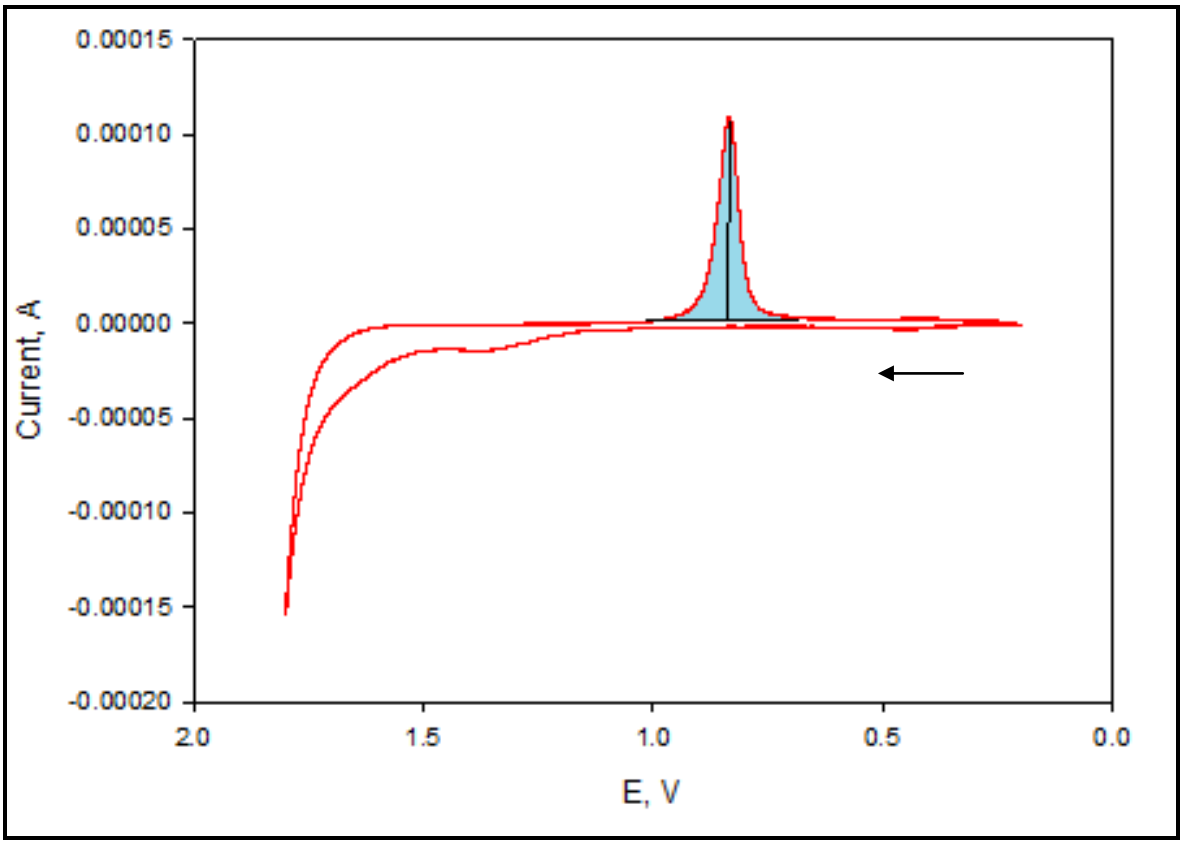

Figure 46: Cyclic voltammogram of flat gold electrode in 0.5 M H_2SO_4. Scan rate: 50 mV/s

In the forward scan that runs from 0.2 V to 1.8 V, gold is oxidised. During the reverse scan from 1.8 V to 0.2 V, a prominent gold oxide reduction peak at around 0.7 V is observed. The area under this peak (shaded region) can be integrated to find out the amount of gold oxide formed during the oxidation cycle. As the area of the electrode increases, the current increases thus increasing the height of the gold oxide reduction peak, Figure 47.

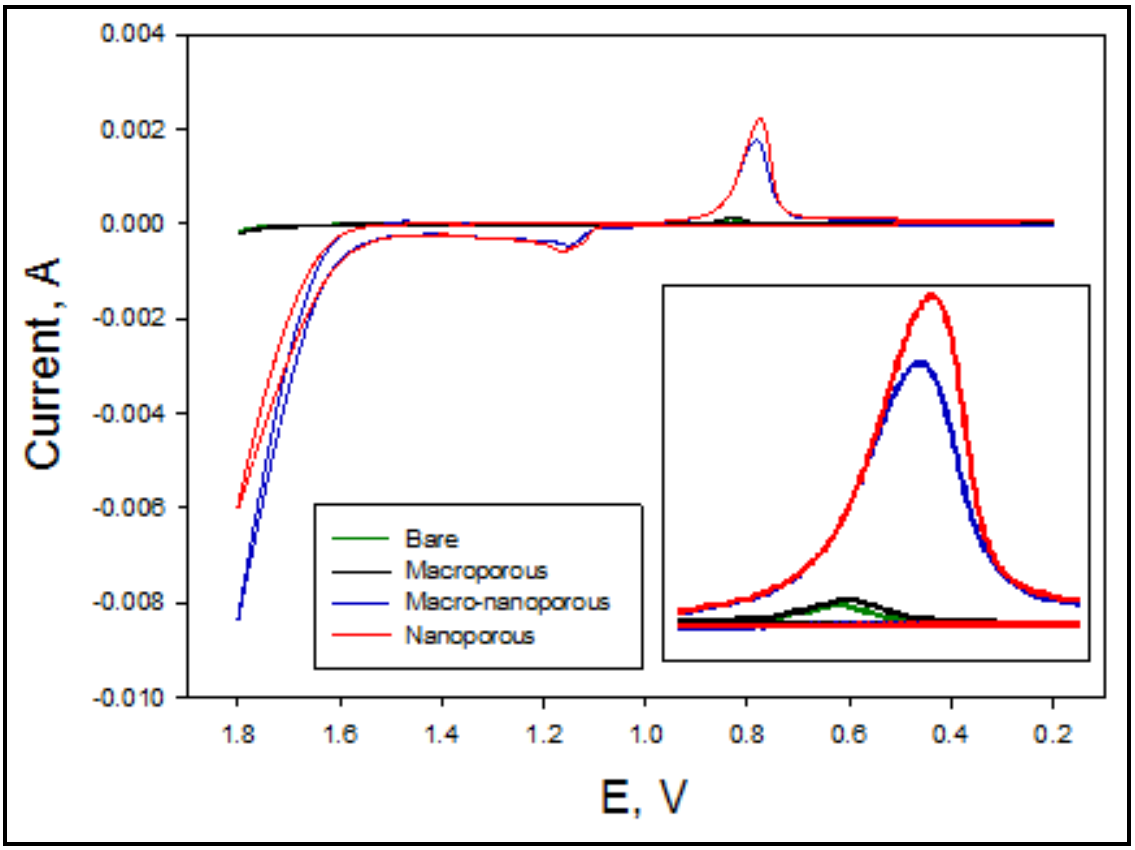

Figure 47: Surface area CV curves of flat, macroporous, macro-nanoporous and nanoporous gold electrodes. Scan rate: 50 mV/s

Figure 47 shows the surface area CV scans of all the electrodes. The inset in the figure shows the magnified gold oxide reduction peaks of the electrodes: flat gold displays the smallest peak and nanoporous gold the highest.

Table 6: Table displaying the surface areas of electrodes and their roughness factors

Electrode	***Surface Area cm^2***	***Geometric Area cm^2***	***Roughness Factor***
Flat	0.0973 ± 0.016	0.078	1.25
Macroporous	0.135 ± 0.009	0.078	1.73
Macro-nanoporous	2.04 ± 0.43	0.078	26.2
Nanoporous	2.53 ± 0.5	0.078	32.4

Table 6 compares the surface areas of macroporous, macro-nanoporous and nanoporous gold electrodes to the flat gold electrode. The charge required to reduce the gold oxide peak (shown in figure 46) is measured and is divided by the conversion factor of 0.4 mC/cm^2.[134] This gives us the real surface area. The geometric surface area defined by the circular hole with radius of 0.159 cm was 0.078 cm^2. The ratio of real surface area to geometric area gives the roughness factor. As expected the nanoporous gold electrode has the highest area on account of the presence of nanopores while macro-nanoporous has an area less than nanoporous but higher than macroporous gold electrode.

4.2 Cyclic Voltammetry in Different Redox Molecule Solutions

As explained in the first chapter, cyclic voltammetry (CV) involves measuring the current as the potential is scanned linearly with time. The switching potential is set such that the oxidation and reduction of the redox molecule occurs between the two set potentials. In all the cyclic voltammetric experiments a three electrode assembly was used: silver wire as the reference electrode, platinum wire as the counter electrode and flat or high surface area gold electrode as the working electrode. Cyclic Voltammograms (CVs) were tested for two kinds of redox molecules – (a) Kinetically reversible redox molecules with fast electron transfer (b)

quasireversible and irreversible redox molecules with slow electron transfer. Figure 48 below, shows the fast and slow electron transfer at an electrode surface.

Figure 48: Fast and slow electron transfer at a porous electrode surface. Red and blue dots show the oxidized and reduced species of the redox molecule.

In case of fast electron transfer, the reduced moiety or the oxidized moiety (red and blue dots in figure 48) exchange electrons rapidly at the electrode surface and as a result their concentration depletes rapidly at the outer surface. Hence, the oxidized or reduced forms of the redox molecule do not enter the pores. In case of slow electron transfer, the concentration of the oxidized or reduced forms does not deplete rapidly due to slow electron transfer but they actually enter the pores where the half reaction reaches completion. As a result, a majority of the electrode surface area is used giving amplified current responses – particularly to redox molecules exhibiting slow electron transfer.[2]

4.2.1 Potassium Ferricyanide in KCl

Potassium Ferricyanide is a reversible redox molecule that exhibits relatively fast electron transfer at the electrode surface. 1 mM of $Fe(CN)_6^{3-}$ was prepared in 0.1 M KCl as the supporting electrolyte and CVs were run at a scan rates of 25, 50 and 100 mV/s (Figure 49).

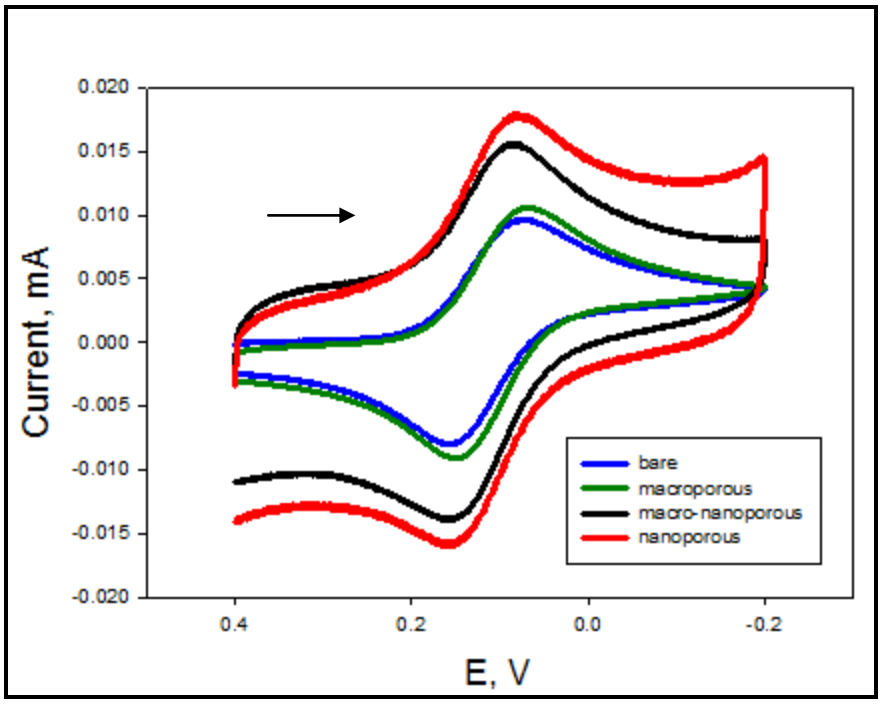

Figure 49: CV scans in 1mM Potassium Ferricyanide in 0.1 M KCl obtained using flat, macroporous, macro-nanoporous and nanoporous gold electrodes. Scan rate: 50 mV/s.

The Faradaic peak current, in case of a reversible redox molecule is given by Randles-Sevcik equation:

$$I_p = 2.69 \times 10^5 \, n^{3/2} \, A \, D^{1/2} \, v^{1/2} \, C \qquad \text{(equation 1)}$$

I_p = peak current in A, n = number of electrons, A = area of the electrode in cm^2, D = Diffusion coefficient in cm^2/s, v = scan rate in V/s, C = concentration in mol/cm^3

As can be deduced from the equation 1, the peak current is directly proportional to the area of the electrode. Hence, the current in Figure 49 should increase with the area of the working electrode. For flat, macroporous and macro-nanoporous the faradaic peak current is 9.29, 12.55 and 14.17 microamperes. Nanoporous exhibits the highest current and the unmodified flat gold electrode the lowest. The capacitance of the electrode is directly proportional to the area of the

electrode. Equation 2 shows the charging current proportional to the area of the electrode. Hence, nanoporous gold electrode shows the highest charging current and capacitance of all the electrodes.

$$I_c = AvC \qquad \text{(equation 2)}$$

Where I_c = non-faradaic current in Amperes, v = scan rate in V/s, A = area in cm^2 and C = capacitance in $\mu F/cm^2$.

As can be deduced from equation 1, current is directly proportional to the square root of scan rate for a kinetically reversible redox molecule. This plot is shown in Figure 50 below.

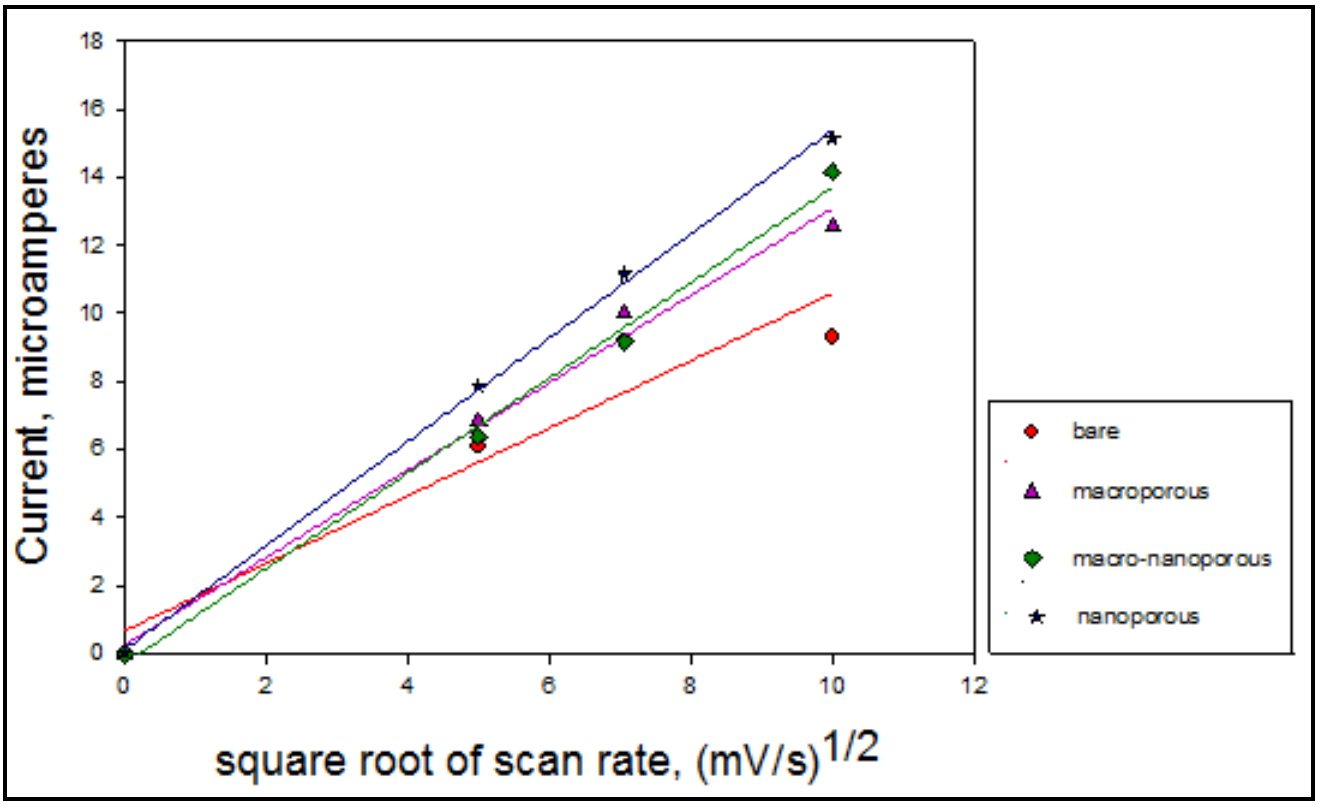

Figure 50: Plot of cathodic peak current versus square root of scan rate for potassium ferricyanide

The differences in the cathodic peak current among the electrodes become more apparent at higher scan rates: nanoporous gold gives the highest current and unmodified flat gold the lowest. This is because faster scan rates reduce the time scale of a CV run which doesn't deplete the concentration of oxidized species as fast as it happens at slow scan rates. This gives some of the oxidized species a chance to enter the pores of the electrode surface and use more surface area. As we can see, the current values for flat gold are not exactly linear. Ideally, the slope of the curve is directly proportional to the surface area of the electrode. As can be seen from the data in Table 7, the slopes of the electrodes are only slightly higher from each other. This is because, as explained earlier, the entire surface area isn't being used due to the fast electron transfer. Had the entire surface area of the electrodes been used, the faradaic peak current values for flat, macroporous, macro-nanoporous and nanoporous gold electrodes would have been higher giving higher slopes than the ones deduced experimentally. Table 8 below shows the slope values calculated using Randles-Sevcik equation. The experimental slope is used to calculate the diffusion coefficient of the redox molecule which, in turn, is used to calculate the faradaic peak current had the entire real surface area of the electrode been used. As expected, there is a significant difference between the experimental and theoretical slope values. Since majority of the real surface area is being unused due to fast electron transfer, the experimental slope values are much lower than the theoretical values.

Table 7: Regression analysis data obtained from the plot of cathodic peak (experimental) current versus square root of scan rate

Electrodes	***R^2***	***Slope ($\mu A.s^{1/2}/(mV)^{1/2}$)***	***Intercept (μA)***
Flat	0.919	0.992	0.674
Macroporous	0.991	1.282	0.264
Macro-nanoporous	0.994	1.399	-0.292
Nanoporous	0.999	1.524	0.133

We used the data obtained from the graph to calculate the diffusion coefficients which were then used to calculate the theoretical slope values i.e. the slope values obtained had the entire surface area of the electrode been used. This data is displayed in Table 8.

Table 8: Regression analysis data obtained from the plot of theoretical cathodic peak current versus square root of scan rate

Electrodes	***R^2***	***Slope ($\mu A.s^{1/2}/(mV)^{1/2}$)***	***Intercept (μA)***	***Diffusion coefficient (cm^2/s)***
Flat	1	1.23	0.0009	1.495E-05
Macroporous	1	2.21	0.0025	1.932E-05
Macro-nanoporous	1	36.7	-0.0191	2.12E-05
Nanoporous	1	49.4	-0.0083	2.297E-05

In order to ensure complete usage of the electrode area, redox molecules with slower electron transfer should be used.

Table 9: Peak splitting and faradaic current values for flat, macroporous, macro-nanoporous and nanoporous gold electrodes at different scan rates

Scan rate (mV/s)	Voltammetric data	Flat	Macroporous	Macro-nanoporous	Nanoporous
25	I_p (A)	6.09E-06	6.81E-06	6.37E-06	7.87E-06
	ΔE_p (V)	0.076	0.071	0.070	0.076
50	I_p (A)	9.19E-06	9.99E-06	1.05E-05	1.11E-05
	ΔE_p (V)	0.085	0.082	0.070	0.077
100	I_p (A)	9.29E-06	1.25E-05	1.41E-05	1.51E-05
	ΔE_p (V)	0.098	0.091	0.077	0.085

Table 9 gives a summary of voltammetric data obtained from the cyclic voltammetric scans for all electrodes in potassium ferricyanide at three different scan rates. The peak splitting for reversible reactions is 0.059 /n where n = number of electrons exchanged in the redox reaction in a completely reversible reaction. The peak splitting values obtained are slightly higher than 0.059 V at a low scan rate of 25 mV/s. As the scan rate increases to 50 and eventually 100 mV/s, differences in the peak splitting become more apparent, in that the peak splitting increases. It's interesting to note that peak splitting at a scan rate of 50 mV/s and 100 mV/s for macro-nanoporous and nanoporous gold electrodes is slightly less than the unmodified flat and macroporous gold electrode. Nanoporous gold and macro-nanoporous gold electrodes show better performance as compared to the flat gold electrode at higher scan rates.

4.2.2 Cyclic Voltammetry in KCl

This section involves measurement of non-Faradaic current by running CVs in 0.1 M KCl over the potential range of 0 V to 0.45 V.

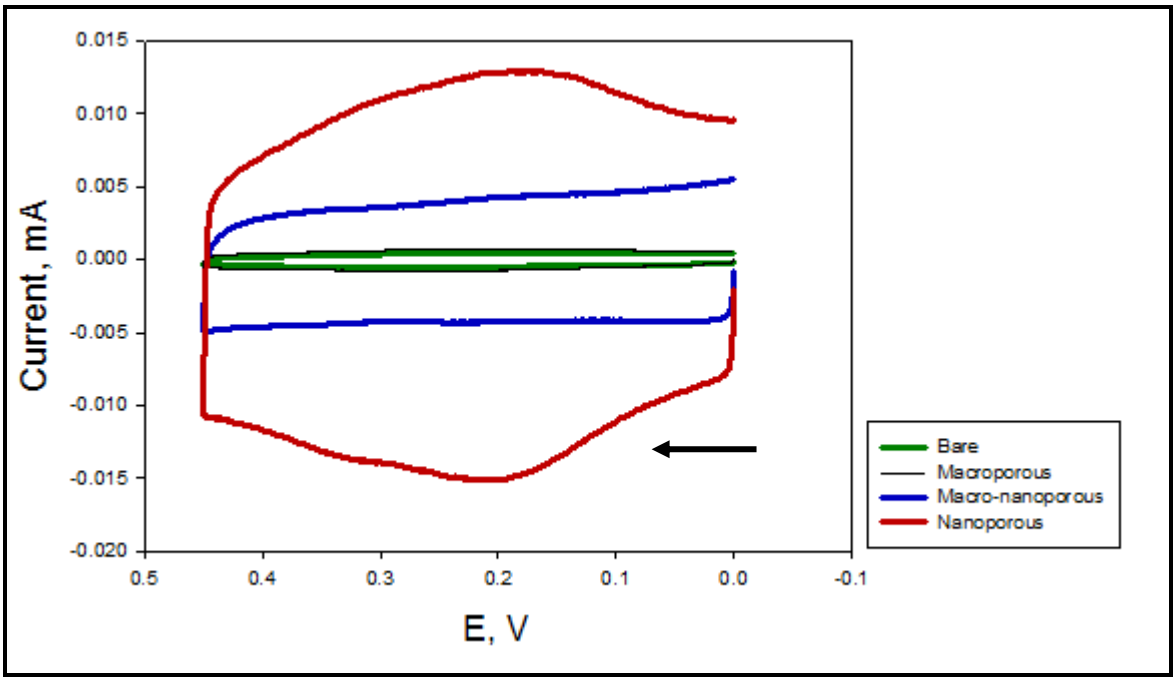

Figure 51: CVs of flat, macroporous, macro-nanoporous and nanoporous in 0.1 M KCl. Scan rate: 50 mV/s

Non-faradaic current is given by the following equation

$$I_c = AvC \qquad \text{(equation 2)}$$

Where I_c = non-faradaic current in Amperes, v = scan rate in V/s, A = area in cm^2 and C = capacitance in $\mu F/cm^2$.

As can be deduced from equation 2, non-Faradaic current is directly proportional to the area of the electrode, scan rate and the capacitance. The capacitance, on application of the potential, is typically in the range of 10-40 $\mu F/cm^2$ for metal electrodes.[135] Figure 50 shows a graph of non-Faradaic current measured at 0.05 V as a function of scan rate. As expected, linear plots are obtained with nanoporous as the steepest slope. Table 10 shows regression analysis data of the plot of charging current versus scan rate.

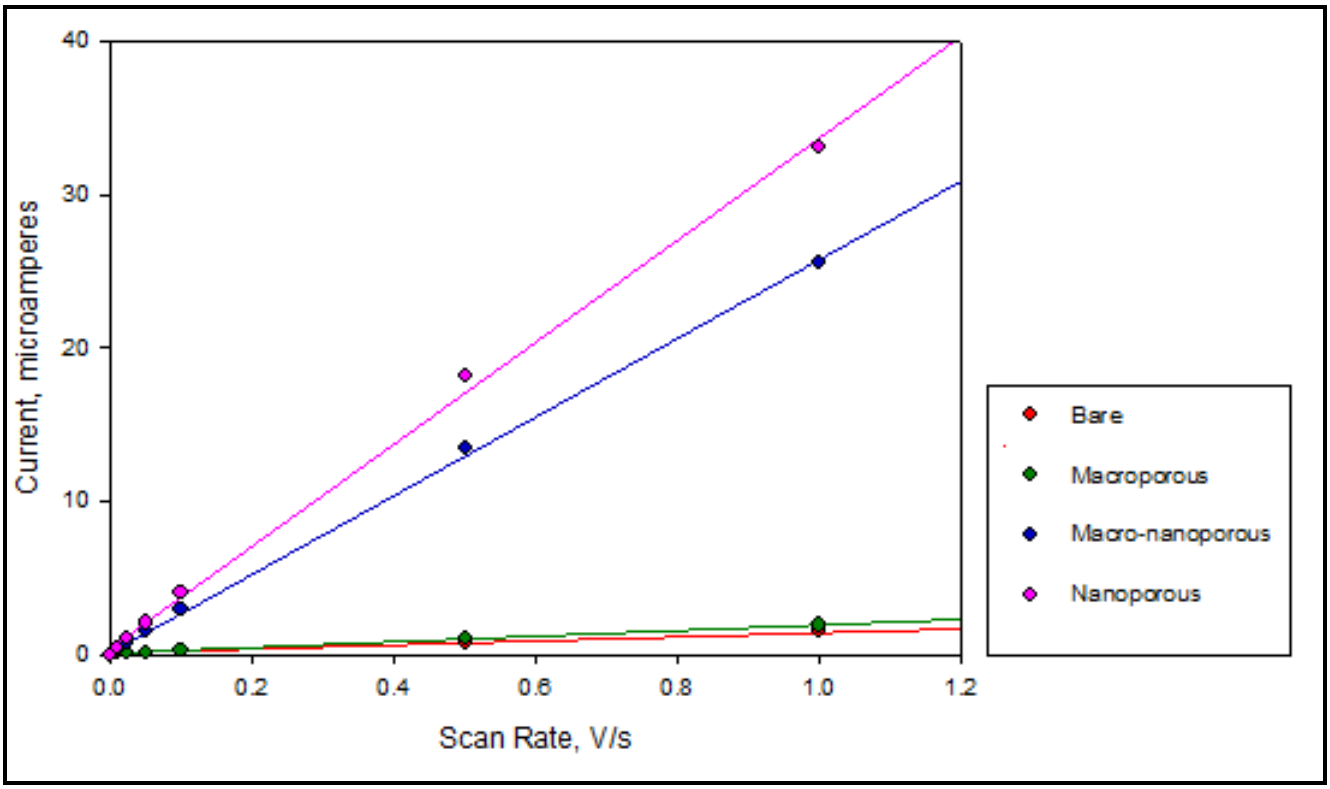

Figure 52: Plot of Charging Current versus Scan Rate in 0.1 M KCl

Table 10: Regression analysis data obtained from the plot of charging current versus scan rate

Electrode	R^2	Slope(μA.s.V^{-1})	Intercept (μA)
Flat	0.9964	1.42	0.055
Macroporous	0.9988	1.87	0.047
Macro-nanoporous	0.9995	25.6	0.197
Nanoporous	0.9979	33.2	0.402

The slopes get increasingly steeper with increasing surface area of the electrode. The slope of nanoporous, macro-nanoporous and macroporous gold electrode is 23, 18 and almost 2 times higher than the flat gold electrode.

4.2.3 Ferrocene Methanol in KCl

Just like potassium ferricyanide, ferrocene methanol is a reversible redox molecule that exhibits fast electron transfer. Flat, macroporous, macro-nanoporous and nanoporous gold electrodes were used to obtain CV curves shown in Figure 53. As expected, the nanoporous and macro-nanoporous gold electrodes show higher peak and capacitive currents as compared to the flat gold electrode owing to their high surface area.

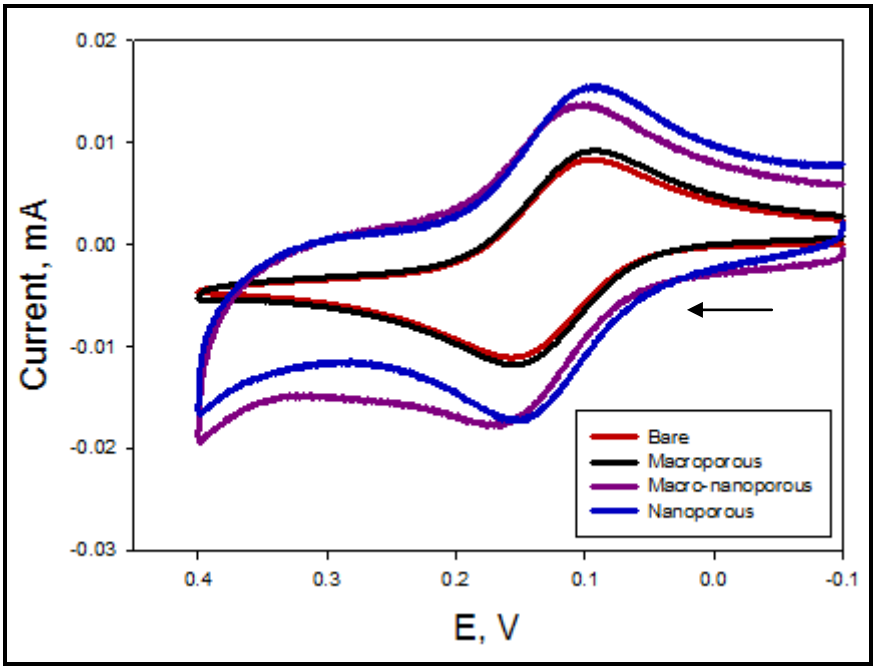

Figure 53: CV curves in 1mM Ferrocene methanol in 0.1 M KCl obtained using flat, macroporous, macro-nanoporous and nanoporous gold electrodes. Scan Rate: 50 mV/s.

Table 11 below shows peak splitting, ΔE_p values obtained for flat and porous gold electrodes in 1 mM Ferrocene methanol in 0.1 M KCl.

Table 11: Peak Splitting data obtained from CV runs carried out using flat, macroporous, macro-nanporous and nanoporous gold electrodes in 1mM ferrocene methanol in 0.1 M KCl

Scan rate (mV/s)	Voltammetric data	Flat	Macroporous	Macro-nanoporous	Nanoporous
25	ΔE_p (V)	0.060	0.058	0.063	0.061
50	ΔE_p (V)	0.065	0.065	0.067	0.065
100	ΔE_p (V)	0.067	0.064	0.066	0.065

Ferrocene methanol, being a kinetically reversible redox molecule, shows peak splitting values around 59 mV/n for all electrodes at a low scan rate of 25 mV/s. For a reversible process, current is directly proportional to square root of scan rate as exhibited in Figure 54. Hence, at higher scan rates higher peak current values are observed.

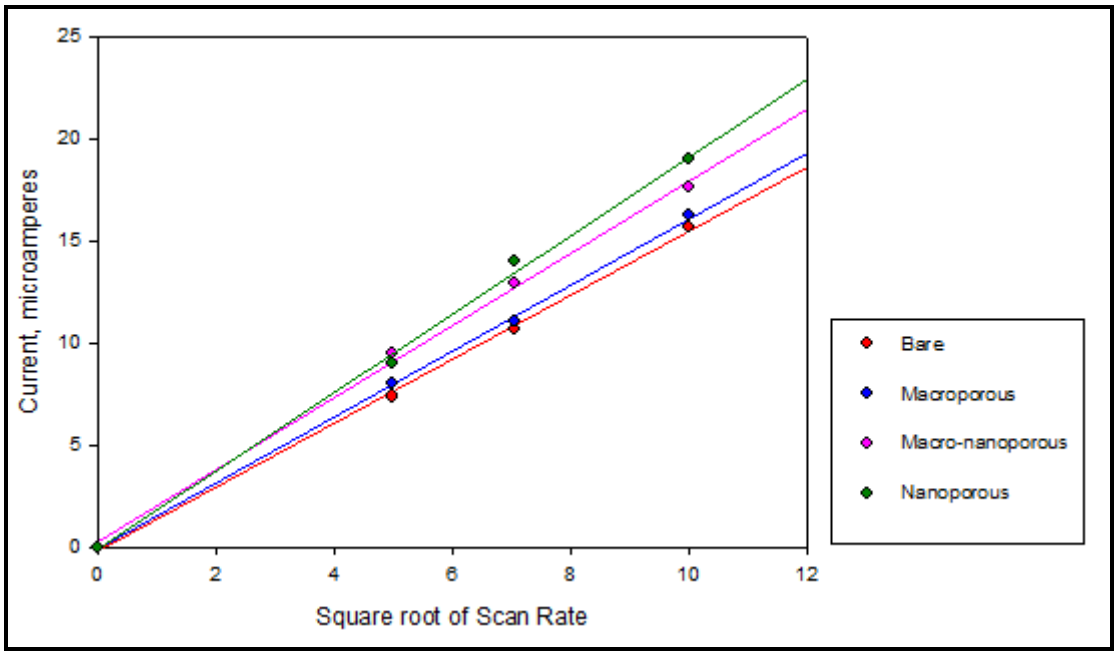

Figure 54: Plot of peak current versus square root of scan rate for Ferrocene Methanol

Table 12 below shows the regression analysis data of the plot of peak current versus square root of scan rate for ferrocene methanol. As explained earlier, most of the area of the electrode remains unused for redox molecules with fast electron transfer and hence the slopes values, although steeper with increasing area, do not significantly differ from each other.

Table 12: Regression analysis data for plot of peak current versus square root of scan rate for Ferrocene Methanol

Electrodes	***R^2***	***Slope*** ***($\mu A.s^{1/2}/(mV)^{1/2}$)***	***Intercept (μA)***
Flat	0.9985	1.56	-0.18
Macroporous	0.9991	1.61	-0.068
Macro-nanoporous	0.9981	1.77	0.235
Nanoporous	0.9972	1.91	-0.097

The signal is further amplified due to higher surface areas: nanoporous gives the highest peak current and flat gold electrode the lowest. The charging current or non-Faradaic current, i_c, is directly proportional to the scan rate and area and hence at fast scan rates, high capacitance is observed for high surface area electrodes.

4.2.4 Dopamine

Cyclic Voltammetric curves were run in 0.2 mM dopamine in 7.4 pH buffer from -0.1 V to 0.5 V (shown in Figure 55 below).

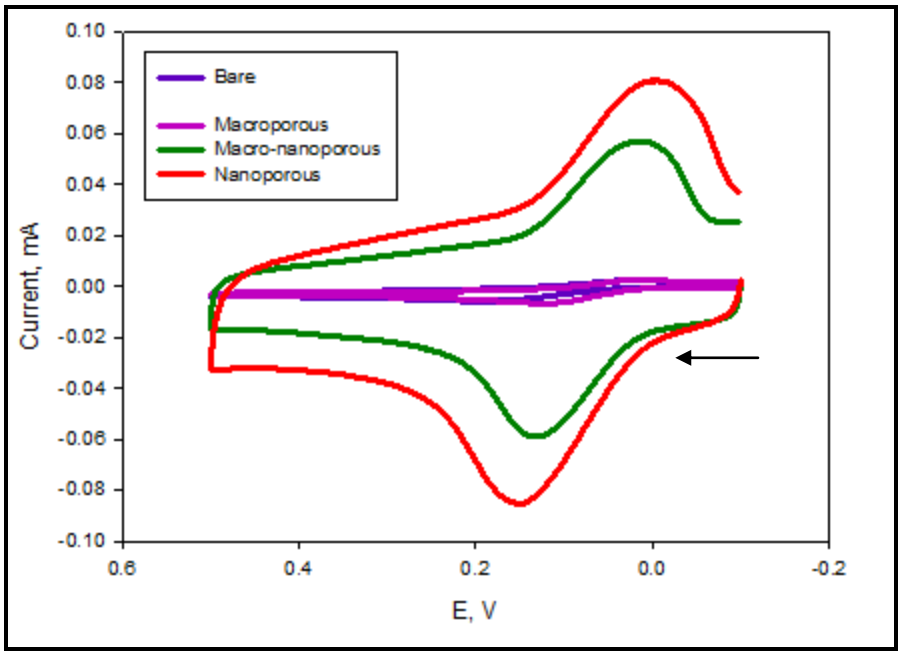

Figure 55: Cyclic Voltammetry in 0.2 mM Dopamine in 0.1 M PBS Buffer (pH 7.4). Scan Rate: 100 mV/s

Oxidation occurs in the first cycle when the potential is scanned from -0.1 V to 0.5 V. As the potential gets more positive, dopamine is slowly oxidized to o-dopaminoquinone (DAQ).[12] The anodic peak is observed around 0.15 V. When the potential is switched and gradually becomes less positive, the DAQ is reduced back to dopamine giving a cathodic peak at around -0.003 V. As can be observed, the anodic peak current is much higher than the cathodic peak current which indicates that the reaction is chemically reversible. The peak currents increase with the increasing surface area of the electrodes: nanoporous giving the highest peak current followed by macro-nanoporous and macroporous gold electrodes

Table 13: Peak positions and peak splitting values of flat, macroporous, macro-nanoporous and nanoporous gold electrodes. Scan rate: 100 mV/s

Electrodes	Anodic peak (V)	Cathodic peak (V)	ΔE_p (V)
Flat	0.194	0.020	0.174
Macroporous	0.125	0.015	0.11
Macro-nanoporous	0.133	0.014	0.119
Nanoporous	0.151	-0.003	0.154

Table 13 above shows the positions of anodic and cathodic peaks observed on flat, macroporous, macro-nanoporous and nanoporous gold electrodes. The peak splitting decreases in case of high surface area porous gold electrodes as compared to that of the flat gold electrode. This agrees well with the results reported in the literature before.[136],[12]. This can be attributed to the fact that the high surface area gold electrodes show better catalytic ability due to better electron transfer than the flat gold electrode. A large amount of surface area is utilized by the redox molecule due to slow electron transfer giving high peak currents for all the porous gold electrodes.

4.2.5 Ascorbic Acid

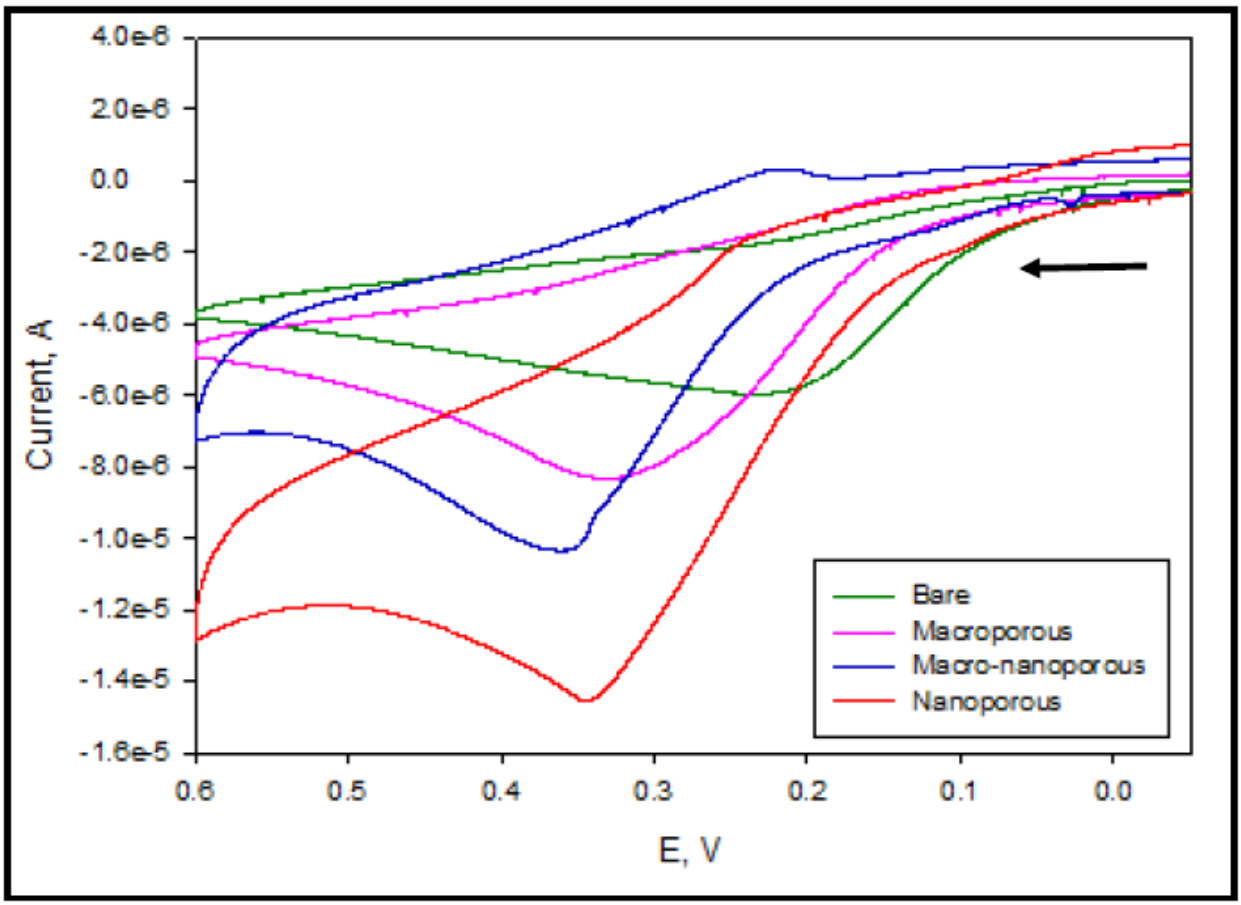

Figure 56: CV curves of flat, macroporous, macro-nanoporous and nanoporous gold electrodes in 1 mM ascorbic acid in 0.1 M PBS buffer (pH 7). Scan rate: 50 mV/s

Figure 56 shows CV curves in 1 mM ascorbic acid in pH 7 PBS buffer scanned from -0.1 V to 0.6 V. The peak observed at a positive potential can be attributed to the ascorbic acid oxidation. No cathodic peak is observed in the figure above because oxidation of ascorbic acid is a chemically irreversible process. The peak current increases with the area of the electrode as the inner surface of the pores get utilized.

4.3 Surface Adsorption of Dopamine on the Electrodes

Dopamine is known to adsorb on the surface of an electrode and foul it. In order to compare the effect of fouling of dopamine on the flat gold electrode and the porous gold electrodes, we ran successive cyclic voltammogram cycles in 0.2 mM dopamine in pH 7 buffer and measured the cathodic and anodic peak current.

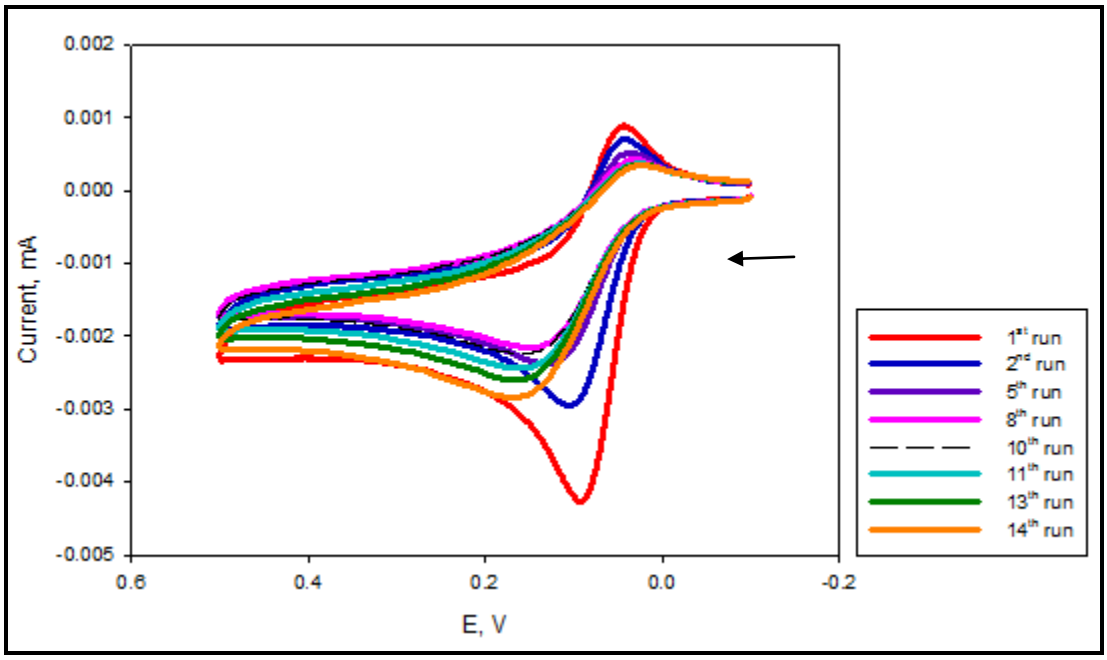

Figure 57: Successive cyclic voltammetric (CV) scans of flat gold electrode in 0.2 mM dopamine in 0.1 M pH 7 PBS Buffer. Scan rate: 25 mV/s

Figure 57 above shows successive CV scans of flat gold electrode in 0.2 mM dopamine. Two peaks are observed in the figure: The one at 0.06 V is the oxidation peak is due to the o-dopaminoquinone (DAQ) and, once the potential is switched, the reduction peak is observed at 0.04 V which can be attributed to the reduction of DAQ to dopamine. We recorded the first, second, fifth, eighth, tenth, eleventh, thirteenth and fourteenth successive scans to observe the effect of adsorption on the cathodic and anodic current.

Table 14: Decrease in the cathodic and anodic current of the flat gold electrode with each successive CV scan

CV Run	Percentage of Cathodic Current	Percentage of Anodic Current
1st	100 %	100 %
2nd	78.8 %	67 %
5th	57.8 %	52.5%
8 th	49.5 %	45.8 %
10 th	43 %	47.6 %
11 th	42 %	52.7 %
13 th	40 %	56.3 %
14 th	38.4 %	62 %

From the data displayed in Table 14 we can deduce that there is a significant decrease in the cathodic peak current for first three scans since dopamine is being adsorbed on the surface of the unmodified flat gold electrode. The current continues to decrease from the 10th scan onwards and although the decrease isn't as significant as the first four scans, it is still a notable decrease in the peak current. For the anodic peak current, the current shows a slight increase from the 10th run onwards probably because of having achieved a pseudo-steady state.

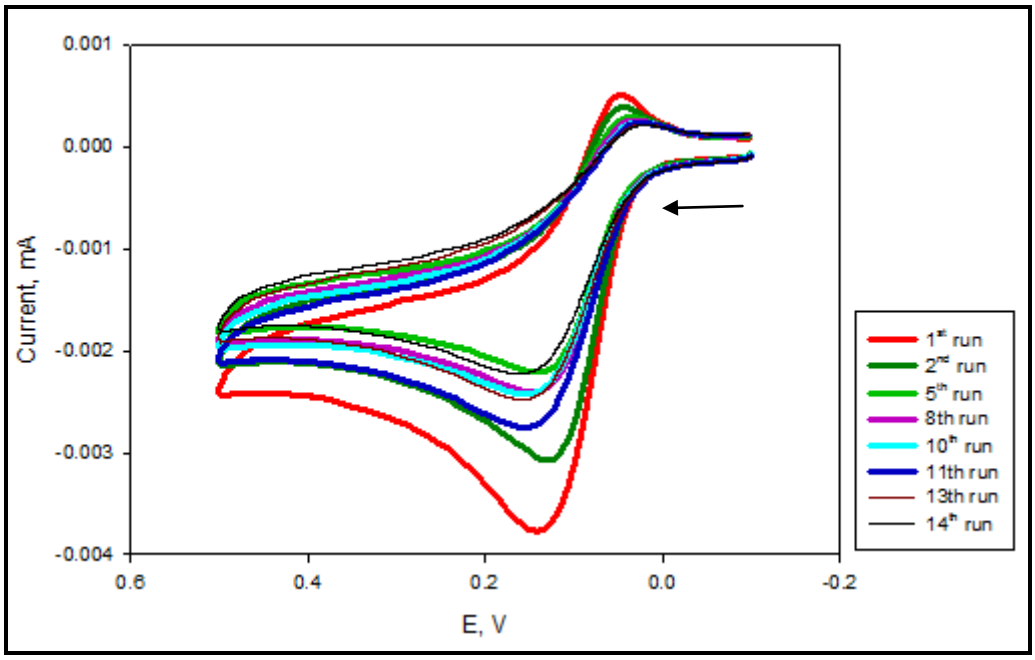

Figure 58: Successive cyclic voltammetric (CV) scans of macroporous gold electrode in 0.2 mM dopamine in 0.1 M pH 7 PBS buffer. Scan rate: 25 mV/s

Successive scans for macroporous gold electrode in 0.2 mM dopamine in pH 7 buffer were recorded (shown in Figure 58). We didn't expect as significant a decrease in the anodic current as was observed for the flat gold electrode because of the presence of macropores.

Table 15: Decrease in the cathodic and anodic current of the macroporous gold electrode with each successive CV scan

CV Run	Percentage of Cathodic Current	Percentage of Anodic Current
1st	100 %	100 %
2nd	77 %	80.5 %
5th	57.5 %	54.7 %
8 th	51.5 %	59.7 %
10 th	47 %	59.7 %
11 th	45.5 %	69.7 %
13 th	42 %	62 %
14 th	41 %	54.2%

As observed for the flat gold electrode, the decrease in the cathodic peak current is high for the first 5 scans since dopamine is being adsorbed on the surface and covering the macropores with each successive scan. Although the values of macroporous gold electrode are slightly better than the flat gold electrode values, we can conclude that the presence of macropores hasn't brought about a major change in the behaviour of the electrode as far as adsorption of dopamine is concerned. For the anodic peak current, after the initial decrease in the current, the current shows slight increase for the 10th run and 11th run before decreasing again.

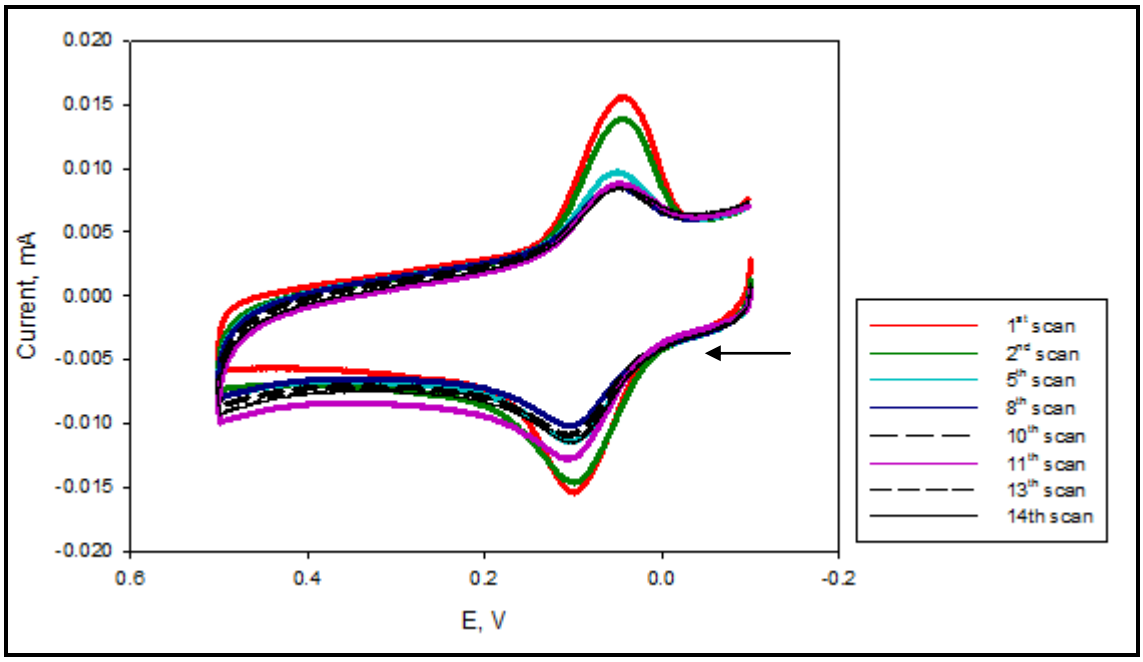

Figure 59: Successive cyclic voltammetric (CV) scans of nanoporous gold electrode in 0.2 mM dopamine in 0.1 M pH 7 PBS buffer. Scan rate: 25 mV/s

Table 16 below gives the cathodic peak and anodic peak current percentage for the nanoporous gold electrode. The rapid decrease in the first three scans was expected as dopamine is being adsorbed on the surface of the electrode. In case of the cathodic current, the values of the peak current become fairly stable after the 5th scan and remain consistent till the 14th scan. For the anodic peak current, the current shows a large drop as expected for the first three runs. For the 10th run onwards, the current increases slightly and then shows slight fluctuations probably because of the pseudo-steady state as explained earlier.

Table 16: Decrease in the cathodic and anodic current of the nanoporous gold electrode with each successive CV scan

CV Run	Percentage of Cathodic Current	Percentage of Anodic Current
1st	100 %	100 %
2nd	89 %	90.5 %
5th	62.5 %	56.1 %
8 th	55.4%	45.5 %
10 th	55 %	56 %
11 th	56.5 %	77.9 %
13 th	54.7 %	50.7 %
14 th	54.3 %	54.8 %

Another parameter that needs to be drawn attention to is the peak splitting, ΔE_p. For a redox molecule with adsorbing properties, peak splitting increases significantly with each scan. This is because, the molecule adsorbing on the surface is blocking the active sites, thus slowing down the electron transfer that manifests itself and increases ΔE_p. In Figure 57, the CV scans of dopamine performed on the flat electrode show shift in the peak positions indicating an increase in the peak splitting. A small change in peak positions is observed for macroporous gold electrode while none is observed for nanoporous gold electrode. This might be because of the morphology of the nanoporous electrode. It offers more active sites that improve the electron transfer than planar gold and hence the low peak splitting. More dopamine experiments need to be conducted on nano and macro-nanoporous to see if these results are reproduced.

4.4 Detection Dopamine (DA) in the Presence of Ascorbic Acid

A Differential Pulse Voltammetry (DPV) experiment was performed to see if a low concentration of dopamine could be detected in the presence of an increasing concentration of ascorbic acid.

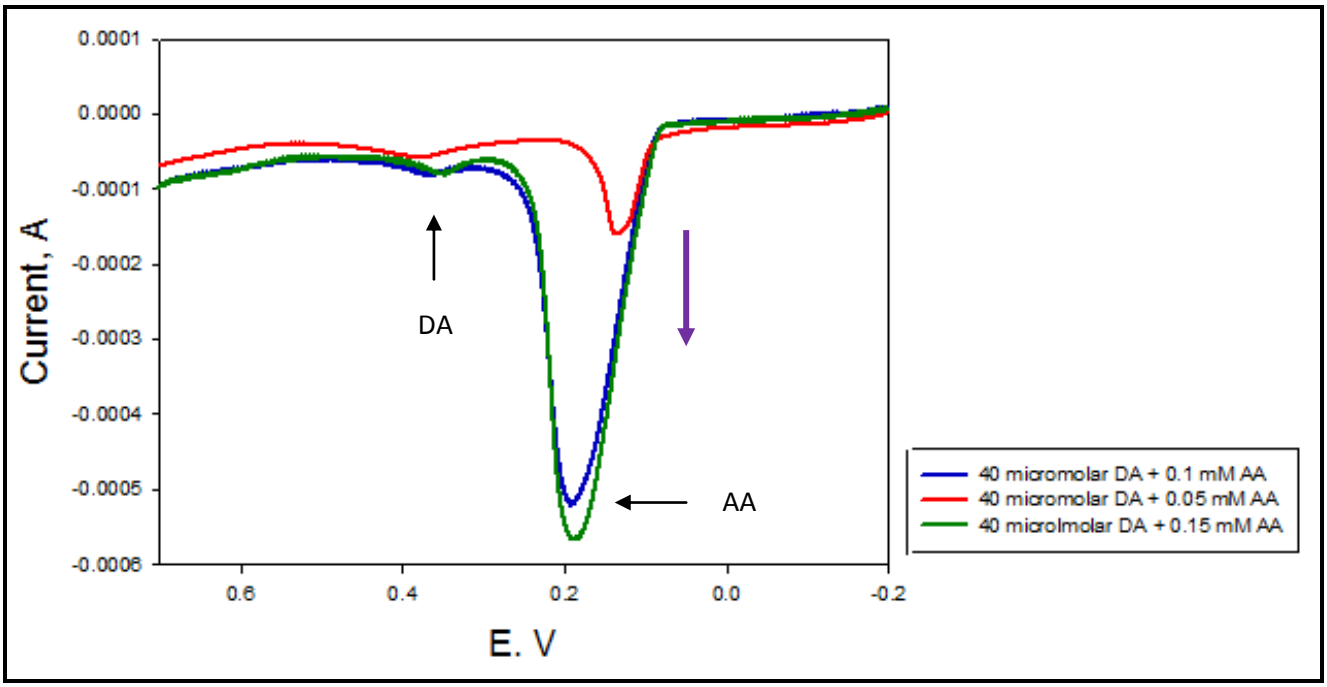

Figure 60: DPV response of macro-nanoporous gold electrode to increasing concentrations of AA in presence of 40 micromolar DA. Scan rate: 100 mV/s

The DPV scan was run from -0.2 V to 0.8 V at 100 mV/s. As the CV runs in the earlier sections exhibit, the oxidations peaks of dopamine and ascorbic acid are very close to each other and it's often difficult to resolve the peaks.[70] DAQ (o-dopaminoquinone) plays a role in the catalytic oxidation of ascorbic acid.[70] As a result, ascorbic acid often interferes in the detection of dopamine. Hence, we decided to test the differential pulse voltammetry (DPV) response of macro-nanoporous gold electrode to a mixture of dopamine and ascorbic acid to see if the two peaks could be resolved. We kept the concentration of dopamine fixed while we increased the concentration of ascorbic acid with each addition. As can be observed from Figure 60, the

ascorbic acid oxidation peak is observed at 0.2 V and the current response increases with increasing concentration of ascorbic acid. Oxidation peak of dopamine is observed at around 0.35 V that does not show any significant change in the current since the concentration is fixed. The two peaks were successfully resolved without ascorbic acid interfering with the detection of dopamine.

4.5 Conclusion and Future Work

Successful fabrication of macroporous, macro-nanoporous and nanoporous gold electrodes have been reported in this work. Polystyrene spheres were synthesized via “surfactant-free emulsion polymerization” procedure that proved time saving and easy to execute. The polystyrene spheres were arranged into an ordered 3D assembly using Langmuir-Blodgett deposition that proved time and resource saving. The colloidal crystal was used as template to fabricate macroporous and macro-nanoporous gold electrode by electrodepositing cyanide-free gold and gold cyanide-silver cyanide alloy solution respectively in the interstices of the spheres. Nanopores were generated into the macropores by etching the macro-nanoporous gold electrode in concentrated nitric acid. Nanoporous gold electrode was fabricated by electrodepositing gold cyanide-silver cyanide alloy solution without the assistance of a template. Surface area of all the electrodes was compared and the faradaic and charging current was measured. The response of these electrodes to various redox molecules of fast and slow electron transfer was tested and the porous gold electrodes with high surface area were proved to perform better than the flat gold electrode. The electrodes were tested for surface adsorption in dopamine and it was concluded that porosity doesn’t allow the redox molecule to foul the surface as quickly as the flat gold electrode. The current response of the porous gold electrode in the event of dopamine adsorption is amplified for the first few cycles before finally decreasing. The macro-nanoporous gold electrode was tested for dopamine detection in the presence of

ascorbic acid differential pulse voltammetry respectively. Dopamine was successfully detected in spite of high concentration of ascorbic acid.

For future studies, the electrodes could be tested on biological fluids to detect heart diseases and Alzheimer's that manifest their onset in the abnormal levels of biomarkers like cysteine, homocysteine and glutathione. By modifying the parameters, the morphology of the porous structure can be changed and any other metal of choice can be used.

References:

(1) Seker, E.; Reed, M. L.; Begley, M. R., Nanoporous Gold: Fabrication, Characterization, and Applications, *Materials,* **2009**, *2*, 2188–2215.

(2) Collinson, M. M., Nanoporous Gold Electrodes and Their Applications in Analytical Chemistry, *ISRN Anal. Chem.* **2013**, *2013*, 1–21.

(3) Zheng, L.-T.; Wei, Y.-L.; Gong, H.-Q.; Qian, L., Application Progress of Nanoporous Gold in Analytical Chemistry, *Chinese J. Anal. Chem.* **2013**, *41*, 137–144.

(4) Park, S.; Kim, H. C.; Chung, T. D., Electrochemical analysis based on nanoporous structures, *Analyst* **2012**, *137*, 3891–3903.

(5) Lai, M.; Riley, D. J. *J,.* Templated electrosynthesis of nanomaterials and porous structures, *Colloid Interface Sci.* **2008**, *323*, 203–212.

(6) Hoa, M. L. K.; Lu, M.; Zhang, Y., Preparation of porous materials with ordered hole structure, *Adv. Colloid Interface Sci.* **2006**, *121*, 9–23.

(7) Liu, Q.; Tang, Z.; Ou, B.; Liu, L.; Zhou, Z.; Shen, S.; Duan, Y., Design, preparation, and application of ordered porous polymer materials, *Mater. Chem. Phys.* **2014**, *144*, 213–225.

(8) Zdravkov, B. D.; Čermák, J. J.; Šefara, M.; Janků, J., Pore classification in the characterization of porous materials: A perspective, *Cent. Eur. J. Chem.* **2007**, *5*, 385–395.

(9) Chen, Y.-L.; Lee, C.-Y.; Chiu, H.-T., Growth of gold nanowires on flexible substrate for highly sensitive biosensing: detection of thrombin as an example, *J. Mater. Chem. B* **2013**, *1*, 186.

(10) Kautek, W.; Reetz, S.; Pentzien, S., Template electrodeposition of nanowire arrays on gold foils fabricated by pulsed-laser deposition, *Electrochim. Acta* **1995**, *40*, 1461–1468.

(11) Menon, V. P.; Martin, C. R., Fabrication and Evaluation of Nanoelectrode Ensembles, *Anal. Chem.* **1995**, *67*, 1920–1928.

(12) Hsu, M.-S.; Chen, Y.-L.; Lee, C.-Y.; Chiu, H.-T., Gold nanostructures on flexible substrates as electrochemical dopamine sensors, *ACS Appl. Mater. Interfaces* **2012**, *4*, 5570–5575.

(13) Jia, F.; Yu, C.; Ai, Z.; Zhang, L., Fabrication of Nanoporous Gold Film Electrodes with Ultrahigh Surface Area and Electrochemical Activity, *Chem. Mater.* **2007**, *19*, 3648–3653.

(14) Brumlik, C. J.; Menon, V. P.; Martin, C. R., Template synthesis of metal microtubule ensembles utilizing chemical, electrochemical, and vacuum deposition techniques, *J. Mater. Res.* **2011**, *9*, 1174–1183.

(15) Jia, F.; Yu, C.; Deng, K.; Zhang, L., Nanoporous Metal (Cu, Ag, Au) Films with High Surface Area: General Fabrication and Preliminary Electrochemical Performance, *J. Phys. Chem. C* **2007**, *111*, 8424–8431.

(16) Chen, L.; Liu, Y., Synthesis and characterization of dendritic and porous Ag-Pd alloy nanostructures, *J. Colloid Interface Sci.* **2011**, *364*, 100–106.

(17) Kloke, A.; von Stetten, F.; Zengerle, R.; Kerzenmacher, S., Strategies for the Fabrication of Porous Platinum Electrodes, *Adv. Mater.* **2011**, *23*, 4976–5008.

(18) Delvaux, M.; Demoustier-Champagne, S., Immobilisation of glucose oxidase within metallic nanotubes arrays for application to enzyme biosensors, *Biosens. Bioelectron.* **2003**, *18*, 943–951.

(19) Zhang, K.; Tan, X.; Zhang, J.; Wu, W.; Tang, Y., Template-dealloying synthesis of ultralow density Au foams with bimodal porous structure, *RSC Adv.* **2014**, *4*, 7196.

(20) Ding, Y.; Erlebacher, J., Nanoporous metals with controlled multimodal pore size distribution, *J. Am. Chem. Soc.* **2003**, *125*, 7772–7773.

(21) Lang, X.; Hirata, A.; Fujita, T.; Chen, M., Nanoporous metal/oxide hybrid electrodes for electrochemical supercapacitors, *Nat. Nanotechnol.* **2011**, *6*, 232–236.

(22) Chen, A.; Holt-Hindle, P., Platinum-based nanostructured materials: synthesis, properties, and applications, *Chem. Rev.* **2010**, *110*, 3767–3804.

(23) Eason, R. *Pulsed Laser Deposition of Thin Films: Applications-Led Growth of Functional Materials (Google eBook)*; John Wiley & Sons, 2007; p. 754.

(24) Navasery, M.; Halim, S. a.; Dehzangi, a.; Soltani, N.; Bahmanrokh, G.; Erfani H, M.; Chen, S. K.; Lim, K. P., Growth and characterization of La0.7Na0.3MnO3 thin films prepared by pulsed laser deposition on different substrates, *J. Alloys Compd.* **2014**, *594*, 197–201.

(25) Vinodkumar, R.; Navas, I.; Porsezian, K.; Ganesan, V.; Unnikrishnan, N. V; Mahadevan Pillai, V. P., Structural, spectroscopic and electrical studies of nanostructured porous ZnO thin films prepared by pulsed laser deposition, *Spectrochim. Acta. A. Mol. Biomol. Spectrosc.* **2014**, *118*, 724–732.

(26) Sun, Y. W.; Gospodyn, J.; Kursa, P.; Sit, J.; DeCorby, R. G.; Tsui, Y. Y., Dense and porous ZnO thin films produced by pulsed laser deposition, *Appl. Surf. Sci.* **2005**, *248*, 392–396.

(27) Chen, X.; Wu, N. J.; Ritums, D. L.; Ignatiev, A., Pulsed laser deposition of conducting porous La-Sr-Co-O films, *Thin Solid Films* **1999**, *342*, 61–66.

(28) Xu, C.; Liu, Y.; Su, F.; Liu, A.; Qiu, H., Nanoporous PtAg and PtCu alloys with hollow ligaments for enhanced electrocatalysis and glucose biosensing, *Biosens. Bioelectron.* **2011**, *27*, 160–166.

(29) Aburada, T.; Fitz-Gerald, J. M.; Scully, Synthesis of nanoporous copper by dealloying of Al-Cu-Mg amorphous alloys in acidic solution: The effect of nickel, J. R. *Corros. Sci.* **2011**, *53*, 1627–1632.

(30) Liu, W. B.; Zhang, S. C.; Li, N.; Zheng, J. W.; Xing, Y. L., Influence of phase constituent and proportion in initial Al–Cu alloys on formation of monolithic nanoporous copper through chemical dealloying in an alkaline solution, *Corros. Sci.* **2011**, *53*, 809–814.

(31) Zhao, C.; Qi, Z.; Wang, X.; Zhang, Z., Fabrication and characterization of monolithic nanoporous copper through chemical dealloying of Mg–Cu alloys, *Corros. Sci.* **2009**, *51*, 2120–2125.

(32) Zhang, Z.; Wang, Y.; Qi, Z.; Lin, J.; Bian, X., Nanoporous Gold Ribbons with Bimodal Channel Size Distributions by Chemical Dealloying of Al - Au Alloys, *J. Phys. Chem. C* **2009**, *113*, 1308–1314.

(33) Zhang, Q.; Wang, X.; Qi, Z.; Wang, Y.; Zhang, Z., A benign route to fabricate nanoporous gold through electrochemical dealloying of Al–Au alloys in a neutral solution, *Electrochim. Acta* **2009**, *54*, 6190–6198.

(34) Wang, X.; Wang, W.; Qi, Z.; Zhao, C.; Ji, H.; Zhang, Z., High catalytic activity of ultrafine nanoporous palladium for electro-oxidation of methanol, ethanol, and formic acid, *Electrochem. commun.* **2009**, *11*, 1896–1899.

(35) Hakamada, M.; Mabuchi, M., Fabrication of nanoporous palladium by dealloying and its thermal coarsening, *J. Alloys Compd.* **2009**, *479*, 326–329.

(36) Singh, N.; Lyon, L. A., Au Nanoparticle Templated Synthesis of pNIPAm Nanogels, *Chem. Mater.* **2007**, *19*, 719–726.

(37) Kresge C.T., Leonowicz M.E., Roth W.J., Vartuli J.C., B. J. S., Ordered mesoporous molecular sieves synthesized by a liquid-crystal template mechanism, *Nature* **1992**, *359*, 710–712.

(38) Furneaux R.C., Rigby W.R., D. A. P., The formation of controlled-porosity membranes from anodically oxidized aluminium, *Nature* **1989**, *337*, 147–149.

(39) Zhao, S.; Roberge, H.; Yelon, A.; Veres, T. *J,* New application of AAO template: a mold for nanoring and nanocone arrays, *Am. Chem. Soc.* **2006**, *128*, 12352–12353.

(40) H. Masuda, H. Asoh, M. Watanabe, K. Nishio, M. Nakao, T. T., Square and Triangular Nanohole Array Architectures in Anodic Alumina, *Adv. Mater.* **2001**, *13*, 189–192.

(41) Toimil Molares, M. E.; Brötz, J.; Buschmann, V.; Dobrev, D.; Neumann, R.; Scholz, R.; Schuchert, I. U.; Trautmann, C.; Vetter, Etched heavy ion tracks in polycarbonate as template for copper nanowires, J. *Nucl. Instruments Methods Phys. Res. Sect. B Beam Interact. with Mater. Atoms* **2001**, *185*, 192–197.

(42) C., S.; Zande, B. M. I. Van Der; Fokkink, L. G. J.; Henny, M.; Schmid, C.; Bachtold, A.; Huber, R.; Birk, H.; Staufer, U., Template Synthesis of Nanowires in Porous Polycarbonate Membranes : Electrochemistry and Morphology, *J. Phys. Chem. B* **1997**, *101*, 5497–5505.

(43) Wu, C.; Bein, T., Conducting Carbon Wires in Ordered , Nanometer-Sized Channels, *Science,* **1994**, *266*, 1013–1015.

(44) Guerret-Plecourt C., Bouar Le Y., Lolseau A., P. H., Relation between metal electronic structure and morphology of metal compounds inside carbon nanotubes, *Nature* **1994**, *372*, 761–765.

(45) Li, Y.; Song, Y.-Y.; Yang, C.; Xia, X.-H., Hydrogen bubble dynamic template synthesis of porous gold for nonenzymatic electrochemical detection of glucose, *Electrochem. commun.* **2007**, *9*, 981–988.

(46) Knez, M.; Bittner, A. M.; Boes, F.; Wege, C.; Jeske, H.; Mai, E.; Kern, K., Biotemplate Synthesis of 3-nm Nickel and Cobalt Nanowires, *Nano Lett.* **2003**, *3*, 1079–1082.

(47) Dujardin, E.; Peet, C.; Stubbs, G.; Culver, J. N.; Mann, S., Organization of Metallic Nanoparticles Using Tobacco Mosaic Virus Templates, *Nano Lett.* **2003**, *3*, 413–417.

(48) Fujikawa, S.; Kunitake, T., Surface Fabrication of Hollow Nanoarchitectures of Ultrathin Titania Layers from Assembled Latex Particles and Tobacco Mosaic Viruses as Templates, *Langmuir* **2003**, *19*, 6545–6552.

(49) S.A., Davis, S.L. Burkett, N. H. M. and S. M., Bacterial Templating of Ordered Macrostructures in Silica and Silica-surfactant Mesophases, *Nature* **1997**, *385*, 420–423.

(50) Liu, Z.; Fan, T.; Zhang, D.; Gong, X.; Xu, Hierarchically porous ZnO with high sensitivity and selectivity to H2S derived from biotemplates, J. *Sensors Actuators B Chem.* **2009**, *136*, 499–509.

(51) Meldrum, F. C.; Seshadri, R., Porous gold structures through templating by echinoid skeletal plates, *Chem. Commun.* **2000**, 29–30.

(52) D. Yang, L. Qi and J. Ma, Eggshell Membrane Templating of Hierarchically Ordered Macroporous Networks Composed, *Adv. Mater.* **2002**, *14*, 1543–1546.

(53) Hall, S. R.; Bolger, H.; Mann, S., Morphosynthesis of complex inorganic forms using pollen grain templates Porous micron-sized particles of silica , calcium carbonate or by template-directed synthesis employing intact pollen, *CHEM COMMUN.* **2003**, *44*, 2784–2785.

(54) Sotiropoulou, S.; Sierra-Sastre, Y.; Mark, S. S.; Batt, C. A., Biotemplated Nanostructured Materials, *Chem. Mater.* **2008**, *20*, 821–834.

(55) Bartlett, P. N.; Birkin, P. R.; Ghanem, M. A., Electrochemical deposition of macroporous platinum, palladium and cobalt films using polystyrene latex sphere templates, *Chem. Commun.* **2000**, 1671–1672.

(56) Bartlett, P. N.; Baumberg, J. J.; Coyle, S.; Abdelsalam, M. E., Optical properties of nanostructured metal films, *Faraday Discuss.* **2004**, *125*, 117.

(57) Chen, Z.; Zhan, P.; Wang, Z. L.; Zhang, J. H.; Zhang, W. Y.; Ming, N. B.; Chan, C. T.; Sheng, P., Two- and Three-Dimensional Ordered Structures of Hollow Silver Spheres Prepared by Colloidal Crystal Templating, *Adv. Mater.* **2004**, *16*, 417–422.

(58) Dokoutchaev, A.; James, J. T.; Koene, S. C.; Pathak, S.; Prakash, G. K. S.; Thompson, M. E., Colloidal Metal Deposition onto Functionalized Polystyrene Microspheres, *Chem. Mater.* **1999**, *11*, 2389–2399.

(59) Yan, H.; Blanford, C. F.; Lytle, J. C.; Carter, C. B.; Smyrl, W. H.; Stein, A., Influence of Processing Conditions on Structures of 3D Ordered Macroporous Metals Prepared by Colloidal Crystal Templating, *Chem. Mater.* **2001**, *13*, 4314–4321.

(60) Sun, X.; Liu, J.; Li, Y., Use of carbonaceous polysaccharide microspheres as templates for fabricating metal oxide hollow spheres, *Chem. - A Eur. J.* **2006**, *12*, 2039–2047.

(61) Zakhidov, A. A., Carbon Structures with Three-Dimensional Periodicity at Optical Wavelengths, *Science,* **1998**, *282*, 897–901.

(62) Braun, P. V; Wiltzius, P., Electrochemically grown photonic crystals, *Nature* **1999**, *402*, 603–604.

(63) Holland, B. T.; Abrams, L.; Stein, A., Dual Templating of Macroporous Silicates with Zeolitic Microporous Frameworks, *J. Am. Chem. Soc.* **1999**, *121*, 4308–4309.

(64) Velev, O. D.; Kaler, E. W., Structured Porous Materials via Colloidal Crystal Templating: From Inorganic Oxides to Metals, *Adv. Mater.*, **2000**, *12*, 531-534.

(65) Stein, A.; Schroden, R. C., Colloidal crystal templating of three-dimensionally ordered macroporous solids : materials for photonics and beyond, *Curr. Opin. Solid State Mater. Sci.* **2001**, *5*, 553–564.

(66) Zhou, W.; Wang, Z. L. *Scanning Microscopy for Nanotechnology: Techniques and Applications*; Springer Science & Business Media, 2007; p. 536.

(67) Sivasankar, B. *Instrumental Methods of Analysis*; Sivasankar, B., Ed.; First.; Oxford University Press, 2012; p. 600.

(68) Bell, D.; Garratt-Reed, A. *Energy Dispersive X-ray Analysis in the Electron Microscope*; Garland Science, 2003; p. 160.

(69) *Encyclopedia of Materials Characterization: Surfaces, Interfaces, Thin Films*; Gulf Professional Publishing, 1992; p. 751.

(70) Ahn, M.; Kim, J. *J*, Electrochemical behavior of dopamine and ascorbic acid at dendritic Au rod surfaces: Selective detection of dopamine in the presence of high concentration of ascorbic acid, *Electroanal. Chem.* **2012**, *683*, 75–79.

(71) Mabbott, G. A., An Introduction to Cyclic Voltammetry, *J. Chem. Educ.* **1983**, *60*, 697–702.

(72) Evans, D. H.; O'Connell, K. M.; Petersen, R. a.; Kelly, M. J., Cyclic voltammetry, *J. Chem. Educ.* **1983**, *60*, 290.

(73) Lee, Y.-J.; Park, J.-Y., Nonenzymatic free-cholesterol detection via a modified highly sensitive macroporous gold electrode with platinum nanoparticles, *Biosens. Bioelectron.* **2010**, *26*, 1353–1358.

(74) El-Said, W. A.; Lee, J.-H.; Oh, B.-K.; Choi, J.-W., 3-D nanoporous gold thin film for the simultaneous electrochemical determination of dopamine and ascorbic acid, *Electrochem. commun.* **2010**, *12*, 1756–1759.

(75) Ding, C.; Li, H.; Hu, K.; Lin, J.-M., Electrochemical immunoassay of hepatitis B surface antigen by the amplification of gold nanoparticles based on the nanoporous gold electrode, *Talanta* **2010**, *80*, 1385–1391.

(76) Li, R.; Wu, D.; Li, H.; Xu, C.; Wang, H.; Zhao, Y.; Cai, Y.; Wei, Q.; Du, B., Label-free amperometric immunosensor for the detection of human serum chorionic gonadotropin based on nanoporous gold and graphene, *Anal. Biochem.* **2011**, *414*, 196–201.

(77) Liu, Z.; Zhang, H.; Hou, S.; Ma, H., Highly sensitive and selective electrochemical detection of L-cysteine using nanoporous gold, *Microchim. Acta* **2012**, *177*, 427–433.

(78) Qiu, H.; Xue, L.; Ji, G.; Zhou, G.; Huang, X.; Qu, Y.; Gao, P., Enzyme-modified nanoporous gold-based electrochemical biosensors, *Biosens. Bioelectron.* **2009**, *24*, 3014–3018.

(79) Zielasek, V.; Jürgens, B.; Schulz, C.; Biener, J.; Biener, M. M.; Hamza, A. V; Bäumer, M., Gold catalysts: nanoporous gold foams, *Angew. Chem. Int. Ed. Engl.* **2006**, *45*, 8241–8244.

(80) Xu, C.; Xu, X.; Su, J.; Ding, Y., Research on unsupported nanoporous gold catalyst for CO oxidation, *J. Catal.* **2007**, *252*, 243–248.

(81) Wittstock, A.; Biener, J.; Bäumer, M., Nanoporous gold: a new material for catalytic and sensor applications, *Phys. Chem. Chem. Phys.* **2010**, *12*, 12919–12930.

(82) Xia, Y.; Huang, W.; Zheng, J.; Niu, Z.; Li, Z., Nonenzymatic amperometric response of glucose on a nanoporous gold film electrode fabricated by a rapid and simple electrochemical method, *Biosens. Bioelectron.* **2011**, *26*, 3555–3561.

(83) Yin, H.; Zhou, C.; Xu, C.; Liu, P.; Xu, X.; Ding, Y., Aerobic Oxidation of D -Glucose on Support-Free Nanoporous Gold, *J. Phys. Chem. C* **2008**, *112*, 9673–9678.

(84) Zeis, R.; Mathur, A.; Fritz, G.; Lee, J.; Erlebacher, J., Platinum-plated nanoporous gold: An efficient, low Pt loading electrocatalyst for PEM fuel cells, *J. Power Sources* **2007**, *165*, 65–72.

(85) Vogel, N.; Goerres, S.; Landfester, K.; Weiss, C. K., A convenient method to produce close- and non-close-packed monolayers using direct assembly at the air-water interface and subsequent plasma-induced size reduction, *Macromol. Chem. Phys.* **2011**, *212*, 1719–1734.

(86) Zhang, J.; Chen, Z.; Wang, Z.; Zhang, W.; Ming, N., Preparation of monodisperse polystyrene spheres in aqueous alcohol system, *Mater. Lett.* **2003**, *57*, 4466–4470.

(87) Gorsd, M. N.; Blanco, M. N.; Pizzio, L. R., Synthesis of Polystyrene Microspheres to be Used as Template in the Preparation of Hollow Spherical Materials: Study of the Operative Variables, *Procedia Mater. Sci.* **2012**, *1*, 432–438.

(88) Reese, C.; Guerrero, C.; Weissman, J.; Lee, K.; Asher, S., Synthesis of Highly Charged, Monodisperse Polystyrene Colloidal Particles for the Fabrication of Photonic Crystals, *J. Colloid Interface Sci.* **2000**, *232*, 76–80.

(89) Stober, W. . A. Fink. E. Bohn., Controlled Growth of Monodisperse Silica Spheres in the Micron Size Range, *J. Colloid Interface Sci.* **1968**, *69*, 62–69.

(90) Xia, Y.; Gates, B.; Yin, Y.; Lu, Y., Monodispersed colloidal spheres: Old materials with new applications, *Adv. Mater.* **2000**, *12*, 693–713.

(91) Ohmori, M. ; M. E., Preparation and Properties of Uniform Coated Colloidal Particles. VII. Silica on Hematite, *J. Colloid Interface Sci.* **1992**, *150*, 594–598.

(92) Sun, X.; Li, Y., Colloidal carbon spheres and their core/shell structures with noble-metal nanoparticles, *Angew. Chemie Int. Ed.* **2004**, *43*, 597–601.

(93) Antl, L.; Goodwin, J. W.; Papworth, S.; Waters, J. A., The Preparation of poly(methyl methacrylate) latices in non-aqueous media, *Colloids and Surfaces* **1986**, *17*, 67–78.

(94) Jardine, R. S.; Bartlett, P., Synthesis of non-aqueous fluorescent hard-sphere polymer colloids, *Colloids Surfaces A Physicochem. Eng. Asp.* **2002**, *211*, 127–132.

(95) Bosma, G.; Pathmamanoharan, C.; de Hoog, E. H. a; Kegel, W. K.; van Blaaderen, A.; Lekkerkerker, H. N. W., Preparation of monodisperse, fluorescent PMMA-latex colloids by dispersion polymerization, *J. Colloid Interface Sci.* **2002**, *245*, 292–300.

(96) Nagao, D.; Anzai, N.; Kobayashi, Y.; Gu, S.; Konno, M., monodisperse poly(methyl methacrylate) particles incorporating fluorescent rhodamine 6G for colloidal crystals, *J. Colloid Interface Sci.* **2006**, *298*, 232–237.

(97) Yamada, Y.; Sakamoto, T.; Gu, S.; Konno, M., Soap-free synthesis for producing highly monodisperse, micrometer-sized polystyrene particles up to 6 microm., *J. Colloid Interface Sci.* **2005**, *281*, 249–252.

(98) Gu, S.; Onishi, J.; Kobayashi, Y.; Nagao, D.; Konno, M., Preparation and colloidal stability of monodisperse magnetic polymer particles, *J. Colloid Interface Sci.* **2005**, *289*, 419–426.

(99) Brinker, C. J.; Lu, Y.; Sellinger, A.; Fan, H., Evaporation-Induced Self-Assembly : Nanostructures Made Easy, *Adv. Mater.* **1999**, *11*, 579–585.

(100) Denkov, N. D.; Velev, O. D.; Kralchevsky, P. A.; Ivanov, I. B.; Yoshimura, H.; Nagayama, K., Mechanism of Formation of Two-Dimensional Crystals from Latex Particles on Substrates, *Langmuir* **1992**, *8*, 3183–3190.

(101) Deckman, H. W.; Dunsmuir, J. H., Natural lithography, *Appl. Phys. Lett.* **1982**, *41*, 377.

(102) Hulteen, J. C.; Van Duyne, R. P., Nanosphere lithography: A materials general fabrication process for periodic particle array surfaces, *J. Vac. Sci. Technol. A Vacuum, Surfaces, Film.* **1995**, *13*, 1553.

(103) Winzer, M.; Kleiber, M.; Dix, N.; Wiesendanger, R., Fabrication of nano-dot- and nano-ring-arrays by nanosphere lithography, *Appl. Phys. A Mater. Sci. Process.* **1996**, *63*, 617–619.

(104) Donselaar, L. N.; Philipse, A. P.; Suurmond, J., Concentration-Dependent Sedimentation of Dilute Magnetic Fluids and Magnetic Silica Dispersions, *Langmuir* **1997**, *13*, 6018–6025.

(105) Miguez, H.; Meseguer, F.; Lopez, C.; Mifsud, A.; Moya, J. S.; Vazquez, L., Evidence of FCC Crystallization of SiO2 Nanospheres, *Langmuir* **1997**, *13*, 6009–6011.

(106) Mayoral, R.; Requena, J.; Moya, J. S.; Lopez, C.; Cintas, A.; Miguez, H.; Meseguer, F.; Vazquez, L.; Holgado, M.; Blanco, A., 3D Long Range Ordering in an SiO2 Submicrometer-Sphere Sintered Superstructure, *Adv. Mater.* **1997**, *9*, 257–260.

(107) Park, S. H.; Qin, D.; Xia, Y., Crystallization of Mesoscale Particles over Large Areas, *Adv. Mater.* **1998**, *10*, 1028–1032.

(108) Park, S. H.; Xia, Y., Macroporous Membranes with Highly Ordered and Three-Dimensionally Interconnected Spherical Pores, *Adv. Mater.* **1998**, *10*, 1045–1048.

(109) Park, S. H.; Xia, Y., Fabrication of Three-Dimensional Macroporous Membranes with Assemblies of Microspheres as Templates, *Chem. Mater.* **1998**, *10*, 1745–1747.

(110) Denkov, N. D.; Velev, O. D.; Kralchevsky, P. A.; Ivanov, I. B.; Yoshimura, H.; Nagayama, K., Two-dimensional Crystallization, *Nature* **1993**, *361*, 26.

(111) Dimitrov, A. S.; Dushkin, C. D.; Yoshimura, H.; Nagayama, K., Observations of Latex Particle Two-Dimensional-Crystal Nucleation in Wetting Films on Mercury, Glass and Mica, *Languir* **1994**, *10*, 432–440.

(112) Yamaki, M.; Higo, J.; Nagayama, K., Size-Dependent Separation of Colloidal Particles In Two-Dimensional Convective Self-Assembly, *Langmuir* **1995**, *11*, 2975–2978.

(113) Jiang, P.; Bertone, J. F.; Hwang, K. S.; Colvin, V. L., Single-Crystal Colloidal Multilayers of Controlled Thickness, *Chem. Mater.* **1999**, *11*, 2132–2140.

(114) Pieranski, P.; Strzelecki, L.; Pansu, B., Thin Colloidal Crystals, *Phys. Rev. Lett.* **1983**, *50*, 900–904.

(115) Velev, O. D.; Jede, T. A.; Lobo, R. F.; Lenhoff, A. M., Microstructured Porous Silica Obtained via Colloidal Crystal Templates, *Chem. Mater.* **1998**, *10*, 3597–3602.

(116) Holland, B. T.; Blanford, C. F.; Stein, A., Synthesis of Macroporous Minerals with Highly Ordered Three-Dimensional Arrays of Spheroidal Voids, *Science,* **1998**, *281*, 538–540.

(117) Huang, Y.-J.; Lai, C.-H.; Wu, P.-W., Fabrication of Large-Area Colloidal Crystals by Electrophoretic Deposition in Vertical Arrangement, *Electrochem. Solid-State Lett.* **2008**, *11*, P20–P22.

(118) Trau, M.; Saville, D. A.; Aksay, I. A., Assembly of Colloidal Crystals at Electrode Interfaces, *Langmuir* **1997**, *13*, 6375–6381.

(119) Holgado, M.; Garcı, F.; Blanco, A.; Ibisate, M.; Cintas, A.; Serna, C. J.; Molpeceres, C.; Requena, J.; Mifsud, A.; Meseguer, F.; Lo, C., Electrophoretic Deposition To Control Artificial Opal Growth, *Langmuir* **1999**, *15*, 4701–4704.

(120) Stein, A., Sphere templating methods for periodic porous solids, *Microporous Mesoporous Mater.* **2001**, *44-45*, 227–239.

(121) Wijnhoven, J. E.; Vos, W. L., Preparation of Photonic Crystals Made of Air Spheres in Titania, *Science,* **1998**, *281*, 802–804.

(122) Kim, M. H.; Im, S. H.; Park, O. O., Rapid Fabrication of Two- and Three-Dimensional Colloidal Crystal Films via Confined Convective Assembly, *Adv. Funct. Mater.* **2005**, *15*, 1329–1335.

(123) Ye, Y.-H.; LeBlanc, F.; Haché, A.; Truong, V.-V., Self-assembling three-dimensional colloidal photonic crystal structure with high crystalline quality, *Appl. Phys. Lett.* **2001**, *78*, 52.

(124) Lu, C.; Möhwald, H.; Fery, A., A lithography-free method for directed colloidal crystal assembly based on wrinkling, *Soft Matter* **2007**, *3*, 1530.

(125) Velev, O. D.; Lenhoff, A. M., Colloidal crystals as templates for porous materials, *Curr. Opin. Colloid Interface Sci.* **2000**, *5*, 56–63.

(126) Telford, A. M.; Pham, B. T. T.; Neto, C.; Hawkett, B. S., Micron-sized polystyrene particles by surfactant-free emulsion polymerization in air: Synthesis and mechanism, *J. Polym. Sci. Part A Polym. Chem.* **2013**, *51*, 3997–4002.

(127) Dziomkina, N. V.; Vancso, G. J., Colloidal crystal assembly on topologically patterned templates, *Soft Matter* **2005**, *1*, 265.

(128) Bartlett, P. N.; Baumberg, J. J.; Birkin, P. R.; Ghanem, M. A.; Netti, M. C., Highly Ordered Macroporous Gold and Platinum Films Formed by Electrochemical Deposition through Templates Assembled from Submicron Diameter Monodisperse Polystyrene Spheres, *Chem. Mater.* **2002**, *14*, 2199–2208.

(129) Seker, E.; Reed, M.; Begley, M., A thermal treatment approach to reduce microscale void formation in blanket nanoporous gold films, *Scr. Mater.* **2009**, *60*, 435–438.

(130) Cox, M. E.; Dunand, D. C., Bulk gold with hierarchical macro-, micro- and nano-porosity, *Mater. Sci. Eng. A* **2011**, *528*, 2401–2406.

(131) Patel, J.; Radhakrishnan, L.; Zhao, B.; Uppalapati, B.; Daniels, R. C.; Ward, K. R.; Collinson, M. M., Electrochemical Properties of Nanostructured Porous Gold Electrodes in Biofouling Solutions, Anal. Chem., 2013, 11610-11618

(132) Erlebacher, J. *J,* An Atomistic Description of Dealloying, *Electrochem. Soc.* **2004**, *151*, C614.

(133) Erlebacher, J.; Aziz, M. J.; Karma, a; Dimitrov, N.; Sieradzki, K., Evolution of nanoporosity in dealloying, *Nature* **2001**, *410*, 450–453.

(134) Lee, Y. J.; Oh, C.; Park, J. Y.; Kim, Y., Fabrication and Characterization of Macroporous Gold Hybrid Sensing Electrodes With Electroplated Platinum Nanoparticles, *IEEE Trans. Nanotechnol.* **2011**, *10*, 1298–1305.

(135) Bard, A. J.; Faulkner, L. R. *Electrochemical Methods: Fundamentals and Applications*; Wiley, 2000; Vol. 6, p. 864.

(136) Sun, W.; Wang, Y.; Zhang, Y.; Ju, X.; Li, G.; Sun, Z., Poly(methylene blue) functionalized graphene modified carbon ionic liquid electrode for the electrochemical detection of dopamine, *Anal. Chim. Acta* **2012**, *751*, 59–65.